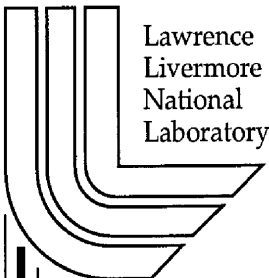


Measurement of Several 239 Pu(n,xn) Partial γ -ray Cross Sections for $x \leq 3$ using GEANIE at LANSCE/WNR

*L.A. Bernstein, J.A. Becker, P.E. Garrett, K. Hauschild,
C.A. McGrath, D.P. McNabb, W. Younes, M. Devlin, N.
Fotiades, G.D. Johns, R.O. Nelson, and W.S. Wilburn*

September 1, 2000

U.S. Department of Energy



DISCLAIMER

This document was prepared as an account of work sponsored by an agency of the United States Government. Neither the United States Government nor the University of California nor any of their employees, makes any warranty, express or implied, or assumes any legal liability or responsibility for the accuracy, completeness, or usefulness of any information, apparatus, product, or process disclosed, or represents that its use would not infringe privately owned rights. Reference herein to any specific commercial product, process, or service by trade name, trademark, manufacturer, or otherwise, does not necessarily constitute or imply its endorsement, recommendation, or favoring by the United States Government or the University of California. The views and opinions of authors expressed herein do not necessarily state or reflect those of the United States Government or the University of California, and shall not be used for advertising or product endorsement purposes.

This work was performed under the auspices of the U. S. Department of Energy by the University of California, Lawrence Livermore National Laboratory under Contract No. W-7405-Eng-48.

This report has been reproduced directly from the best available copy.

Available electronically at <http://www.doc.gov/bridge>

Available for a processing fee to U.S. Department of Energy
And its contractors in paper from
U.S. Department of Energy
Office of Scientific and Technical Information
P.O. Box 62
Oak Ridge, TN 37831-0062
Telephone: (865) 576-8401
Facsimile: (865) 576-5728
E-mail: reports@adonis.osti.gov

Available for the sale to the public from
U.S. Department of Commerce
National Technical Information Service
5285 Port Royal Road
Springfield, VA 22161
Telephone: (800) 553-6847
Facsimile: (703) 605-6900
E-mail: orders@ntis.fedworld.gov
Online ordering: <http://www.ntis.gov/ordering.htm>

OR

Lawrence Livermore National Laboratory
Technical Information Department's Digital Library
<http://www.llnl.gov/tid/Library.html>

Measurement of several $^{239}\text{Pu}(n,xn)$ partial γ -ray cross sections for $x \leq 3$ using GEANIE at LANSCE/WNR

L.A.Bernstein, J.A.Becker, P.E.Garrett, K.Hauschild, C.A.McGrath,
D.P. McNabb, W. Younes
LLNL

M. Devlin, N. Fotiades, G.D.Johns, R.O.Nelson, W.S.Wilburn
LANL

I.) Introduction

Previous experimental efforts to measure the $^{239}\text{Pu}(n,2n)$ reaction cross section have relied on the detection of evaporated neutrons [Mat72, Fre85]. These efforts were hampered by the presence of the large ($\sigma \approx 2$ barns) neutron-induced fission channel which produces on average 3-4 neutrons [How71]. This paper is one of three manuscripts that document an effort to determine the $^{239}\text{Pu}(n,2n)$ channel cross section using the GERmanium Array for Neutron Induced Excitations (GEANIE) spectrometer [Bec97] at the Los Alamos Neutron Science Center/Weapons Neutron Research (LANSCE/WNR) [Lis90] facility. In this document we report the measurement of several $^{239}\text{Pu}(n,xn\gamma)^{240-x}\text{Pu}$ partial cross sections. The other two papers report results for a parallel proof-of-principle experiment using a ^{235}U target as a surrogate for ^{239}Pu [Youn00] and a detailed calculation and measurement of the efficiency of the GEANIE spectrometer [McN00]. Results from these two works are frequently referred to in this paper. A later report from Becker et al. will use the partial $(n,2n\gamma)$ cross sections reported here, together with the predictions of the GNASH [Cha99, Cha00] and IDA [Ros99] reaction models, to extract a total cross section for the $(n,2n)$ channel.

The results of three experiments are reported here. Two were carried out in 1998 using a 0.010 inch (referred to as "thin") and 0.020 inch (referred to as "thick") ^{239}Pu target. The remaining one was run in 1999 using the same thin target. This work is being carried out in parallel with a similar effort to measure $(n,xn\gamma)$ cross sections on a ^{235}U target being analyzed by Younes et al., [You00]. This experiment was performed using the same γ -ray spectrometer and a similar analysis approach, thereby allowing a detailed comparison between the two data sets and a check on the techniques used.

The report is comprised of three portions. In the first part the experimental techniques used for all three runs will be presented. The next section will describe how the partial $(n,xn\gamma)$ cross sections were extracted from a combination of all three data sets, including a detailed discussion of the level spectroscopy of levels in ^{238}Pu populated in this experiment. The last portion of the report will focus on a comparison between the observed partial cross sections and the predictions of the GNASH reaction model [Cha99, Cha00]. Several methods will be suggested in which the model predictions may be coupled with the measured partial cross sections to extract a $(n,2n)$ channel cross section. A separate appendix will present the results from the three separate experiments individually.

This work was performed under the auspices of the U.S. Department of Energy by the University of California, Lawrence Livermore National Laboratory under Contract No. W-7405-Eng-48.

II.) Experimental Set-up

Figure 1 shows a schematic description of the GEANIE spectrometer at LANSCE/WNR. The experiments were performed by exposing a ^{239}Pu targets in the neutron beam and recording the γ -ray energy (pulse height) and the neutron time-of-flight (TOF) using the GEANIE spectrometer. In-beam and beam-off γ -rays were recorded. The capabilities of a prior implementation of the GEANIE spectrometer were highlighted in an earlier study of neutron-induced reactions on a ^{196}Pt target [Ber98]. GEANIE is currently comprised of 9 Compton suppressed and 6 unsuppressed coaxial Ge detectors with approximately 25% of the efficiency of a 3" X 3" NaI crystal and 11 Compton suppressed planar Ge detectors (LEPS – Low Energy Photon Spectrometers). GEANIE is located 20.34 m from the Weapons Neutron Research (WNR) spallation neutron source at the Los Alamos Neutron Scattering Center (LANSCE) on the 60°-right flight path. Neutron energies at the WNR "white" source cover the range from less than 1 MeV to \approx 600 MeV. Neutron fluences on target were measured with a $^{235}\text{U}/^{238}\text{U}$ fission chamber [Wen93] located 18.48 m from the center of the spallation target.

Spallation neutrons were produced at the ^{nat}W spallation target irradiated by an 800 MeV proton beam with an average current of \approx 2 μA during the 1998 experiments and \approx 6 μA during the 1999 run. The neutron flux decreases by approximately a factor of 5 between 5 and 20 MeV. The beam time structure consisted of a train of 1.8 μs micropulses (referred to as a "macropulse") at a rep rate of 120 Hz. However, the last 1-20 macropulses were "missing". Table 1 below give the specific beam structure for the three experiments. The beam intensity varied considerably during the course of the experiment and there were sizable (> 12 hour) periods of time when the beam was off. In-beam recorded data consisted of γ -ray pulse heights with $20 \text{ keV} \leq E_{\gamma} \leq 1 \text{ MeV}$ for the LEPS and $50 \text{ keV} \leq E_{\gamma} \leq 4 \text{ MeV}$ for the coaxial detectors together with the event time, correlated to the beam micropulse RF signal. Beam-off recorded data included the same γ -ray pulse height information together with a 100 ns-per-tick "long-range clock" that was reset at the beginning of every macropulse. The neutron energy of an event that produced a specific detected in-beam γ -ray was obtained from the difference in the time of arrival of the γ -ray the " γ -flash" coming from the spallation target. This is referred to as the time-of-flight (TOF) technique. Data were recorded onto magnetic tape using a specially modified version of the VME-based Michigan State University data acquisition system [Mai94]. Three separate measurements were made. The 1998 measurements were made on two different targets (10 mil thickness and 20 mil thickness respectively). The 1999 experiment used the 10 mil target only. The normal of the targets were oriented at an angle of 19° with respect to the beam. Table 2 below discuss the properties of the thin and thick targets used.

Table 1: Beam timing structure and total number of neutrons in the beam with $1 < E_n (\text{MeV}) < 25$ (from the ^{235}U fission chamber) for the 1998 10 mil, 1998 20 mil and 1999 10 mil data sets.

Run	Macropulse Length (μs)	Rep Rate (Hz)	N_{neutrons} with $1 < E_n (\text{MeV}) < 25$
1998 0.010" target	625	100-110	$7.9868(209) \times 10^{13}$
1998 0.020" target	625	100-110	$6.5305(188) \times 10^{13}$
1999 0.010" target	750	119	$8.3577(215) \times 10^{13}$

Table 2: Isotopic and chemical composition of the thin and thick targets used in all three experiment.

Thickness (cm)	Isotopic Composition (atom %)						Weight % Gallium
	^{238}Pu	^{239}Pu	^{240}Pu	^{241}Pu	^{242}Pu	^{241}Am	
0.0277 ± 0.0008	0.0027	98.014	1.973	0.0093	0.0013	0.00015(3)	0.98(1)
0.0500 ± 0.0003	0.0027	98.014	1.973	0.0093	0.0013	0.00015(3)	0.98(1)

The efficiency and the attenuation of the target-array combination were determined using a combination of point- and distributed calibration source measurements performed and cross-checked with the results of a MCNP model calculation. This process is described in [McN00]. However, in order to gain confidence in the array+target attenuation and efficiency calibration an additional cross-check was added during the 1999 thin target run a pair of 0.004" ^{54}Fe foils were placed on either side of the ^{239}Pu target. This allowed for a cross-check of the efficiency calibration using the partial γ -ray cross section of the 846.7 keV $2^+ \rightarrow 0^+$ transition in ^{54}Fe as a calibration standard.

IIIa.) Data Analysis

In this section the techniques used to analyze the γ -ray-Time-of-Flight (TOF) correlated data will be presented. Figure 2 shows a projection onto the time-of-flight axis for the planar detectors from the thin target 1999 data set. Even for this data set, which had the highest peak-to-background ratio of all three runs, the background from target activity (the area under the red-dashed line in figure 2) is nearly half of the total counts. This large target activity background, together with the background due to neutron-induced fission, necessitated that the analysis be focused on the planar detector data, which had better energy resolution than the coaxial detectors. In addition, the planar detector background due to the Compton scatter of incident γ -rays is less than half that found in the coaxial detectors. This becomes increasingly important at lower-energies where background from higher energy peaks “piles up” to contaminate low-energy lines.

Data obtained from the experiments were replayed off-line and sorted into a separate set of two-dimensional γ -ray pulse height versus time-of-flight (E_γ vs. TOF) arrays for each data set (thin target 1998, thick target 1998 and thin target 1999). Gains were dynamically aligned during playback using the technique developed by Younes et al., [You00] to minimize the widths of the γ -ray peaks and therefore maximize the resolving power ($\Delta E_\gamma/E_\gamma$) of the array. A γ -ray pulse height spectrum corresponding to incident neutron energies of 1-25 MeV was then formed by “gating” on the TOF-axis of this two-dimensional array. Portions of this spectrum were chosen that had as close to a flat background as possible and contained no more than 15 peaks each. These regions were then fit using the GF2 code from David Radford [Rad98]. Peak shapes were assumed to be a normal plus a skewed gaussian. Table 3 below describes the parameters used in a GF2 fit and give some of the typical values for the region near the ^{238}Pu $6 \rightarrow 4$ γ -ray. These parameters are then varied until the χ^2/ν for the fit is minimized. Occasionally this results in a negative peak area. This does not substantially alter the results as long as the negative peak area is consistent with zero within statistical errors.

Table 3: Parameters used in the GF2 fitting program from D. Radford [Rad98]. The example shown is for the region near the ^{238}Pu $6 \rightarrow 4$ ground state band transition.

Parameter	Description	Example
A	Constant Background Term	3436.85 ± 21.32
B	Linear Background Term	0.1527 ± 0.5150
C	Quadratic Background Term	0.0000 ± 0.0000
R _A	Constant Skew Percentage Term (default=10)	0
R _B	Linear Skew Percentage Term (default=0)	0
BETA ₁	Constant Skewness Decay Constant term	1.876 ± 0.000
BETA ₂	Linear Skewness Decay Constant term	0
STEP	Step (percentage of peak-height in step function	0.0000 ± 0.0000
F	Full width half maximum constant term	3.00
G	Full width half maximum linear term	2.00
H	Full width half maximum quadratic term	0.00
P _i	Peak location (up to 15 peaks/fit)	Various

The approach used in this analysis, modeling the γ -ray pulse height spectrum using a series of "piece-wise" fits, differs from that used by Younes et al. to fit the entire $^{235}\text{U}(n,xn\gamma)$ γ -ray pulse height spectra simultaneously [You00]. However, the results, in the form of the γ -ray peak areas, are nearly identical. This can be seen in Table 4 which shows the areas obtained for the peaks in the region near the ^{238}Pu $6 \rightarrow 4$ transition obtained using both GF2 and XGAM. The decision was made to use the GF2 package instead of the XGAM package after a comparison was made to the γ -ray pulse height spectra fit using both methods. As the size of the region of the γ -ray spectrum used to fix the background was increased in XGAM the sensitivity of the fit to the choice of the background parameters increased as well. The smaller peak-to-background ratio found in the ^{239}Pu data as compared to the ^{235}U data results in a far greater sensitivity to the choice of background parameters, necessitating the use of local, rather than global fits. The choice was then made to use GF2 rather than XGAM due to the presence of a more readily accessible user interface and the prior establishment of the best fitting parameters in the 1998 data sets.

Table 4: Peak areas obtained from a local fit with the same limits using the GF2 program from [Rad98] and the XGAM program from [You00]. The peak areas in GF2 are fixed while those in XGAM are free to vary. Note that every peak in the GF2 fit falls within the stated uncertainty of a corresponding XGAM peak.

Peak Number	GF2		XGAM	
	Location	Area	Location	Area
1	1224.681	1610(343)	1224.63(1.79)	1131(451)
2	1232.954	7649(331)	1231.82(1.50)	6823(1283)
3	1238.297	4827(383)	1236.06(1.37)	6494(1470)
4	1242.678	9769(400)	1242.72(0.40)	11069(1103)
5	1248.736	5020(350)	1249.89(1.75)	4646(2755)
6	1253.876	18978(425)	1254.03(0.49)	18457(2706)
7	1262.559	65419(618)	1263.04(0.06)	66666(1606)
8	1268.966	10187(431)	1269.50(0.41)	10151(1020)
9	1274.083	-93(344)	1280.2954(3E+72)	0(0)
10	1279.358	2311(314)	1280.61(1.59)	2868(916)
11	1285.690	4870(302)	1286.70(1.02)	4950 (762)
12	1293.668	1905(355)	1294.93(0.97)	2172(376)
13	1307.700	905(399)	1308.85(0.79)	1448(326)
14	1316.829	-553(394)	1315.12(3E+38)	0(0)

Once the local fits were established the $E_n=1-25$ MeV pulse height spectrum was then sub-divided into a series of γ -ray pulse height spectra corresponding to adjacent 20 ns wide time-of-flight bins. The average and uncertainty in the neutron energy for each of these spectra was calculated from the detector timing response as determined from the width of the γ -flash following the impact of the proton beam on the spallation target source [You99]. These neutron-energy-gated spectra were then fit using the parameters derived from the 1-25 MeV pulse height spectrum where all of the parameters other than the peak heights and the background (which was limited to a quadratic in γ -ray energy)

were fixed. Examples of these fits are presented in Figures 3a-c. The peak area from these fits is referred to as the γ -ray yield.

The main source of background in the data was due to target activity and was therefore independent of the TOF. In order to gain an understanding of this portion of the pulse height γ -ray background, a “TOF-random” flat baseline spectrum was subtracted from each of the pulse height spectra and the γ -ray fitting procedure repeated. The effect of this type of background subtraction on (n,2n) and (n,3n) transitions is minor. This can be seen in figure 4a,b for the $6 \rightarrow 4$ transition in ^{238}Pu . Although the two pulse height spectra differ considerably in appearance the resulting yield curves are identical within the resolution of the measurement. However, the background subtraction does have a major effect on (n,n'γ) transitions resulting from levels in ^{239}Pu with an excitation energy less than $E_x \approx 600$ keV. These levels can be populated by two or more previous beam bursts due to beam “wrap-around”. Although, the flat baseline subtraction is still not equivalent to “non-wrapped” data, it is the best technique available for these data sets. A longer micropulse spacing is required to eliminate any ambiguity in the γ -ray yield for any transitions originating from a level with $E_x < 600$ keV (a 1.8 μs time-of-flight). Nonetheless, a flat baseline subtraction is in this report for the (n,n'γ) partial cross sections since it is likely to approximate the background due to wrap-around.

In order to obtain the absolute partial γ -ray cross sections it is necessary to divide the γ -ray yield by the corresponding neutron fluence. The neutron fluence was determined from the $^{235}\text{U}/^{238}\text{U}$ fission chamber data using the same procedure as described in [You00,Wen93]. An error in either the electronics caused some uncertainty in the ^{238}U fission chamber data from the 1998 data sets. Therefore, the ^{235}U fission chamber was exclusively used throughout in order to insure consistency between the analysis of the three data sets. A two-dimensional array of the fission chamber pulse height versus the time-of-flight relative to the beam bursts was formed. Figure 5a,b shows the pulse height and the fission-gated TOF spectrum from this array for the ^{235}U fission chamber in the 1999 data set. A gate was applied in the pulse-height direction corresponding to neutron-induced fission events (as opposed to α -decay from the actinide foils). The resulting TOF spectrum was used to determine the neutron flux. Figure 6 shows the neutron fluences for both fission chambers from the 1999 data. The results for the 1999 data can be compared to the recently evaluated value for the ^{54}Fe 847 keV $2 \rightarrow 0$ partial γ -ray cross section [Sim98]. Although there is a difference between the evaluated value and the extrapolated measurement at an incident neutron energy of 14 MeV, the difference is well within the 1σ confidence limit.

The final step in the analysis is to correct for a number of effects including, target attenuation, array efficiency, internal conversion of the γ -ray transitions, the number of target atoms in the neutron beam and the angular distribution of the γ -rays observed. The product of the first two of these factors were determined using a combination of γ -ray source measurements and monte carlo modeling of the GEANIE spectrometer by McNabb *et al.*, [McN00]. Internal conversion is the process by which a nuclear transition occurs via the emission of an inner shell electron with a kinetic energy equal to the transition energy less than the atomic binding energy. The magnitude of this process is well modeled and understood and the values used were obtained using the HSICC code from the National Nuclear Data Center at Brookhaven National Laboratory [ENS00]. The number of target atoms in the neutron beam was determined from a set of thickness measurements performed at Los Alamos. The absolute partial γ -ray cross sections for an incident neutron energy, i , were then deduced using the relation:

$$\sigma^{(i)} = (1 + \alpha_{\gamma}) \frac{I_{\gamma}^{(i)} LT_{FC} f_{\gamma}(\theta)}{N \epsilon_{\gamma} \Phi^{(i)} LT_{ADC}}$$

Where σ is the cross section, α_{γ} is the conversion coefficient which depends on the γ -ray energy and multipolarity, I_{γ} is the number of counts in a γ -ray peak, Φ is the number of neutrons incident on the targets, N is the number of atoms in exposed to the neutron beam (which is determined by the target thickness (in barns/atom) and the inclination angle of the target normal with respect to the beam ($\theta=19^{\circ}$)), ϵ_{γ} is the efficiency for detecting the transition (including attenuation in the target), LT is the live-time for the fission chamber or the ADCs and $f_{\gamma}(\theta)$ is the angular distribution correction factor (see below). The live-times for detection of the neutrons and the γ -rays were determined using scalars gated by the beam macropulse.

Table 5 below shows the live-times and efficiencies for the ground state band transitions in ^{238}Pu , number of target atoms, and ratio of fission chamber to ADC live-times for the three runs.

Run	Efficiencies @ E_{γ} (keV)			Target Thickness (barns/atom)	Live-time Ratio (γ -ray/FC)
	102	158	210		
Thick Target 1998	0.019201	0.011571	0.012600	1.958(34) x 10^{-3}	0.890769
Thin Target 1998	0.026026	0.016837	0.015710	1.070(37) x 10^{-3}	0.684486
Thin Target 1999	0.026026	0.016837	0.015710	1.070(37) x 10^{-3}	0.853771

The derivation of the array efficiency and target attenuation effects is described in [McN00]. Additional confidence in the efficiency measurement and the entire procedure is provided by the γ -ray partial cross section from the ^{57}Fe foils used during the 1999 run. Figure 7 shows the extracted cross sections for both fission chambers. Table 7 at the end of the report shows the extracted partial cross section for the 847 keV transition for both fission chamber foils. The agreement between the data and the evaluated value [END00] is quite good. The efficiency-corrected excitation functions were then multiplied by the ratio of live-time for the Ge detectors over live-time for the fission chamber. Table 8 at the end of this report presents the total number of counts, extracted number of neutrons and the 1/barns factor (defined as $N\Phi\epsilon_{\gamma}$) for the ^{235}U fission chamber for the three data sets.

One factor still needs to be taken into consideration to extract the cross section; the angular distribution of the γ -rays. The γ -rays are emitted from the residual nucleus at specific angles with respect to the direction of the incoming neutrons resulting in an angle and incoming neutron energy dependent variation in the γ -ray intensity. The data exhibits this variation. Figure 8a-b shows the intensity of the $6 \rightarrow 4$ transition in the ground state band of ^{238}Pu for the 11 planar detectors normalized in two different ways; with respect to the efficiency and live-times of the detectors, and b) the intensity of a 161.3 keV background contaminant associated with the radioactive decay of the target material. The agreement in the relative magnitude for the different detectors helps to build confidence in the efficiency measurements [McN00]. Figures 8c-d show the averages of the detectors at each of the four angles with respect to the beam, as well as a least-squares fit for the angular distribution of the γ -rays.

This physical process governing the γ -ray angular distribution are well understood and can be modeled from first principles. The predicted angular distribution shown in figure

8c-d for the $6 \rightarrow 4$ transition is consistent with the best fit of the observed angular distribution. This angular distribution can then be used to obtain a correction factor to convert the γ -ray yields at the measured angles to the average cross section over all incoming angles. Table 6a below shows the detector angles for the planar detectors for the three data sets.

Table 6a: Angles with respect to the incident neutron beam and types (planar or coaxial) for the Compton suppressed GEANIE detectors.

Detector #	Type	Angle with respect to beam (degrees)
1	Planar	141.07
2	Planar	141.82
3	Planar	143.62
4	Planar	144.13
5	Coaxial	129.50
6	Coaxial	100.48
7	Coaxial	100.91
8	Coaxial	78.50
9	Planar	58.24
10	Planar	58.65
11	Planar	26.50
12	Planar	29.02
13	Planar	29.02
14	Planar	25.20
15	Coaxial	56.69
16	Coaxial	56.60
17	Coaxial	76.90
18	Coaxial	100.22
19	Coaxial	100.48
20	Planar	128.00

The cross sections from the three data sets were found to be in good agreement. This can be seen in Figure 9a which shows the partial cross section for the yrast ^{238}Pu $6^+ \rightarrow 4^+$ transition from all three data sets. Nonetheless, there are some significant differences between the results from the three experiments. The most striking of these differences is between the 1999 and the two 1998 data sets for $E_n=7\text{-}12$ MeV. In this energy range the 1999 data is significantly lower than either of the 1998 data sets. The main difference between the two runs is the 1999 neutron flux, which was considerably higher. This results in a higher peak-to-background and therefore a difference in the peak-fitting result. This difference is somewhat indicative of the systematic uncertainties involved in analyzing the γ -ray data. In order to minimize this systematic uncertainty the time-of-flight gated pulse height spectra from the two 1998 data sets (thick and thin target) were gain-shifted to match the 1999 thin target data and then the three added together to form a single set of spectra. A combination known ^{239}Pu radioactivity lines and X-rays [MIR00], and the ^{54}Fe $2 \rightarrow 0$ transition in the case of the 1999 target data, were used as references for the energy calibration. The resulting sum spectra had improved statistics, thereby minimizing the uncertainty associated with the fitting procedure. Figure 9b shows the resulting cross section for the ^{238}Pu $6^+ \rightarrow 4^+$ γ -ray. The γ -ray energy calibration is shown in Figure 10. The addition of the three data sets and the propagation of errors through the procedure was done using the following expression:

$$I_\gamma^{total} = \sum_{\text{data sets}} I_\gamma = \frac{\sigma}{1 + \alpha_\gamma} \sum_{\text{data sets}} \Phi N \epsilon_\gamma \frac{LT_{ADC}}{LT_{FC}}$$

Solving for cross section yields:

$$\sigma = \frac{(1 + \alpha_\gamma) I_\gamma^{total}}{\sum_{\text{data sets}} \Phi N \epsilon_\gamma \frac{LT_{ADC}}{LT_{FC}}}$$

For a single data set the errors would be propagated using the following formula:

$$\left(\frac{\delta\sigma}{\sigma}\right)^2 = \left(\frac{\Delta I_\gamma}{I_\gamma}\right)^2 + \left(\frac{\Delta\Phi}{\Phi}\right)^2 + \left(\frac{\Delta N_{thin}}{N_{thin}}\right)^2 + \left(\frac{\Delta N_{thick}}{N_{thick}}\right)^2 + \left(\frac{\Delta\epsilon_\gamma}{\epsilon_\gamma}\right)^2$$

However, the propagation of the errors through the addition of the three data sets results necessitates the use of a different procedure. First, the statistical errors from the γ -ray counts and the neutron-flux monitor are added for each of the three data sets (i):

$$\left(\frac{\Delta\sigma_{statistical}^{(i)}}{\sigma_{statistical}^{(i)}}\right)^2 = \left(\frac{\Delta I_\gamma^{(i)}}{I_\gamma^{(i)}}\right)^2 + \left(\frac{\Delta\Phi_n^{(i)}}{\Phi_n^{(i)}}\right)^2$$

These errors are then combined with the uncertainty for the efficiency and the total number of target atoms. These uncertainties are only added for the 1998 thin target and thick target data. They are not added to the 1999 thin target data since this would amount to "double counting" the errors.

$$\left(\frac{\Delta\sigma^{(98-thin)}}{\sigma^{(98-thin)}}\right)^2 = \left(\frac{\Delta\sigma_{statistical}^{(98-thin)}}{\sigma_{statistical}^{(98-thin)}}\right)^2 + \left(\frac{\Delta N_{thin}}{N_{thin}}\right)^2 + \left(\frac{\Delta\epsilon_{thick}^\gamma}{\epsilon_{thick}^\gamma}\right)^2$$

$$\left(\frac{\Delta\sigma^{(98-thick)}}{\sigma^{(98-thick)}}\right)^2 = \left(\frac{\Delta\sigma_{statistical}^{(98-thick)}}{\sigma_{statistical}^{(98-thick)}}\right)^2 + \left(\frac{\Delta N_{thick}}{N_{thick}}\right)^2 + \left(\frac{\Delta\varepsilon_{thick}^\gamma}{\varepsilon_{thick}^\gamma}\right)^2$$

Finally, all three errors are added using the summation formula to yield the error on the summed data:

$$(\Delta\sigma^{(sum)})^2 = (\Delta\sigma^{(98-thick)})^2 + (\Delta\sigma^{(98-thin)})^2 + (\Delta\sigma^{(99-thin)})^2$$

A total of 13 transitions in $^{237-239}\text{Pu}$ were observed in the summed data sets. Figures 11-17 display the partial γ -ray cross sections obtained from the summed 1998 and 1999 data together with the predictions of the two models (where they are available) for transitions in $^{237-9}\text{Pu}$. The measured values are presented at the end of this report in tables 9-21. The total uncertainty in the γ -ray cross section as well as the uncertainty due to the γ -ray statistics and the fitting procedure are tabulated in the last two columns of these tables. It should be noted that, with the exception of the strongest transitions, almost the entire error arises from the γ -ray statistics and fitting procedure. The statistical component of this error can be assumed to follow Poisson statistics. A comparison between the number of counts in the γ -ray peaks and the uncertainty in the cross section due to the γ -ray statistics and the fitting procedure indicates that the vast majority of the uncertainty in the cross sections arises from the γ -ray fitting procedure. This can be attributed to the large background and the presence of strong contaminant γ -rays in the γ -ray pulse height spectra.

Tables 7a,b below lists the transitions, the conversion coefficients and target-array γ -ray efficiency used to obtain the partial transition cross sections, and their peak cross section. In addition, table 7b lists the average cross section value below the neutron energy threshold as an apparent "offset" due to systematic uncertainties in the peak-fitting procedure for weak transitions described above. Assignments were made based on a combination of γ -ray energy and the threshold neutron energy. Conversion coefficient and multipolarity assignments (as well as mixing ratios, when appropriate) for all of the transitions were taken from ENSDF [ENS00]. Tables 8a-g shows the angular distribution correction factors applied to the summed 98+99 data for the transitions in $^{237-9}\text{Pu}$.

Tables 7a: γ -ray transitions in $^{237-239}\text{Pu}$ for which partial cross sections were measured in the summed data.

Number	Mass	Parent Level		Final Level		E_γ (keV)	Observed/ Comments
		J^π	E_x (keV)	J^π	E_x (keV)		
1	238	6^+	303.4	4^+	145.96	157.4	Yes
2	238	8^+	513.4	6^+	303.4	210.0	Yes
3	238	4^-	1082.57	4^+	145.96	936.5	Yes
4	238	2^-	968.1	2^+	44.1	924.0*	Yes
5	238	1^-	962.77	2^+	44.1	918.7*	Yes-weak
6	238	1^-	962.77	0^+	0	962.8	Yes-weak
7	238	5^-	763.2	6^+	303.4	459.8	Yes
8(a)	238	$3/5^-$	661.4/763.2	$2^+/4^+$	145.96/44.1	617.3	Yes
9	239	$13/2^+$	318.1	$9/2^+$	163.76	154.3	Yes
10	239	$5/2^-$	511.84	$5/2^+$	285.46	226.4*	Yes
11	239	$5/2^+$	285.46	$5/2^+$	75.71	228.18	Yes
12	239	$5/2^+$	285.46	$3/2^+$	7.86	277.60	Yes
13	237	$7/2^+$	321.0	$9/2^-$	47.7	273.3	Yes

- (a) Two transitions in ^{238}Pu have γ -ray energies that are within the resolving power of the array. Therefore no information about their separate yields can be made using the data.

Table 7b: Conversion Coefficients, array-target efficiencies, peak cross sections, and apparent background offset (if any) for the transitions listed in table 7a above.

Peak #	E_γ (keV)	Conversion Coefficient	Thin target Efficiency (%)	Thick target Efficiency (%)	σ_{peak} (mb)	Offset (mb)
1	157.4	2.242	1.424(71)	0.972(53)	92.8(92)	0
2	210.0	0.6891	1.433(71)	1.139(57)	34.9(35)	0
3	936.5	<0.001	0.29(1)	0.29(1)	47.1(47)	0
4	924.0	<0.001	0.29(1)	0.28(1)	16.0(23)	0
5	918.7	<0.001	0.29(1)	0.28(1)	13.8(20)	5.5(26)
6	962.8	<0.001	0.29(1)	0.26(1)	15.0(40)	1.1(5)
7	459.8	0.0171	0.624(30)	0.624(29)	12.3(16)	2.9(11)
8	617.3	0.0097	0.440(21)	0.426(21)	34.8(40)	13.6(63)
9	154.3	2.352	1.409(71)	0.952(52)	47.8(59)	0
10	226.4	0.0779	1.371(62)	1.126(54)	12.4(16)	0
11	228.18	2.734	1.365(62)	1.124(54)	197.5(16)	0
12	277.60	1.548	1.145(54)	1.005(47)	155.6(13)	0
13	273.3	0.2925	1.166(53)	1.019(47)	24.6(26)	0

Table 8a: Angular distribution correction factors for the $E_{\gamma}=157.4$ keV $6 \rightarrow 4$ and the $E_{\gamma}=210.0$ keV $8 \rightarrow 6$ transitions in ^{328}Pu .

E_n (MeV)	δE_n (MeV)	98-thin $6 \rightarrow 4$	98-thick $6 \rightarrow 4$	99-thin $6 \rightarrow 4$	98-thin $8 \rightarrow 6$	98-thick $8 \rightarrow 6$	99-thin $8 \rightarrow 6$
6.0640	0.1760	0.8627	0.8628	0.8602	0.8560	0.8559	0.8538
6.5000	0.1950	0.8666	0.8666	0.8641	0.8591	0.8590	0.8569
6.9690	0.2150	0.8707	0.8707	0.8682	0.8624	0.8623	0.8601
7.4980	0.2430	0.8689	0.8689	0.8664	0.8627	0.8627	0.8605
8.1050	0.2720	0.8696	0.8696	0.8671	0.8644	0.8644	0.8621
8.7730	0.3060	0.8875	0.8876	0.8850	0.8737	0.8736	0.8714
9.5200	0.3460	0.8994	0.8995	0.8970	0.8831	0.8830	0.8807
10.3920	0.3950	0.9057	0.9058	0.9033	0.8901	0.8900	0.8877
11.3730	0.4530	0.9085	0.9086	0.9062	0.8932	0.8931	0.8909
12.4990	0.5250	0.9089	0.9090	0.9066	0.8939	0.8938	0.8916
13.8240	0.6060	0.9086	0.9087	0.9063	0.8948	0.8947	0.8924
15.3590	0.7190	0.9227	0.9228	0.9206	0.9067	0.9066	0.9044
17.1830	0.8460	0.9353	0.9353	0.9334	0.9180	0.9180	0.9159
19.3360	1.0180	0.9388	0.9388	0.9370	0.9219	0.9218	0.9198

Table 8b: Angular distribution correction factors for the $E_{\gamma}=936.5$ keV $4^- \rightarrow 4^+$ and the $E_{\gamma}=924.0$ keV $2^- \rightarrow 2^+$ transitions in ^{238}Pu .

E_n (MeV)	δE_n (MeV)	98-thin $4^- \rightarrow 4^+$	98-thick $4^- \rightarrow 4^+$	99-thin $4^- \rightarrow 4^+$	98-thin $3^+ \rightarrow 4^+$	98-thick $3^+ \rightarrow 4^+$	99-thin $3^+ \rightarrow 4^+$
6.0640	0.1760	0.8832	0.8831	0.8794	1.0689	1.0690	1.0714
6.5000	0.1950	0.8878	0.8876	0.8841	1.0657	1.0658	1.0681
6.9690	0.2150	0.8927	0.8925	0.8891	1.0622	1.0623	1.0644
7.4980	0.2430	0.8978	0.8976	0.8944	1.0586	1.0587	1.0607
8.1050	0.2720	0.9019	0.9017	0.8985	1.0560	1.0561	1.0580
8.7730	0.3060	0.8965	0.8963	0.8931	1.0613	1.0614	1.0634
9.5200	0.3460	0.9151	0.9149	0.9122	1.0465	1.0466	1.0481
10.3920	0.3950	0.9362	0.9361	0.9340	1.0302	1.0302	1.0313
11.3730	0.4530	0.9399	0.9398	0.9378	1.0289	1.0289	1.0299
12.4990	0.5250	0.9372	0.9371	0.9350	1.0312	1.0312	1.0323
13.8240	0.6060	0.9351	0.9350	0.9328	1.0334	1.0335	1.0346
15.3590	0.7190	0.9485	0.9484	0.9467	1.0250	1.0250	1.0259
17.1830	0.8460	0.9598	0.9597	0.9583	1.0182	1.0182	1.0188
19.3360	1.0180	0.9621	0.9621	0.9608	1.0169	1.0169	1.0175

Table 8c: Angular distribution correction factors for the $E_{\gamma}=918.7$ keV $1^- \rightarrow 2^+$ and the $E_{\gamma}=962.8$ keV $1^- \rightarrow 0^+$ transitions in ^{238}Pu .

E_n (MeV)	δE_n (MeV)	98-thin $1^- \rightarrow 2^+$	98-thick $1^- \rightarrow 2^+$	99-thin $1^- \rightarrow 2^+$	98-thin $1^- \rightarrow 0^+$	98-thin $1^- \rightarrow 0^+$	99-thin $1^- \rightarrow 0^+$
6.0640	0.1760	1.0021	1.0021	1.0021	1.0208	1.0208	1.0215
6.5000	0.1950	1.0020	1.0020	1.0020	1.0198	1.0198	1.0205
6.9690	0.2150	1.0018	1.0018	1.0019	1.0187	1.0187	1.0194
7.4980	0.2430	1.0017	1.0017	1.0018	1.0175	1.0175	1.0182
8.1050	0.2720	1.0016	1.0016	1.0017	1.0167	1.0167	1.0173
8.7730	0.3060	1.0018	1.0018	1.0019	1.0183	1.0183	1.0190
9.5200	0.3460	1.0014	1.0014	1.0014	1.0135	1.0136	1.0141
10.3920	0.3950	1.0009	1.0009	1.0009	1.0084	1.0085	1.0088
11.3730	0.4530	1.0008	1.0008	1.0008	1.0081	1.0081	1.0084
12.4990	0.5250	1.0008	1.0008	1.0009	1.0088	1.0088	1.0091
13.8240	0.6060	1.0009	1.0009	1.0010	1.0095	1.0095	1.0098
15.3590	0.7190	1.0007	1.0007	1.0007	1.0069	1.0069	1.0071
17.1830	0.8460	1.0005	1.0005	1.0005	1.0046	1.0046	1.0048
19.3360	1.0180	1.0004	1.0004	1.0004	1.0043	1.0043	1.0045

Table 8d: Angular distribution correction factors for the $E_{\gamma}=459.8$ keV $5^- \rightarrow 6^+$ and the $E_{\gamma}=617.3$ keV $5^- \rightarrow 4^+$ transitions in $^{238}\text{Pu}^*$.

E_n (MeV)	δE_n (MeV)	98-thin $5^- \rightarrow 6^+$	98-thick $5^- \rightarrow 6^+$	99-thin $5^- \rightarrow 6^+$	98-thin $5^- \rightarrow 4^+$	98-thick $5^- \rightarrow 4^+$	99-thin $5^- \rightarrow 4^+$
6.0640	0.1760	1.0579	1.0578	1.0601	1.1045	1.1049	1.1088
6.5000	0.1950	1.0561	1.0560	1.0582	1.1011	1.1015	1.1053
6.9690	0.2150	1.0541	1.0540	1.0561	1.0974	1.0978	1.1015
7.4980	0.2430	1.0520	1.0520	1.0540	1.0936	1.0939	1.0974
8.1050	0.2720	1.0502	1.0502	1.0521	1.0903	1.0906	1.0939
8.7730	0.3060	1.0515	1.0514	1.0534	1.0925	1.0929	1.0963
9.5200	0.3460	1.0445	1.0445	1.0462	1.0797	1.0800	1.0829
10.3920	0.3950	1.0368	1.0368	1.0382	1.0656	1.0658	1.0682
11.3730	0.4530	1.0350	1.0350	1.0363	1.0622	1.0624	1.0647
12.4990	0.5250	1.0354	1.0354	1.0367	1.0630	1.0632	1.0654
13.8240	0.6060	1.0359	1.0359	1.0372	1.0638	1.0640	1.0662
15.3590	0.7190	1.0289	1.0289	1.0300	1.0512	1.0514	1.0532
17.1830	0.8460	1.0232	1.0232	1.0241	1.0409	1.0410	1.0424
19.3360	1.0180	1.0218	1.0218	1.0226	1.0385	1.0386	1.0399

* This γ -ray is a doublet with the $3^- \rightarrow 2^+$ transition in ^{238}Pu . The angular distribution correction factor shown is only for the $5^- \rightarrow 4^+$ transition since the data supports this assignment alone (see section IIIb.) below

Table 8e: Angular distribution correction factors for the $E_{\gamma}=154.3$ keV $13/2^+ \rightarrow 9/2^+$ and the $E_{\gamma}=226.4$ keV $5/2^- \rightarrow 5/2^+$ transitions in ^{238}Pu .

E_n (MeV)	δE_n (MeV)	98-thin $13/2^+ \rightarrow 9/2^+$	98-thick $13/2^+ \rightarrow 9/2^+$	99-thin $13/2^+ \rightarrow 9/2^+$	98-thin $5/2^- \rightarrow 5/2^+$	98-thin $5/2^- \rightarrow 5/2^+$	99-thin $5/2^- \rightarrow 5/2^+$
6.0640	0.1760	1.0040	1.0040	1.0041	1.0090	1.0090	1.0093
6.5000	0.1950	1.0041	1.0041	1.0042	1.0091	1.0091	1.0093
6.9690	0.2150	1.0041	1.0041	1.0042	1.0091	1.0091	1.0094
7.4980	0.2430	1.0042	1.0042	1.0043	1.0092	1.0092	1.0095
8.1050	0.2720	1.0043	1.0043	1.0044	1.0094	1.0094	1.0097
8.7730	0.3060	1.0042	1.0042	1.0044	1.0094	1.0094	1.0097
9.5200	0.3460	1.0042	1.0042	1.0043	1.0093	1.0093	1.0096
10.3920	0.3950	1.0042	1.0042	1.0043	1.0091	1.0091	1.0094
11.3730	0.4530	1.0039	1.0039	1.0040	1.0087	1.0087	1.0089
12.4990	0.5250	1.0035	1.0035	1.0036	1.0078	1.0078	1.0080
13.8240	0.6060	1.0032	1.0032	1.0033	1.0072	1.0072	1.0075
15.3590	0.7190	1.0031	1.0031	1.0032	1.0070	1.0070	1.0073
17.1830	0.8460	1.0031	1.0031	1.0032	1.0070	1.0070	1.0072
19.3360	1.0180	1.0033	1.0033	1.0034	1.0074	1.0074	1.0077

Table 8f: Angular distribution correction factors for the $E_{\gamma}=228.2$ keV $5/2^+ \rightarrow 5/2^+$ and the $E_{\gamma}=277.6$ keV $5/2^+ \rightarrow 3/2^+$ transitions in ^{238}Pu .

E_n (MeV)	δE_n (MeV)	98-thin $5/2^+ \rightarrow 5/2^+$	98-thick $5/2^+ \rightarrow 5/2^+$	99-thin $5/2^+ \rightarrow 5/2^+$	98-thin $5/2^+ \rightarrow 3/2^+$	98-thick $5/2^+ \rightarrow 3/2^+$	99-thin $5/2^+ \rightarrow 3/2^+$
6.0640	0.1760	0.9701	0.97	0.969	1.0040	1.0040	1.0041
6.5000	0.1950	0.9698	0.9697	0.9687	1.0041	1.0041	1.0042
6.9690	0.2150	0.9694	0.9693	0.9683	1.0041	1.0041	1.0042
7.4980	0.2430	0.9687	0.9687	0.9676	1.0042	1.0042	1.0043
8.1050	0.2720	0.968	0.968	0.9669	1.0043	1.0043	1.0044
8.7730	0.3060	0.9682	0.9681	0.9671	1.0042	1.0042	1.0044
9.5200	0.3460	0.9685	0.9685	0.9675	1.0042	1.0042	1.0043
10.3920	0.3950	0.969	0.969	0.968	1.0042	1.0042	1.0043
11.3730	0.4530	0.9706	0.9705	0.9696	1.0039	1.0039	1.0040
12.4990	0.5250	0.9737	0.9737	0.9729	1.0035	1.0035	1.0036
13.8240	0.6060	0.9756	0.9756	0.9748	1.0032	1.0032	1.0033
15.3590	0.7190	0.9763	0.9762	0.9755	1.0031	1.0031	1.0032
17.1830	0.8460	0.9763	0.9762	0.9755	1.0031	1.0031	1.0032
19.3360	1.0180	0.9748	0.9748	0.974	1.0033	1.0033	1.0034

Table 8g: Angular distribution correction factors for the $E_{\gamma}=273.3$ keV $7/2^+ \rightarrow 7/2^-$ transition in ^{237}Pu .

E_n (MeV)	δE_n (MeV)	98-thin $7/2^+ \rightarrow 7/2^-$	98-thick $7/2^+ \rightarrow 7/2^-$	99-thin $7/2^+ \rightarrow 7/2^-$
12.4990	0.5250	1.0294	1.0294	1.0304
13.8240	0.6060	1.0190	1.0191	1.0197
15.3590	0.7190	1.0172	1.0173	1.0178
17.1830	0.8460	1.0147	1.0148	1.0153
19.3360	1.0180	1.0074	1.0074	1.0077

IIIb.) Level Spectroscopy in $^{238-9}\text{Pu}$

In this section the assignment and cross sections as a function of incident neutron energy of the γ -rays observed in ^{238}Pu and ^{239}Pu following the (n,2n) and (n,3n) reactions will be discussed in light of the known level schemes for these nuclei [ENS00]. Only a single transition in ^{237}Pu following (n,3n γ) was observed in the planar detectors, thereby limiting discussion.

Figure 18 shows a portion of the low-lying level scheme of ^{238}Pu from [ENS00]. Although numerous transitions were observed in the current work, several were not. The two ground state band transitions that were observed, the $8 \rightarrow 6$ and $6 \rightarrow 4$ γ -rays, are presented in figure 11a,b. However the two lowest transitions in the ground state band, the $2^+ \rightarrow 0^+$ and $4^+ \rightarrow 2^+$, were not observed. The lack of observation of the ground state band $2^+ \rightarrow 0^+$ transition is attributable to a number of factors. These include attenuation of the γ -ray in the target, poor low-energy γ -ray efficiency (which is in turn due in part to the use of 0.010" Molybdenum absorbers in front of the γ -ray detectors), and internal conversion of the γ -ray into an electron and an atomic X-ray. The net effect is to decrease the intensity of the $2^+ \rightarrow 0^+$ transition relative to the observed $6^+ \rightarrow 4^+$ transition by more than a factor of 1000.

The same factors are responsible for the lack of observation of the ground state band $4^+ \rightarrow 2^+$ transition, but to a lesser degree. However, the observation of this transition is much more greatly hindered by the large γ -ray background due to the presence of the Plutonium and Uranium K-shell X-rays. These transitions are by far the strongest lines in the entire γ -ray spectrum. Figure 19 (bottom) shows the γ -ray pulse height spectrum observed in the planar detectors at an energy where the (n,2n) reaction channel is near peak (11.373 ± 0.453 MeV). This same spectrum is shown expanded around the X-ray region in figure 19 (top). The location of the $4^+ \rightarrow 2^+$ ground state band transition is shown (E _{γ} =102 keV). A simple argument can be used to show why the $4^+ \rightarrow 2^+$ transition is not visible in the data. Assuming that the $4^+ \rightarrow 2^+$ γ -ray has approximately the same cross section at peak as the $6^+ \rightarrow 4^+$ γ -ray, then the number of counts expected in the $4^+ \rightarrow 2^+$ peak is given by the expression:

$$\frac{\text{Counts}(4 \rightarrow 2)}{\text{Counts}(6 \rightarrow 4)} = \frac{(1 + \alpha_{6 \rightarrow 4})}{(1 + \alpha_{4 \rightarrow 2})} \times \frac{\varepsilon_{4 \rightarrow 2}}{\varepsilon_{6 \rightarrow 4}}$$

Inserting efficiencies from [McN00] and conversion coefficients from [ENS00] we obtain a ratio of counts of approximately 6.5. The $6 \rightarrow 4$ peak area at E_n = 11.373 ± 0.453 MeV is 7662 ± 330 . Therefore, the predicted number of counts in the $4 \rightarrow 2$ peak would be 1179 ± 51 . This corresponds to a peak height of approximately 150 counts. The height of the 11.373 MeV spectrum at the energy of the $4 \rightarrow 2$ transition is 18828 counts, corresponding to an uncertainty due to counting (Poisson) statistics of $(18828)^{1/2} = 137$ counts. This implies that the peak height for the $2 \rightarrow 0$ transition would be approximately equal to the Poisson background fluctuations due to the X-ray contaminants at this γ -ray energy. The situation is further complicated by the presence of one or more fission contaminants with the same γ -ray energy. Therefore, it was impossible to unambiguously identify the $4 \rightarrow 2$ transition in the ground state band in the data.

In contrast, the non-ground state band transitions are often considerably more amenable to analysis. The majority of the transitions connecting these side-bands to the ground state band are higher in γ -ray energy, thereby making them less susceptible to target attenuation and internal conversion. Furthermore, since these γ -rays are higher in energy the background due to Compton scattering of target activity γ -rays and beam-related sources (i.e., fission etc.) is lower. The result is that the majority of the transitions seen in ^{238}Pu come from these states. However, the limited amount of information available regarding the spectrum of these excited side-bands in ^{238}Pu introduces some ambiguity in the assignment of any specific transition.

The strongest of these transitions has been identified as the $E_\gamma=936.6$ keV ($E_x = 1083$ keV) $4^- \rightarrow 4^+$ ground state band transition. The cross section as a function of incident neutron energy for this transition is shown in figure 12a. This transition is the second strongest transition in the data, surpassing even the $8^+ \rightarrow 6^+$ ground state band transition. The assignment of this transition is based on a combination of the γ -ray energy and the threshold behavior of the partial cross section. Furthermore, the $E_\gamma=119.9$ keV γ -ray populating the 1083 keV level from the 3^- level at $E_x=1202.7$ keV, is seen in the a time-of-flight random background subtracted spectrum, further supporting the assignment of the $E_\gamma=936.6$ keV γ -ray to the $4^- \rightarrow 4^+$ transition. The most likely explanation for the large intensity of this γ -ray is the conservation of aligned angular momentum, referred to as K, in a deformed nucleus like ^{238}Pu . This state contains the largest K, 4 units, of any low-lying transition in ^{238}Pu , thereby rendering it a “K-collector” transition for the nucleus. This phenomenon is clearly seen in neutron-induced reactions on deformed rare earth nuclei [Yat00].

Transitions from three other side-bands are evident in the data; the 1^- band with a band-head energy of $E_x=962.8$ keV, the 2^- band with a band-head at $E_x=968.1$ keV, and the 1^- “Octupole” band with a band-head energy of $E_x=605.2$ keV. Assignments were made from a combination of their excitation energy and the threshold and peak location of their cross section as a function of incident neutron energy. All three of these bands decay into the ground state band through numerous paths. However, only a few of the transitions are unambiguously identifiable in our data. We will address each one of them here.

The 1^- band at $E_x=962.8$ keV decays primarily into the ground state band through two transitions; a $E_\gamma=962.8$ keV E1 transition directly to the ground state, and a $E_\gamma=918.7$ keV E1 into the 2^+ member of the ground state band [ENS00]. The cross section as a function of neutron energy for these two lines are presented in figures 13a-b. Both transitions are very weak. The $E_\gamma=918.7$ keV $1^- \rightarrow 2^+$ transition appears to have a slight offset in its baseline which can be attributed to the difficulty involved in obtaining a good background fit for such a weak γ -ray. The relative intensities of the $E_\gamma=962.8$ and $E_\gamma=918.7$ keV γ -rays are, within error, similar to what is reported in ENSDF (100 and 84 respectively).

The 2^- band with a band-head energy of $E_x=968.1$ decays consists of only one level and decays to the ground state band through the single transition $2^- \rightarrow 2_{g.s.}^+$ with $E_\gamma=924.0$ keV. Other possible assignments for this γ -ray include the $3^+ \rightarrow 4^+$ transition from the $J^\pi = 2^+$ band with $E_x=1028$ keV. However, the non-observation of the stronger $3^+ \rightarrow 2^+$ transition in the coaxial detector data from the same state makes this assignment unlikely. The cross section as a function of incident neutron energy for this line is shown in figure 12b.

The final band populated was the 1^- band with a band-head energy of $E_\gamma=605$ keV. Three members of this band have been assigned by earlier work including the band-head, a 3^- state at $E_\xi=661.43$ keV and a 5^- state at $E_\xi=763.2$ keV. This spin-J members of the band decays into ground state band states with spin $J_{g.s.}=\pm 1$. Two of these transitions; the $3^- \rightarrow 2^+$ and the $5^- \rightarrow 4^+$ are degenerate with a γ -ray energy of $E_\gamma=617$ keV. The $E_\gamma=617$ keV “doublet”, together with the decay from the 5^- state into the ground state band, the $E_\gamma=459.8$ keV $5^- \rightarrow 6^+$ are observed in our data and are shown in figures 14 a-b. However, the other decay from the 3^- level, the $3^- \rightarrow 4^+$ has not been observed. Taken together, this indicates that the majority of the $E_\gamma=617$ keV γ -ray intensity is likely to have come from the 5^- rather than the 3^- level.

The data in ^{239}Pu is far more limited. Although 4 γ -rays have been definitely assigned, all of them come from excited states in ^{239}Pu which are subject to “wrap-around” in the neutron spectrum. The cross sections for these lines are shown in figures 15 and 16. The wrap-around is caused by the beam time structure which is comprised of pulses every 1.8 μs (see experiment section above). The repetition of the beam causes low-energy neutrons from the N^{th} beam pulse to arrive at the target location at the same time with respect to the beam as the $N+1^{\text{th}}$ beam pulse. This produces

an uncertainty in the energy assignment of the neutron flux for low ($E_n < 600$ keV) energy neutrons. This in turn effect the population of the lowest-lying states in ^{239}Pu with excitation energies less than the wrap-around threshold of approximately 600 keV. All 4 γ -rays observed in ^{239}Pu arise from levels below this incident neutron energy.

Furthermore, the two transitions coming from the $E_\xi=285.46$ keV level have an additional ambiguity in the interpretation of their partial cross sections as a function of incident neutron energy. The $E_\xi=285.36$ keV level is populated from a number of discrete states. One of these states is a $7/2^-$ isomer state at $E_\xi=330.125$ keV with a lifetime of $T_{1/2}=193$ ns [ENS00]. The isomer causes a distortion in the TOF of any transition which arises from it. The net effect is to displace intensity from higher neutron energies (i.e., shorter time-of-flight) to lower neutron energies (higher time-of-flight). It is unclear how much of the population of the $E_\xi=285.46$ keV level comes through the isomer because the strongest transition from this state is a $E_\gamma=106.125$ keV γ -ray which is blocked due to contamination from Pu K-shell X-rays. (see figure 18). Therefore, the magnitude of the effect of the isomeric state on these transitions is unclear.

IV.) Comparison with Reaction Models

In this section we will compare the experimental results with the predictions of GNASH calculations performed by Chadwick [Cha99, Cha00]. A comparison between the model calculation and the $(n,n'\gamma)$ cross sections are complicated by the effects of "wrap-around" population of levels in ^{239}Pu with excitation energies less than ≈ 600 keV. Comparison between the model and the single $(n,3n\gamma)$ cross section measured is hampered by the lack of any other $(n,3n)$ lines in the data and the fact that GNASH calculations only exist for $E_n > 20$ MeV. Therefore, the discussion will center on the $(n,2n\gamma)$ partial cross sections.

Two sets of GNASH calculations were available to the authors at the time of this article's release. The first set is well described in [Cha99] and used a discrete level scheme from [ENS00]. More recently [Cha00], new calculations were run with an expanded discrete level scheme from W.E. Ormand and H. Chen that included levels "borrowed" from neighboring nuclei. In addition, the more recent calculations included a $\Delta\sigma_R \approx 130$ mb reduction in the total reaction cross section used.

In both cases the fission channel was adjusted to reproduce existing evaluated cross sections. The measured cross sections together with the results of the two sets of calculations, when available, are plotted in figures 11-17.

An important factor to note when comparing the model calculations to the data is that the absolute magnitude of the partial cross sections is uncertain due to the large error in the measured total reaction cross section. Changes in the optical model (the portion of the reaction model that calculates the total reaction cross section at a given incident neutron energy) on the order of $\pm 5\%$ are well within keeping of the total reaction measurements. This corresponds to a ± 150 mb change at $E_n = 14$ MeV. Therefore, the most reliable measure of the calculations is their behavior as a function of neutron energy (i.e., their "shape"), and not their magnitude.

Overall, the shape of the cross sections, particularly the two ground state band transitions is remarkably good. A separate indicator of the success of the model can be seen in the ratio of these individual transitions in the exit channel. These ratios are insensitive to the choice of the reaction cross section used. These ratios are an excellent measure of the portion of the model that calculates the cascade of γ -rays from the entry region down to the ground state. Figure 20a shows the ground state band $8 \rightarrow 6/6 \rightarrow 4$ ratio from the data as well as the two GNASH calculations. There is a marked improvement due to the use of the new level scheme. Figure 20b shows the ratio of the strongest side-band transition, the $4^- \rightarrow 4^+$, over the ground state band $6 \rightarrow 4$. Again, the new level scheme appears to improve the case for this side-band transition, although there is still a sizable discrepancy between the experimental results and the model calculations. As mentioned above, this might in part be attributable to conservation of K quantum number in a deformed nucleus. The effect of K is not considered in the generation of the γ -ray cascade by the model and therefore success here is not expected. A later work will comment on how to use the side-band γ -ray cross sections to lessen the discrepancy between the model and experiment.

In short, qualitative agreement between the model and experiment exists for the ground state band and the strongest side-band transitions.

V.) Conclusion

In conclusion, the GEANIE spectrometer at LANSCE/WNR was used to measure a total of 13 partial γ -ray cross section from the $^{239}\text{Pu}(n,x\gamma)^{240-x}\text{Pu}$ channels with $x=1-3$. The results reported here cover the incident neutron energy range from $E_n=1-20$ MeV. The partial cross sections were measured using the observation of discrete state γ -rays using high-resolution γ -rays spectroscopy. Neutron energies were determined using the time-of-flight technique. The majority (8) of the partial cross sections measured were from the $^{239}\text{Pu}(n,2n)^{238}\text{Pu}$ reaction channel. Uncertainties in the partial cross sections come from Poisson counting statistics as well as systematic sources.

Results from these measurements were compared the predictions the GNASH and IDA reaction models. Although the models and the shape of the measured values qualitatively agree, significant discrepancies exist which may in large part be attributable to the model treatment of the γ -ray cascade process within the final residual nucleus and the role of K quantum number conservation in the nucleus.

The authors would like to thank Mark Chadwick from Los Alamos and H. Chen, M. Alan Ross and W. Erich Ormand for offering invaluable insight into reaction modeling. We would also like to thank R. Bauer from LLNL for helping with the experiment and for crucial discussions regarding interpretation of the results. This work has been made possible through the U.S. Department of Energy Contract numbers W-7405-ENG-48 (LLNL) and W-4705-ENG-36 (LANL).

References

- [Bec98] J.A. Becker and R.O.Nelson, Nuclear Physics News Article (1998).
- [Lis90] P.W. Lisowski, C.D. Bowman, G.J. Russell and S.A. Wender, Nucl. Sci. Eng. 106, 208 (1990).
- [Wen93] S.A. Wender et al., Nucl. Instrum. and Meth. A336 2 (1993).
- [Ber98] L.A. Bernstein et al., Phys. Rev. C57, R2799 (1998).
- [Mai94] M. Maier, M. Robertson, A. Vander Molen, and G.D. Westfall, Nucl. Instrum. and Meth. A337 619 (1994)
- [ENS00] Evaluated Nuclear Structure Data Files. Brookhaven National Laboratory, Upton, N.Y. (2000).
- [Ros99] M. Alan Ross, H. Chen, G. Reffo, and R.M. White, The $^{239}\text{Pu}(n,2n)^{238}\text{Pu}$ Cross Section: Preliminary Calculations. UCRL-ID-133497.
- [END00] Evaluated Nuclear Data Library, Brookhaven National Laboratory, Upton, N.Y. (2000).
- [Sim98] S.P. Simakov, A. Pavlik, H. Vonach and S. Hlavac. IAEA Nuclear Data Section IDC(CCP)-413 (1998).
- [MIR00] Measured Intensity Radiation Dose Library. National Nuclear Data Center, Upton, NY (2000).
- [Cha99] M.B. Chadwick and P.G. Young, Calculated Plutonium reactions for determining $^{239}\text{Pu}(n,2n)^{238}\text{Pu}$. LA-UR-99-2885 (1999).
- [Cha00] M.B. Chadwick. Private communications (1985).
- [McN00] D.P. McNabb, Uncertainty Budget and efficiency analysis for the $^{239}\text{Pu}(n,2n)$ reaction cross section measurements. Unpublished.
- [You00] W. Younes et al., The $^{235}\text{U}(n,2n_{-})$ Yраст Partial Gamma-Ray Cross Sections: A Report on the 1998 and 1999 GEANIE Data and Analysis Techniques. Unpublished.
- [How71] R.J. Howerton. Nucl.Sci. and Eng. 46, 414 (1971).
- [Mat72] Mather et al., EANDC(UK) 142-AL (1972).
- [Fre80] J. Frehaut et al., Nucl. Sci. and Eng. 74, 29 (1980)
- [Lou85] R.W. Lougheed, et al., Private communication (1985).
- [Yat00] S.W. Yates, et al., Private communications (2000).

runs.

Table 8: Summed ^{235}U fission chamber data for the 1998 10 mil, 20 mil and 1999 10 mil

E_{γ} (MeV)	gE_{γ} (MeV)	Counts	Δ Counts	Neutrons	Δ Neutrons	$1/\text{barns}$	$\Delta 1/\text{barns}$
1.3210	0.0180	1.004E+04	1.640E+02	7.230E+12	2.249E+11	1.238E+07	3.030E+05
1.3650	0.0190	1.088E+04	1.763E+02	7.431E+12	2.222E+11	1.342E+07	3.173E+05
1.4090	0.0190	1.113E+04	1.752E+02	7.219E+12	2.222E+11	1.342E+07	3.173E+05
1.4550	0.0210	1.216E+04	1.828E+02	7.469E+12	2.122E+11	1.460E+07	3.309E+05
1.5040	0.0220	1.225E+04	1.835E+02	7.120E+12	2.018E+11	1.510E+07	3.429E+05
1.5560	0.0230	1.294E+04	1.906E+02	7.116E+12	1.964E+11	1.578E+07	3.429E+05
1.6100	0.0240	1.373E+04	1.964E+02	7.147E+12	1.917E+11	1.627E+07	3.485E+05
1.6670	0.0250	1.350E+04	1.947E+02	6.619E+12	1.794E+11	1.632E+07	3.480E+05
1.7280	0.0270	1.396E+04	1.947E+02	6.473E+12	1.727E+11	1.684E+07	3.537E+05
1.7920	0.0280	1.539E+04	2.055E+02	6.722E+12	1.713E+11	1.779E+07	3.643E+05
1.8580	0.0290	1.555E+04	2.078E+02	6.405E+12	1.625E+11	1.840E+07	3.701E+05
1.9290	0.0320	1.579E+04	2.082E+02	6.134E+12	1.547E+11	1.880E+07	3.751E+05
2.0040	0.0330	1.657E+04	2.174E+02	6.067E+12	1.493E+11	1.900E+07	3.769E+05
2.0840	0.0350	1.620E+04	2.113E+02	5.590E+12	1.393E+11	1.924E+07	3.773E+05
2.2590	0.0400	1.835E+04	2.303E+02	5.627E+12	1.324E+11	2.124E+07	4.038E+05
2.3540	0.0420	1.769E+04	2.224E+02	5.136E+12	1.229E+11	2.112E+07	4.018E+05
2.4550	0.0450	1.789E+04	2.207E+02	4.989E+12	1.168E+11	2.125E+07	4.040E+05
2.5640	0.0480	1.849E+04	2.324E+02	4.771E+12	1.118E+11	2.175E+07	4.101E+05
2.6800	0.0520	1.813E+04	2.249E+02	4.410E+12	1.044E+11	2.196E+07	4.143E+05
2.8020	0.0550	1.774E+04	2.251E+02	4.104E+12	9.791E+10	2.183E+07	4.137E+05
3.0280	0.0600	1.871E+04	2.268E+02	4.067E+12	9.569E+10	2.277E+07	4.299E+05
3.2310	0.0680	1.884E+04	2.328E+02	3.630E+12	8.604E+10	2.330E+07	4.485E+05
3.5080	0.0630	1.911E+04	2.365E+02	3.915E+12	9.211E+10	2.373E+07	4.791E+05
3.7660	0.0860	2.045E+04	2.346E+02	3.189E+12	7.316E+10	2.570E+07	4.775E+05
4.2000	0.1100	2.104E+04	2.441E+02	2.881E+12	6.505E+10	2.800E+07	5.068E+05
4.4450	0.1100	2.198E+04	2.442E+02	2.786E+12	6.192E+10	2.883E+07	5.167E+05
4.7130	0.1190	2.192E+04	2.468E+02	2.589E+12	5.751E+10	3.008E+07	5.350E+05
5.0010	0.1320	2.202E+04	2.493E+02	2.438E+12	5.400E+10	3.092E+07	5.485E+05
5.3250	0.1440	2.224E+04	2.493E+02	2.326E+12	5.066E+10	3.148E+07	5.485E+05
5.6780	0.1590	2.243E+04	2.506E+02	2.098E+12	4.610E+10	3.250E+07	5.683E+05
6.0640	0.1760	2.259E+04	2.506E+02	2.018E+12	4.207E+10	3.401E+07	5.725E+05
6.5000	0.1950	3.175E+04	2.831E+02	1.902E+12	3.632E+10	3.475E+07	5.725E+05
6.9690	0.2150	3.516E+04	3.114E+02	1.652E+12	3.023E+10	3.396E+07	5.123E+05
7.4980	0.2430	3.598E+04	3.184E+02	1.371E+12	2.483E+10	3.173E+07	4.710E+05
8.1050	0.2720	3.770E+04	3.232E+02	1.223E+12	2.167E+10	3.090E+07	4.554E+05
8.7730	0.3060	3.663E+04	3.260E+02	1.044E+12	1.876E+10	3.042E+07	4.506E+05
9.5200	0.3460	3.502E+04	3.155E+02	8.914E+11	1.627E+10	2.921E+07	4.385E+05
10.3920	0.3950	3.339E+04	3.157E+02	7.560E+11	1.381E+10	2.796E+07	4.223E+05
11.3730	0.4530	3.502E+04	2.915E+02	6.060E+10	1.150E+10	2.648E+07	4.065E+05
12.4990	0.5250	3.168E+04	2.887E+02	5.218E+10	9.586E+09	2.572E+07	3.887E+05
13.8240	0.6060	3.390E+04	3.066E+02	4.314E+10	7.665E+09	2.436E+07	3.619E+05
15.3590	0.7190	3.413E+04	3.087E+02	3.570E+10	6.506E+09	2.435E+07	3.637E+05
17.1830	0.8460	3.403E+04	3.053E+02	3.093E+10	5.904E+09	2.435E+07	3.862E+05
19.3360	1.0180	3.113E+04	1.763E+02	2.222E+10	1.342E+10	3.173E+07	3.030E+05
21.9600	1.2250	3.828E+04	3.170E+02	2.334E+10	4.1153E+09	2.738E+07	4.218E+05
25.1210	1.5160	4.445E+04	3.415E+02	2.178E+10	3.391E+09	3.029E+07	3.993E+05

Table 9: Neutron energy, γ -ray peak area, and cross sections (σ) for the 157.4 keV $6^+ \rightarrow 4^+$ transition in ^{238}Pu from the 98+99 data. $\Delta\sigma_\gamma$ is the uncertainty in the cross section due to γ -ray statistics and peak-fitting.

E_n (MeV)	δE_n (MeV)	Area	Δ_{Area}	σ (barns)	$\Delta\sigma_\gamma$ (barns)	$\Delta\sigma$ (barns)
1.3210	0.0180	1170	238	0.0379	0.0077	0.0083
1.3650	0.0190	972	248	0.0287	0.0073	0.0077
1.4090	0.0190	543	243	0.0153	0.0068	0.0069
1.4550	0.0210	955	245	0.0255	0.0065	0.0069
1.5040	0.0220	849	246	0.0217	0.0063	0.0065
1.5560	0.0230	679	251	0.0166	0.0061	0.0063
1.6100	0.0240	923	254	0.0215	0.0059	0.0062
1.6670	0.0250	631	252	0.0147	0.0059	0.0060
1.7280	0.0270	885	255	0.0201	0.0058	0.0060
1.7920	0.0280	742	260	0.0158	0.0055	0.0057
1.8580	0.0290	1167	258	0.0237	0.0052	0.0056
1.9290	0.0320	803	261	0.0159	0.0052	0.0053
2.0040	0.0330	626	261	0.0122	0.0051	0.0052
2.0840	0.0350	711	269	0.0138	0.0052	0.0053
2.1690	0.0370	975	267	0.0178	0.0049	0.0051
2.2590	0.0400	871	273	0.0151	0.0047	0.0049
2.3540	0.0420	610	267	0.0106	0.0046	0.0047
2.4550	0.0450	201	267	0.0035	0.0046	0.0046
2.5640	0.0480	779	284	0.0131	0.0048	0.0049
2.6800	0.0520	470	280	0.0078	0.0046	0.0047
2.8020	0.0550	917	277	0.0154	0.0047	0.0048
2.9380	0.0600	193	286	0.0032	0.0047	0.0047
3.0780	0.0630	252	279	0.0038	0.0042	0.0043
3.2310	0.0680	756	278	0.0118	0.0043	0.0044
3.3960	0.0740	357	284	0.0056	0.0045	0.0045
3.5740	0.0790	511	287	0.0078	0.0044	0.0044
3.7660	0.0860	521	278	0.0075	0.004	0.0040
3.9730	0.0930	530	291	0.0071	0.0039	0.0040
4.2000	0.1010	241	289	0.0031	0.0037	0.0038
4.4450	0.1100	446	295	0.0057	0.0038	0.0038
4.7130	0.1190	550	290	0.0066	0.0035	0.0035
5.0010	0.1320	-392	300	-0.0038	0.0029	0.0030
5.3250	0.1440	225	295	0.0022	0.0029	0.0029
5.6780	0.1590	-317	301	-0.0030	0.0028	0.0029
6.0640	0.1760	263	309	0.0025	0.0029	0.0030
6.5000	0.1950	1356	317	0.0125	0.0029	0.0031
6.9690	0.2150	2406	326	0.0218	0.003	0.0034
7.4980	0.2430	3482	328	0.0336	0.0032	0.0041
8.1050	0.2720	4551	326	0.0450	0.0032	0.0047
8.7730	0.3060	4940	327	0.0498	0.0033	0.0051
9.5200	0.3460	5751	323	0.0614	0.0034	0.0059
10.3920	0.3950	7236	327	0.0814	0.0037	0.0073
11.3730	0.4530	7662	330	0.0928	0.004	0.0082
12.4990	0.5250	7254	321	0.0922	0.0041	0.0082
13.8240	0.6060	5495	324	0.0721	0.0043	0.0070
15.3590	0.7190	3955	318	0.0527	0.0042	0.0059
17.1830	0.8460	3324	316	0.0443	0.0042	0.0054
19.3360	1.0180	2664	310	0.0343	0.004	0.0048
21.9600	1.2250	2840	313	0.0347	0.0038	0.0047
25.1210	1.5160	2206	320	0.0245	0.0036	0.0040

Table 10: Neutron energy, γ -ray peak area, and cross sections (σ_c) for the 210.0 keV 8^+ $\rightarrow 6^+$ transition in ^{238}Pu from the 98+99 data. $\delta\sigma_\gamma$ is the uncertainty in the cross section due to γ -ray statistics and peak-fitting

E_n (MeV)	δE_n (MeV)	Area	Δ_{Area}	σ (barns)	$\Delta\sigma_\gamma$ (barns)	$\Delta\sigma$ (barns)
1.3210	0.0180	725	297	0.0117	0.0048	0.0048
1.3650	0.0190	-321	288	-0.0047	0.0042	0.0042
1.4090	0.0190	-63	300	-0.0009	0.0042	0.0042
1.4550	0.0210	334	298	0.0044	0.0040	0.0040
1.5040	0.0220	-13	301	-0.0002	0.0038	0.0038
1.5560	0.0230	-370	296	-0.0045	0.0036	0.0036
1.6100	0.0240	-575	301	-0.0066	0.0035	0.0035
1.6670	0.0250	376	303	0.0044	0.0035	0.0035
1.7280	0.0270	35	313	0.0004	0.0035	0.0035
1.7920	0.0280	-125	306	-0.0013	0.0032	0.0032
1.8580	0.0290	37	320	0.0004	0.0032	0.0032
1.9290	0.0320	-270	307	-0.0027	0.0030	0.0030
2.0040	0.0330	358	320	0.0035	0.0031	0.0031
2.0840	0.0350	217	315	0.0021	0.0030	0.0030
2.1690	0.0370	-167	313	-0.0015	0.0028	0.0028
2.2590	0.0400	120	321	0.0010	0.0028	0.0028
2.3540	0.0420	260	315	0.0022	0.0027	0.0027
2.4550	0.0450	-727	322	-0.0062	0.0028	0.0028
2.5640	0.0480	-711	334	-0.0059	0.0028	0.0028
2.6800	0.0520	-298	333	-0.0025	0.0028	0.0028
2.8020	0.0550	116	338	0.0010	0.0028	0.0028
2.9380	0.0600	-32	346	-0.0003	0.0028	0.0028
3.0780	0.0630	-164	340	-0.0012	0.0026	0.0026
3.2310	0.0680	-8	335	-0.0001	0.0026	0.0026
3.3960	0.0740	219	340	0.0017	0.0026	0.0026
3.5740	0.0790	620	355	0.0047	0.0027	0.0027
3.7660	0.0860	599	350	0.0043	0.0025	0.0025
3.9730	0.0930	116	352	0.0008	0.0024	0.0024
4.2000	0.1010	-356	340	-0.0023	0.0022	0.0022
4.4450	0.1100	-73	355	-0.0005	0.0022	0.0022
4.7130	0.1190	742	363	0.0044	0.0022	0.0022
5.0010	0.1320	-397	355	-0.0019	0.0017	0.0017
5.3250	0.1440	405	351	0.0020	0.0017	0.0017
5.6780	0.1590	525	359	0.0025	0.0017	0.0017
6.0640	0.1760	89	360	0.0004	0.0017	0.0017
6.5000	0.1950	-394	347	-0.0018	0.0016	0.0016
6.9690	0.2150	1052	379	0.0047	0.0017	0.0017
7.4980	0.2430	1146	370	0.0055	0.0018	0.0018
8.1050	0.2720	1124	359	0.0055	0.0018	0.0018
8.7730	0.3060	2815	361	0.0139	0.0018	0.0019
9.5200	0.3460	3818	364	0.0199	0.0019	0.0020
10.3920	0.3950	4589	368	0.0252	0.0020	0.0022
11.3730	0.4530	5102	376	0.0302	0.0022	0.0025
12.4990	0.5250	5623	365	0.0349	0.0023	0.0026
13.8240	0.6060	4473	356	0.0287	0.0023	0.0025
15.3590	0.7190	4319	368	0.0281	0.0024	0.0026
17.1830	0.8460	2585	374	0.0168	0.0024	0.0025
19.3360	1.0180	2395	380	0.0151	0.0024	0.0025
21.9600	1.2250	1433	377	0.0086	0.0023	0.0023
25.1210	1.5160	2096	399	0.0114	0.0022	0.0022

Table 11: Neutron energy, γ -ray peak area, and cross sections (σ) for the 936.6 keV $4^- \rightarrow 4^+$ transition in ^{238}Pu from the 98+99 data. $\delta\sigma_\gamma$ is the uncertainty in the cross section due to γ -ray statistics and peak-fitting

E_n (MeV)	δE_n (MeV)	Area	Δ_{Area}	σ (barns)	$\Delta\sigma_\gamma$ (barns)	$\Delta\sigma$ (barns)
1.3210	0.0180	-85	47	-0.0038	0.0021	0.0021
1.3650	0.0190	36	50	0.0015	0.0020	0.0020
1.4090	0.0190	10	53	0.0004	0.0021	0.0021
1.4550	0.0210	22	59	0.0008	0.0022	0.0022
1.5040	0.0220	-13	54	-0.0005	0.0019	0.0019
1.5560	0.0230	-1	55	-0.0000	0.0019	0.0019
1.6100	0.0240	4	57	0.0001	0.0018	0.0018
1.6670	0.0250	20	61	0.0006	0.0020	0.0020
1.7280	0.0270	3	57	0.0001	0.0018	0.0018
1.7920	0.0280	20	58	0.0006	0.0017	0.0017
1.8580	0.0290	-154	65	-0.0043	0.0018	0.0018
1.9290	0.0320	14	65	0.0004	0.0018	0.0018
2.0040	0.0330	-108	62	-0.0029	0.0017	0.0017
2.0840	0.0350	9	63	0.0002	0.0017	0.0017
2.1690	0.0370	-170	65	-0.0043	0.0016	0.0016
2.2590	0.0400	-181	68	-0.0043	0.0016	0.0016
2.3540	0.0420	95	67	0.0023	0.0016	0.0016
2.4550	0.0450	24	71	0.0006	0.0017	0.0017
2.5640	0.0480	-61	74	-0.0014	0.0017	0.0017
2.6800	0.0520	-162	79	-0.0037	0.0018	0.0018
2.8020	0.0550	22	79	0.0005	0.0018	0.0018
2.9380	0.0600	-204	78	-0.0046	0.0018	0.0018
3.0780	0.0630	-9	79	-0.0002	0.0017	0.0017
3.2310	0.0680	-64	77	-0.0014	0.0017	0.0017
3.3960	0.0740	-130	77	-0.0028	0.0017	0.0017
3.5740	0.0790	35	80	0.0007	0.0017	0.0017
3.7660	0.0860	99	82	0.0020	0.0016	0.0016
3.9730	0.0930	17	86	0.0003	0.0016	0.0016
4.2000	0.1010	-139	85	-0.0025	0.0015	0.0015
4.4450	0.1100	6	92	0.0001	0.0016	0.0016
4.7130	0.1190	-125	88	-0.0021	0.0015	0.0015
5.0010	0.1320	-51	91	-0.0008	0.0015	0.0015
5.3250	0.1440	-65	95	-0.0010	0.0015	0.0015
5.6780	0.1590	-24	93	-0.0004	0.0015	0.0015
6.0640	0.1760	-90	91	-0.0012	0.0012	0.0012
6.5000	0.1950	96	95	0.0013	0.0013	0.0013
6.9690	0.2150	125	97	0.0016	0.0013	0.0013
7.4980	0.2430	758	96	0.0105	0.0013	0.0014
8.1050	0.2720	1400	105	0.0199	0.0015	0.0016
8.7730	0.3060	2062	114	0.0290	0.0016	0.0018
9.5200	0.3460	2294	119	0.0345	0.0018	0.0020
10.3920	0.3950	2340	113	0.0377	0.0018	0.0021
11.3730	0.4530	2712	122	0.0471	0.0021	0.0025
12.4990	0.5250	2128	116	0.0387	0.0021	0.0024
13.8240	0.6060	1449	103	0.0272	0.0019	0.0021
15.3590	0.7190	1292	102	0.0245	0.0019	0.0020
17.1830	0.8460	1138	103	0.0216	0.0020	0.0020
19.3360	1.0180	1078	102	0.0198	0.0019	0.0019
21.9600	1.2250	1331	103	0.0244	0.0019	0.0020
25.1210	1.5160	1331	107	0.0220	0.0018	0.0019

Table 12: Neutron energy, γ -ray peak area, and cross sections (Q_γ) for the 924.0 keV 2^+ $\rightarrow 2^+$ transition in ^{28}Pu from the 98+99 data. Q_γ is the uncertainty in the cross section due to γ -ray statistics and peak-fitting

E_n (MeV)	δE (MeV)	Area	A_{Area}	Q (bars)	ΔQ (bars)	ΔQ (bars)
1.3210	0.0180	131	49	0.0059	0.0022	0.0022
1.3650	0.0190	120	50	0.0049	0.0020	0.0020
1.4090	0.0190	180	54	0.0070	0.0021	0.0021
1.4550	0.0210	248	62	0.0091	0.0023	0.0023
1.5040	0.0220	196	56	0.0069	0.0020	0.0020
1.5560	0.0230	195	57	0.0066	0.0019	0.0019
1.6100	0.0240	290	60	0.0093	0.0019	0.0019
1.6670	0.0250	189	62	0.0061	0.0020	0.0020
1.7280	0.0270	241	58	0.0075	0.0018	0.0018
1.7920	0.0280	122	58	0.0036	0.0017	0.0017
1.8580	0.0290	94	66	0.0026	0.0019	0.0019
1.9290	0.0320	105	65	0.0029	0.0018	0.0018
2.0040	0.0330	132	61	0.0035	0.0016	0.0016
2.0840	0.0350	75	63	0.0020	0.0017	0.0017
2.1690	0.0370	39	66	0.0010	0.0017	0.0017
2.2590	0.0400	69	68	0.0016	0.0016	0.0016
2.3540	0.0420	94	66	0.0022	0.0016	0.0016
2.4550	0.0450	69	72	0.0023	0.0017	0.0017
2.5640	0.0480	98	72	0.0016	0.0017	0.0017
2.6800	0.0520	26	80	0.0006	0.0018	0.0018
2.8020	0.0550	191	80	0.0044	0.0018	0.0019
2.9380	0.0600	143	80	0.0032	0.0018	0.0018
3.0780	0.0630	142	79	0.0030	0.0017	0.0017
3.2310	0.0680	191	78	0.0041	0.0017	0.0017
3.3960	0.0740	113	77	-0.0024	0.0017	0.0017
3.5740	0.0790	304	82	0.0064	0.0017	0.0017
3.7660	0.0860	176	82	0.0035	0.0016	0.0016
3.9730	0.0930	73	86	0.0014	0.0016	0.0016
4.2000	0.1010	37	85	0.0007	0.0015	0.0015
4.4450	0.1100	252	93	0.0044	0.0016	0.0016
4.7130	0.1190	107	89	0.0018	0.0015	0.0015
5.0010	0.1320	109	91	0.0018	0.0015	0.0015
5.3250	0.1440	85	93	-0.0013	0.0015	0.0015
5.6780	0.1590	116	93	0.0018	0.0014	0.0014
6.0640	0.1760	19	90	0.0003	0.0015	0.0015
6.5000	0.1950	166	94	0.0026	0.0015	0.0015
6.9690	0.2150	82	96	0.0013	0.0015	0.0015
7.4980	0.2430	382	92	0.0062	0.0015	0.0015
8.1050	0.2720	430	94	0.0071	0.0016	0.0016
8.7730	0.3060	832	98	0.0118	0.0016	0.0017
9.5200	0.3460	688	98	0.0138	0.0016	0.0017
10.3920	0.3950	805	93	0.0142	0.0016	0.0017
11.3730	0.4530	844	96	0.0160	0.0018	0.0019
12.4990	0.5250	764	95	0.0152	0.0019	0.0019
13.8240	0.6060	656	92	0.0135	0.0019	0.0019
15.3590	0.7190	412	92	0.0084	0.0019	0.0019
17.1830	0.8460	268	93	0.0054	0.0019	0.0019
19.3360	1.0180	397	95	0.0077	0.0018	0.0018
21.9600	1.2250	486	94	0.0089	0.0017	0.0017
25.1210	1.5160	485	98	0.0080	0.0016	0.0016

Table 13: Neutron energy, γ -ray peak area, and cross sections (σ_c) for the 918.7 keV $1^- \rightarrow 2^+$ transition in ^{238}Pu from the 98+99 data. . $\delta\sigma_\gamma$ is the uncertainty in the cross section due to γ -ray statistics and peak-fitting

E_n (MeV)	δE_n (MeV)	Area	Δ_{Area}	σ (barns)	$\Delta\sigma_\gamma$ (barns)	$\Delta\sigma$ (barns)
1.3210	0.0180	284	51	0.0114	0.0020	0.0021
1.3650	0.0190	279	56	0.0103	0.0021	0.0021
1.4090	0.0190	140	53	0.0050	0.0019	0.0019
1.4550	0.0210	264	61	0.0090	0.0021	0.0021
1.5040	0.0220	359	60	0.0117	0.0020	0.0020
1.5560	0.0230	286	59	0.0090	0.0018	0.0019
1.6100	0.0240	276	62	0.0083	0.0019	0.0019
1.6670	0.0250	177	61	0.0053	0.0018	0.0018
1.7280	0.0270	171	59	0.0050	0.0017	0.0017
1.7920	0.0280	210	62	0.0058	0.0017	0.0017
1.8580	0.0290	307	68	0.0082	0.0018	0.0018
1.9290	0.0320	244	68	0.0064	0.0018	0.0018
2.0040	0.0330	185	68	0.0047	0.0017	0.0017
2.0840	0.0350	210	67	0.0054	0.0017	0.0017
2.1690	0.0370	201	71	0.0048	0.0017	0.0017
2.2590	0.0400	51	72	0.0012	0.0017	0.0017
2.3540	0.0420	117	73	0.0027	0.0017	0.0017
2.4550	0.0450	45	75	0.0010	0.0017	0.0017
2.5640	0.0480	311	81	0.0069	0.0018	0.0018
2.6800	0.0520	176	86	0.0039	0.0019	0.0019
2.8020	0.0550	207	86	0.0046	0.0019	0.0019
2.9380	0.0600	132	88	0.0029	0.0019	0.0019
3.0780	0.0630	181	83	0.0037	0.0017	0.0017
3.2310	0.0680	98	83	0.0020	0.0017	0.0017
3.3960	0.0740	152	85	0.0031	0.0018	0.0018
3.5740	0.0790	198	86	0.0040	0.0017	0.0017
3.7660	0.0860	306	88	0.0059	0.0017	0.0017
3.9730	0.0930	182	91	0.0033	0.0016	0.0016
4.2000	0.1010	230	92	0.0040	0.0016	0.0016
4.4450	0.1100	271	96	0.0046	0.0016	0.0016
4.7130	0.1190	235	94	0.0038	0.0015	0.0015
5.0010	0.1320	271	96	0.0042	0.0015	0.0015
5.3250	0.1440	355	98	0.0055	0.0015	0.0015
5.6780	0.1590	374	99	0.0057	0.0015	0.0015
6.0640	0.1760	440	97	0.0066	0.0015	0.0015
6.5000	0.1950	394	100	0.0058	0.0015	0.0015
6.9690	0.2150	548	103	0.0079	0.0015	0.0015
7.4980	0.2430	401	97	0.0062	0.0015	0.0015
8.1050	0.2720	613	101	0.0096	0.0016	0.0016
8.7730	0.3060	545	97	0.0086	0.0015	0.0015
9.5200	0.3460	787	101	0.0129	0.0017	0.0017
10.3920	0.3950	794	98	0.0136	0.0017	0.0017
11.3730	0.4530	568	97	0.0104	0.0018	0.0018
12.4990	0.5250	525	96	0.0101	0.0018	0.0018
13.8240	0.6060	408	92	0.0081	0.0018	0.0018
15.3590	0.7190	396	95	0.0079	0.0019	0.0019
17.1830	0.8460	350	93	0.0069	0.0018	0.0018
19.3360	1.0180	289	93	0.0055	0.0018	0.0018
21.9600	1.2250	491	92	0.0089	0.0017	0.0017
25.1210	1.5160	550	99	0.0091	0.0016	0.0016

Table 14: Neutron energy, γ -ray peak area, and cross sections (g) for the 962.8 keV I-

E _a (MeV)	SE(MeV)	Area	A _{ave}	g(bars)	ΔG _b (bars)	ΔG _d (bars)
1.3210	0.0180	59	55	0.0006	0.0006	0.0006
1.3650	0.0190	149	60	0.0014	0.0005	0.0006
1.4090	0.0190	100	59	0.0005	0.0005	0.0005
1.4550	0.0210	147	63	0.0012	0.0005	0.0005
1.5040	0.0220	125	65	0.0017	0.0005	0.0005
1.5560	0.0230	128	61	0.0010	0.0005	0.0005
1.6100	0.0240	61	67	0.0004	0.0005	0.0005
1.6670	0.0250	189	68	0.0014	0.0005	0.0005
1.7280	0.0270	96	73	0.0007	0.0005	0.0005
1.7920	0.0280	169	68	0.0011	0.0004	0.0004
1.8580	0.0290	48	73	0.0003	0.0005	0.0005
1.9290	0.0320	274	71	0.0017	0.0004	0.0004
2.0040	0.0330	173	77	0.0010	0.0005	0.0005
2.0840	0.0350	63	73	0.0004	0.0005	0.0004
2.1690	0.0370	150	78	0.0009	0.0004	0.0004
2.2590	0.0400	185	80	0.0010	0.0004	0.0004
2.3540	0.0420	229	81	0.0012	0.0004	0.0004
2.4550	0.0450	164	83	0.0009	0.0004	0.0004
2.5640	0.0480	267	87	0.0014	0.0005	0.0004
2.6800	0.0520	282	98	0.0015	0.0005	0.0005
2.8020	0.0550	229	99	0.0012	0.0005	0.0005
2.9380	0.0600	242	97	0.0012	0.0005	0.0005
3.0780	0.0630	493	102	0.0023	0.0005	0.0005
3.2310	0.0680	251	100	0.0012	0.0005	0.0005
3.3960	0.0740	284	97	0.0014	0.0005	0.0005
3.5740	0.0790	316	103	0.0015	0.0005	0.0005
3.7660	0.0860	35	101	0.0002	0.0005	0.0005
3.9730	0.0930	308	105	0.0013	0.0005	0.0005
4.2000	0.1010	531	109	0.0021	0.0004	0.0004
4.4450	0.1100	385	113	0.0015	0.0004	0.0004
4.7130	0.1190	204	110	0.0008	0.0004	0.0004
5.0010	0.1320	119	115	0.0008	0.0004	0.0004
5.3250	0.1440	219	120	0.0008	0.0004	0.0004
5.6780	0.1590	261	118	0.0009	0.0004	0.0004
6.0640	0.1760	220	126	0.0009	0.0004	0.0004
6.5000	0.1950	143	128	0.0005	0.0004	0.0004
6.9690	0.2150	143	128	0.0005	0.0004	0.0004
7.4980	0.2430	468	119	0.0015	0.0004	0.0004
8.1050	0.2720	281	130	0.0010	0.0005	0.0005
8.7730	0.3060	101	121	0.0004	0.0004	0.0004
9.5200	0.3460	282	121	0.0004	0.0005	0.0005
10.3920	0.3950	369	130	0.0011	0.0005	0.0005
11.3730	0.4530	73	121	0.0014	0.0005	0.0005
12.4990	0.5250	451	118	0.0032	0.0005	0.0005
13.8240	0.6060	508	114	0.0020	0.0005	0.0005
15.3590	0.7190	256	107	0.0012	0.0005	0.0005
17.1830	0.8460	232	119	0.0010	0.0005	0.0005
19.3360	1.0180	289	119	0.0012	0.0005	0.0005
21.9600	1.2250	320	118	0.0013	0.0005	0.0005
25.1210	1.5160	356	123	0.0013	0.0005	0.0005

due to γ -ray statistics and peak-fitting

→ γ -transition in ^{208}Po from the 98+99 data. $\delta\sigma$ is the uncertainty in the cross section

Table 15: Neutron energy, γ -ray peak area, and cross sections (σ_c) for the 459.8 keV $5^- \rightarrow 6^+$ transition in ^{238}Pu from the 98+99 data. . $\delta\sigma_c$ is the uncertainty in the cross section due to γ -ray statistics and peak-fitting

E_n (MeV)	δE_n (MeV)	Area	Δ_{Area}	$\sigma(\text{barns})$	$\Delta\sigma_c(\text{barns})$	$\Delta\sigma(\text{barns})$
1.3210	0.0180	64	84	0.0013	0.0017	0.0017
1.3650	0.0190	96	89	0.0018	0.0017	0.0017
1.4090	0.0190	146	88	0.0026	0.0016	0.0016
1.4550	0.0210	174	91	0.0029	0.0015	0.0015
1.5040	0.0220	211	93	0.0034	0.0015	0.0015
1.5560	0.0230	82	93	0.0013	0.0014	0.0014
1.6100	0.0240	255	96	0.0037	0.0014	0.0014
1.6670	0.0250	97	94	0.0014	0.0014	0.0014
1.7280	0.0270	161	96	0.0023	0.0014	0.0014
1.7920	0.0280	336	102	0.0045	0.0014	0.0014
1.8580	0.0290	319	102	0.0041	0.0013	0.0013
1.9290	0.0320	141	100	0.0018	0.0013	0.0013
2.0040	0.0330	84	103	0.0010	0.0013	0.0013
2.0840	0.0350	189	104	0.0023	0.0013	0.0013
2.1690	0.0370	384	108	0.0044	0.0012	0.0013
2.2590	0.0400	178	110	0.0019	0.0012	0.0012
2.3540	0.0420	428	110	0.0047	0.0012	0.0012
2.4550	0.0450	268	114	0.0029	0.0012	0.0012
2.5640	0.0480	240	119	0.0026	0.0013	0.0013
2.6800	0.0520	256	123	0.0027	0.0013	0.0013
2.8020	0.0550	80	124	0.0008	0.0013	0.0013
2.9380	0.0600	281	124	0.0029	0.0013	0.0013
3.0780	0.0630	292	123	0.0028	0.0012	0.0012
3.2310	0.0680	376	124	0.0037	0.0012	0.0012
3.3960	0.0740	212	121	0.0021	0.0012	0.0012
3.5740	0.0790	394	126	0.0038	0.0012	0.0012
3.7660	0.0860	402	123	0.0037	0.0011	0.0011
3.9730	0.0930	255	127	0.0022	0.0011	0.0011
4.2000	0.1010	426	130	0.0035	0.0011	0.0011
4.4450	0.1100	359	136	0.0029	0.0011	0.0011
4.7130	0.1190	593	134	0.0045	0.0010	0.0010
5.0010	0.1320	481	138	0.0035	0.0010	0.0010
5.3250	0.1440	347	136	0.0025	0.0010	0.0010
5.6780	0.1590	413	140	0.0029	0.0010	0.0010
6.0640	0.1760	639	141	0.0047	0.0010	0.0011
6.5000	0.1950	452	142	0.0032	0.0010	0.0010
6.9690	0.2150	883	148	0.0061	0.0010	0.0010
7.4980	0.2430	796	144	0.0059	0.0011	0.0011
8.1050	0.2720	959	147	0.0072	0.0011	0.0011
8.7730	0.3060	1083	147	0.0082	0.0011	0.0011
9.5200	0.3460	1475	145	0.0116	0.0011	0.0012
10.3920	0.3950	1515	144	0.0123	0.0012	0.0012
11.3730	0.4530	1313	138	0.0115	0.0012	0.0012
12.4990	0.5250	977	138	0.0089	0.0013	0.0013
13.8240	0.6060	946	135	0.0090	0.0013	0.0013
15.3590	0.7190	675	137	0.0063	0.0013	0.0013
17.1830	0.8460	737	138	0.0068	0.0013	0.0013
19.3360	1.0180	556	139	0.0049	0.0012	0.0012
21.9600	1.2250	896	142	0.0075	0.0012	0.0012
25.1210	1.5160	881	149	0.0066	0.0011	0.0011

Table 16: Neutron energy, γ -ray peak area, and cross sections (σ) for the 617.3 keV $3^- \rightarrow 2^+/5^- \rightarrow 4^+$ doublet in ^{238}Pu from the 98+99 data. . $\delta\sigma_\gamma$ is the uncertainty in the cross section due to γ -ray statistics and peak-fitting

E_n (MeV)	δE_n (MeV)	Area	Δ_{Area}	σ (barns)	$\Delta\sigma_\gamma$ (barns)	$\Delta\sigma$ (barns)
1.3210	0.0180	246	117	0.0071	0.0034	0.0034
1.3650	0.0190	-85	151	-0.0022	0.0040	0.0040
1.4090	0.0190	12	127	0.0003	0.0032	0.0032
1.4550	0.0210	327	129	0.0078	0.0031	0.0031
1.5040	0.0220	558	142	0.0127	0.0032	0.0033
1.5560	0.0230	597	146	0.0130	0.0032	0.0032
1.6100	0.0240	1059	169	0.0220	0.0035	0.0036
1.6670	0.0250	1492	171	0.0311	0.0036	0.0037
1.7280	0.0270	1151	181	0.0233	0.0037	0.0037
1.7920	0.0280	1030	162	0.0196	0.0031	0.0031
1.8580	0.0290	911	154	0.0165	0.0028	0.0028
1.9290	0.0320	896	158	0.0159	0.0028	0.0028
2.0040	0.0330	810	168	0.0141	0.0029	0.0029
2.0840	0.0350	407	154	0.0071	0.0027	0.0027
2.1690	0.0370	1086	178	0.0177	0.0029	0.0029
2.2590	0.0400	661	180	0.0102	0.0028	0.0028
2.3540	0.0420	1287	191	0.0199	0.0030	0.0030
2.4550	0.0450	1004	209	0.0155	0.0032	0.0033
2.5640	0.0480	1416	196	0.0213	0.0029	0.0030
2.6800	0.0520	1485	214	0.0221	0.0032	0.0032
2.8020	0.0550	817	200	0.0122	0.0030	0.0030
2.9380	0.0600	705	216	0.0103	0.0032	0.0032
3.0780	0.0630	789	191	0.0107	0.0026	0.0026
3.2310	0.0680	799	195	0.0111	0.0027	0.0027
3.3960	0.0740	1265	195	0.0176	0.0027	0.0028
3.5740	0.0790	841	195	0.0114	0.0026	0.0027
3.7660	0.0860	725	187	0.0093	0.0024	0.0024
3.9730	0.0930	865	192	0.0104	0.0023	0.0023
4.2000	0.1010	958	200	0.0111	0.0023	0.0023
4.4450	0.1100	1051	216	0.0119	0.0024	0.0025
4.7130	0.1190	1174	195	0.0126	0.0021	0.0021
5.0010	0.1320	1113	206	0.0115	0.0021	0.0022
5.3250	0.1440	1318	198	0.0135	0.0020	0.0021
5.6780	0.1590	1111	211	0.0112	0.0021	0.0021
6.0640	0.1760	1555	197	0.0171	0.0022	0.0022
6.5000	0.1950	1129	204	0.0119	0.0022	0.0022
6.9690	0.2150	1660	220	0.0170	0.0023	0.0023
7.4980	0.2430	1589	188	0.0173	0.0020	0.0021
8.1050	0.2720	2387	233	0.0264	0.0026	0.0027
8.7730	0.3060	2757	213	0.0306	0.0024	0.0025
9.5200	0.3460	2755	205	0.0316	0.0023	0.0025
10.3920	0.3950	2938	216	0.0348	0.0026	0.0027
11.3730	0.4530	2647	207	0.0335	0.0026	0.0028
12.4990	0.5250	1676	187	0.0223	0.0025	0.0026
13.8240	0.6060	2341	224	0.0322	0.0031	0.0032
15.3590	0.7190	1749	200	0.0237	0.0027	0.0028
17.1830	0.8460	1224	194	0.0162	0.0026	0.0026
19.3360	1.0180	1584	214	0.0202	0.0027	0.0028
21.9600	1.2250	1314	225	0.0155	0.0027	0.0027
25.1210	1.5160	1522	217	0.0162	0.0023	0.0024

Table 17: Neutron energy, γ -ray peak area, and cross sections (σ) for the $273.3 \text{ keV } 7/2^+ \rightarrow 5/2^-$ ^{237}Pu γ -ray from the 98+99 data. . $\delta\sigma_\gamma$ is the uncertainty in the cross section due to γ -ray statistics and peak-fitting

$E_n (\text{MeV})$	$\delta E_n (\text{MeV})$	Area	Δ_{Area}	$\sigma(\text{barns})$	$\Delta\sigma_\gamma(\text{barns})$	$\Delta\sigma(\text{barns})$
1.504	0.022	-126	159	-0.0014	0.0018	0.0018
1.556	0.023	-152	151	-0.0016	0.0016	0.0016
1.61	0.024	36	166	0.0004	0.0017	0.0017
1.667	0.025	-63	166	-0.0006	0.0017	0.0017
1.728	0.027	-170	160	-0.0017	0.0016	0.0016
1.792	0.028	171	172	0.0016	0.0016	0.0016
1.858	0.029	-360	172	-0.0032	0.0015	0.0015
1.929	0.032	-386	173	-0.0034	0.0015	0.0015
2.004	0.033	-100	161	-0.0009	0.0014	0.0014
2.084	0.035	8	176	0.0001	0.0015	0.0015
2.169	0.037	-540	171	-0.0043	0.0014	0.0014
2.259	0.04	-143	182	-0.0011	0.0014	0.0014
2.354	0.042	-295	169	-0.0023	0.0013	0.0013
2.455	0.045	-189	177	-0.0014	0.0013	0.0013
2.564	0.048	-80	192	-0.0006	0.0014	0.0014
2.68	0.052	-214	190	-0.0016	0.0014	0.0014
2.802	0.055	-48	187	-0.0004	0.0014	0.0014
2.938	0.06	-240	192	-0.0017	0.0014	0.0014
3.078	0.063	-246	195	-0.0016	0.0013	0.0013
3.231	0.068	-4	187	-0.0000	0.0013	0.0013
3.396	0.074	-13	187	-0.0001	0.0013	0.0013
3.574	0.079	28	197	0.0002	0.0013	0.0013
3.766	0.086	-217	186	-0.0014	0.0012	0.0012
3.973	0.093	-653	196	-0.0039	0.0012	0.0012
4.2	0.101	-87	193	-0.0005	0.0011	0.0011
4.445	0.11	26	197	0.0001	0.0011	0.0011
4.713	0.119	-180	193	-0.0010	0.0010	0.0010
5.001	0.132	-31	202	-0.0002	0.0010	0.0010
5.325	0.144	-193	203	-0.0014	0.0015	0.0015
5.678	0.159	-70	217	-0.0003	0.0011	0.0011
6.064	0.176	-307	217	-0.0015	0.0011	0.0011
6.5	0.195	-8	214	-0.0000	0.0010	0.0010
6.969	0.215	-250	222	-0.0011	0.0010	0.0010
7.498	0.243	205	226	0.0010	0.0011	0.0011
8.105	0.272	-68	225	-0.0003	0.0011	0.0011
8.773	0.306	-430	214	-0.0022	0.0011	0.0011
9.52	0.346	300	224	0.0016	0.0012	0.0012
10.392	0.395	-217	214	-0.0012	0.0012	0.0012
11.373	0.453	-61	227	-0.0004	0.0013	0.0013
12.499	0.525	-234	224	-0.0015	0.0014	0.0014
13.824	0.606	-296	217	-0.0019	0.0014	0.0014
15.359	0.719	589	205	0.0038	0.0013	0.0013
17.183	0.846	1733	210	0.0110	0.0013	0.0014
19.336	1.018	2904	219	0.0177	0.0013	0.0015
21.96	1.225	3600	226	0.0209	0.0013	0.0015
25.121	1.516	4688	255	0.0246	0.0013	0.0016
29.076	1.882	4534	293	0.0209	0.0014	0.0015
34.014	2.397	2853	260	0.0113	0.0010	0.0011
40.376	3.096	1006	343	0.0034	0.0011	0.0012

Table 18: Neutron energy, γ -ray peak area, and cross sections (σ_c) for the 154.3 keV $13/2^+ \rightarrow 9/2^+$ ^{239}Pu γ -ray from 98+99 data. . $\delta\sigma_c$ is the uncertainty in the cross section due to γ -ray statistics and peak-fitting

E_n (MeV)	δE_n (MeV)	Area	Δ_{Area}	σ (barns)	$\Delta\sigma_\gamma$ (barns)	$\Delta\sigma$ (barns)
1.3210	0.0180	472	338	0.0159	0.0114	0.0115
1.3650	0.0190	358	261	0.0110	0.0080	0.0081
1.4090	0.0190	346	180	0.0101	0.0053	0.0053
1.4550	0.0210	242	273	0.0067	0.0076	0.0076
1.5040	0.0220	501	264	0.0133	0.0070	0.0071
1.5560	0.0230	605	286	0.0154	0.0073	0.0073
1.6100	0.0240	391	166	0.0095	0.0040	0.0041
1.6670	0.0250	592	294	0.0144	0.0072	0.0072
1.7280	0.0270	553	210	0.0131	0.0050	0.0051
1.7920	0.0280	1068	302	0.0236	0.0067	0.0069
1.8580	0.0290	1145	270	0.0242	0.0057	0.0060
1.9290	0.0320	425	201	0.0088	0.0042	0.0042
2.0040	0.0330	813	259	0.0165	0.0052	0.0054
2.0840	0.0350	1612	403	0.0326	0.0082	0.0085
2.1690	0.0370	1065	299	0.0202	0.0057	0.0059
2.2590	0.0400	553	200	0.0100	0.0036	0.0037
2.3540	0.0420	1241	276	0.0224	0.0050	0.0052
2.4550	0.0450	1249	346	0.0225	0.0062	0.0064
2.5640	0.0480	1271	297	0.0223	0.0052	0.0055
2.6800	0.0520	1152	297	0.0200	0.0052	0.0054
2.8020	0.0550	1708	308	0.0298	0.0054	0.0058
2.9380	0.0600	2147	363	0.0366	0.0062	0.0067
3.0780	0.0630	1820	336	0.0289	0.0053	0.0057
3.2310	0.0680	1509	315	0.0246	0.0051	0.0054
3.3960	0.0740	1976	376	0.0321	0.0061	0.0065
3.5740	0.0790	1907	348	0.0301	0.0055	0.0059
3.7660	0.0860	2257	349	0.0339	0.0052	0.0058
3.9730	0.0930	2853	407	0.0401	0.0057	0.0064
4.2000	0.1010	2645	343	0.0358	0.0046	0.0053
4.4450	0.1100	3477	449	0.0459	0.0059	0.0068
4.7130	0.1190	3418	409	0.0428	0.0051	0.0060
5.0010	0.1320	3942	385	0.0478	0.0047	0.0058
5.3250	0.1440	3686	411	0.0442	0.0049	0.0058
5.6780	0.1590	3944	448	0.0464	0.0053	0.0062
6.0640	0.1760	3961	424	0.0460	0.0049	0.0059
6.5000	0.1950	3235	382	0.0362	0.0043	0.0050
6.9690	0.2150	2183	335	0.0238	0.0037	0.0040
7.4980	0.2430	1241	305	0.0144	0.0035	0.0037
8.1050	0.2720	1599	300	0.0190	0.0036	0.0038
8.7730	0.3060	962	272	0.0114	0.0032	0.0033
9.5200	0.3460	527	342	0.0065	0.0042	0.0043
10.3920	0.3950	155	350	0.0020	0.0046	0.0046
11.3730	0.4530	59	247	0.0008	0.0034	0.0034
12.4990	0.5250	406	262	0.0059	0.0038	0.0039
13.8240	0.6060	691	299	0.0104	0.0045	0.0046
15.3590	0.7190	486	270	0.0073	0.0041	0.0041
17.1830	0.8460	558	312	0.0083	0.0046	0.0047
19.3360	1.0180	828	291	0.0119	0.0042	0.0043

Table 19: Neutron energy, γ -ray peak area, and cross sections (σ) for the 226.4 keV $5/2^- \rightarrow 5/2^+$ ^{238}Pu γ -ray from the 98+99 data. $\delta\sigma_\gamma$ is the uncertainty in the cross section due to γ -ray statistics and peak-fitting.

E_n (MeV)	δE_n (MeV)	Area	Δ_{Area}	σ (barns)	$\Delta\sigma_\gamma$ (barns)	$\Delta\sigma$ (barns)
1.3210	0.0180	290	279	0.0033	0.0031	0.0031
1.3650	0.0190	487	270	0.0050	0.0028	0.0028
1.4090	0.0190	462	272	0.0045	0.0027	0.0027
1.4550	0.0210	1069	263	0.0099	0.0024	0.0024
1.5040	0.0220	452	272	0.0040	0.0024	0.0024
1.5560	0.0230	671	275	0.0057	0.0023	0.0023
1.6100	0.0240	477	279	0.0038	0.0022	0.0022
1.6670	0.0250	614	281	0.0050	0.0023	0.0023
1.7280	0.0270	1180	281	0.0093	0.0022	0.0022
1.7920	0.0280	1452	300	0.0107	0.0022	0.0022
1.8580	0.0290	612	274	0.0043	0.0019	0.0019
1.9290	0.0320	1119	280	0.0077	0.0019	0.0019
2.0040	0.0330	1004	277	0.0068	0.0019	0.0019
2.0840	0.0350	1263	287	0.0085	0.0019	0.0019
2.1690	0.0370	820	287	0.0052	0.0018	0.0018
2.2590	0.0400	1340	299	0.0081	0.0018	0.0018
2.3540	0.0420	965	296	0.0058	0.0018	0.0018
2.4550	0.0450	614	282	0.0037	0.0017	0.0017
2.5640	0.0480	1314	303	0.0077	0.0018	0.0018
2.6800	0.0520	1026	310	0.0059	0.0018	0.0018
2.8020	0.0550	1301	308	0.0076	0.0018	0.0018
2.9380	0.0600	694	305	0.0039	0.0017	0.0017
3.0780	0.0630	1349	302	0.0071	0.0016	0.0016
3.2310	0.0680	2044	314	0.0111	0.0017	0.0017
3.3960	0.0740	2014	321	0.0109	0.0017	0.0018
3.5740	0.0790	2233	315	0.0117	0.0017	0.0017
3.7660	0.0860	1406	301	0.0070	0.0015	0.0015
3.9730	0.0930	1754	318	0.0082	0.0015	0.0015
4.2000	0.1010	2244	325	0.0101	0.0015	0.0015
4.4450	0.1100	2142	320	0.0094	0.0014	0.0014
4.7130	0.1190	1676	313	0.0070	0.0013	0.0013
5.0010	0.1320	3049	328	0.0123	0.0013	0.0013
5.3250	0.1440	2431	337	0.0097	0.0013	0.0014
5.6780	0.1590	3166	348	0.0124	0.0014	0.0014
6.0640	0.1760	2493	330	0.0097	0.0013	0.0013
6.5000	0.1950	2131	354	0.0080	0.0013	0.0013
6.9690	0.2150	1742	359	0.0064	0.0013	0.0013
7.4980	0.2430	477	347	0.0019	0.0014	0.0014
8.1050	0.2720	147	358	0.0006	0.0014	0.0014
8.7730	0.3060	754	359	0.0030	0.0014	0.0014
9.5200	0.3460	393	366	0.0016	0.0015	0.0015
10.3920	0.3950	629	388	0.0027	0.0017	0.0017
11.3730	0.4530	4	376	0.0000	0.0018	0.0018
12.4990	0.5250	-139	393	-0.0007	0.0019	0.0019
13.8240	0.6060	-187	391	-0.0009	0.0020	0.0020
15.3590	0.7190	-175	411	-0.0009	0.0021	0.0021
17.1830	0.8460	159	413	0.0008	0.0021	0.0021
19.3360	1.0180	-408	440	-0.0020	0.0021	0.0021

Table 20: Neutron energy, γ -ray peak area, and cross sections (σ) for the 228.2 keV $5/2^+$ $\rightarrow 7/2^+$ ^{238}Pu γ -ray from the 98+99 data. $\delta\sigma_\gamma$ is the uncertainty in the cross section due to γ -ray statistics and peak-fitting.

E_n (MeV)	δE_n (MeV)	Area	Δ_{Area}	σ (barns)	$\Delta\sigma_\gamma$ (barns)	$\Delta\sigma$ (barns)
1.3210	0.0180	3288	351	0.1280	0.0137	0.0188
1.3650	0.0190	3580	329	0.1267	0.0116	0.0174
1.4090	0.0190	3581	345	0.1212	0.0117	0.0168
1.4550	0.0210	4145	341	0.1329	0.0109	0.0173
1.5040	0.0220	4277	341	0.1312	0.0105	0.0168
1.5560	0.0230	4739	363	0.1388	0.0106	0.0175
1.6100	0.0240	5338	360	0.1490	0.0100	0.0180
1.6670	0.0250	5091	349	0.1426	0.0098	0.0174
1.7280	0.0270	6009	371	0.1639	0.0101	0.0192
1.7920	0.0280	6130	361	0.1567	0.0092	0.0180
1.8580	0.0290	7080	368	0.1730	0.0090	0.0193
1.9290	0.0320	7027	358	0.1676	0.0085	0.0187
2.0040	0.0330	7629	368	0.1783	0.0086	0.0196
2.0840	0.0350	7737	376	0.1807	0.0088	0.0199
2.1690	0.0370	8309	392	0.1822	0.0086	0.0201
2.2590	0.0400	8890	394	0.1850	0.0082	0.0203
2.3540	0.0420	7897	369	0.1646	0.0077	0.0180
2.4550	0.0450	8050	390	0.1673	0.0081	0.0184
2.5640	0.0480	9504	406	0.1923	0.0082	0.0208
2.6800	0.0520	9404	419	0.1884	0.0084	0.0206
2.8020	0.0550	8489	387	0.1707	0.0078	0.0187
2.9380	0.0600	10046	412	0.1976	0.0081	0.0212
3.0780	0.0630	9561	393	0.1748	0.0072	0.0189
3.2310	0.0680	9756	408	0.1832	0.0077	0.0198
3.3960	0.0740	10034	413	0.1879	0.0077	0.0203
3.5740	0.0790	10057	405	0.1831	0.0074	0.0196
3.7660	0.0860	10372	406	0.1795	0.0070	0.0191
3.9730	0.0930	10896	418	0.1761	0.0068	0.0188
4.2000	0.1010	10687	408	0.1668	0.0064	0.0178
4.4450	0.1100	10869	407	0.1658	0.0062	0.0174
4.7130	0.1190	11457	421	0.1655	0.0061	0.0175
5.0010	0.1320	12164	431	0.1699	0.0060	0.0179
5.3250	0.1440	11571	436	0.1599	0.0060	0.0170
5.6780	0.1590	11046	423	0.1498	0.0057	0.0159
6.0640	0.1760	10241	432	0.1325	0.0056	0.0142
6.5000	0.1950	7829	418	0.0976	0.0052	0.0108
6.9690	0.2150	6095	399	0.0740	0.0048	0.0087
7.4980	0.2430	3749	394	0.0485	0.0051	0.0070
8.1050	0.2720	3934	392	0.0520	0.0052	0.0073
8.7730	0.3060	3394	403	0.0448	0.0053	0.0069
9.5200	0.3460	2395	411	0.0331	0.0057	0.0065
10.3920	0.3950	2100	408	0.0304	0.0059	0.0066
11.3730	0.4530	1891	429	0.0294	0.0067	0.0073
12.4990	0.5250	1812	425	0.0297	0.0070	0.0075
13.8240	0.6060	1287	452	0.0218	0.0077	0.0080
15.3590	0.7190	1254	438	0.0213	0.0074	0.0077
17.1830	0.8460	1299	482	0.0217	0.0080	0.0083
19.3360	1.0180	1362	490	0.0219	0.0079	0.0082

Table 21: Neutron energy, γ -ray peak area, and cross sections (σ_c) for the 277.6 keV $5/2^+ \rightarrow 3/2^+$ ^{239}Pu γ -ray from the 98+99 data. $\delta\sigma_\gamma$ is the uncertainty in the cross section due to γ -ray statistics and peak-fitting.

E_n (MeV)	δE_n (MeV)	Area	Δ_{Area}	σ (barns)	$\Delta\sigma_\gamma$ (barns)	$\Delta\sigma$ (barns)
1.3210	0.0180	3834	333	0.1115	0.0123	0.0097
1.3650	0.0190	3777	314	0.0998	0.0107	0.0083
1.4090	0.0190	4113	342	0.1040	0.0111	0.0086
1.4550	0.0210	4798	348	0.1149	0.0114	0.0083
1.5040	0.0220	4902	353	0.1123	0.0111	0.0081
1.5560	0.0230	4645	295	0.1016	0.0094	0.0065
1.6100	0.0240	5530	333	0.1153	0.0104	0.0069
1.6670	0.0250	5671	343	0.1187	0.0108	0.0072
1.7280	0.0270	5719	330	0.1165	0.0103	0.0067
1.7920	0.0280	7055	361	0.1347	0.0113	0.0069
1.8580	0.0290	7392	357	0.1349	0.0111	0.0065
1.9290	0.0320	7322	367	0.1305	0.0109	0.0065
2.0040	0.0330	7672	341	0.1339	0.0107	0.0060
2.0840	0.0350	8416	378	0.1468	0.0118	0.0066
2.1690	0.0370	8486	367	0.1390	0.0111	0.0060
2.2590	0.0400	9259	383	0.1440	0.0114	0.0060
2.3540	0.0420	8520	352	0.1326	0.0104	0.0055
2.4550	0.0450	8976	373	0.1393	0.0109	0.0058
2.5640	0.0480	9604	399	0.1451	0.0114	0.0060
2.6800	0.0520	9760	397	0.1460	0.0114	0.0059
2.8020	0.0550	9882	376	0.1484	0.0114	0.0056
2.9380	0.0600	10596	397	0.1556	0.0119	0.0058
3.0780	0.0630	10709	399	0.1462	0.0112	0.0054
3.2310	0.0680	10626	398	0.1490	0.0114	0.0056
3.3960	0.0740	10774	400	0.1507	0.0115	0.0056
3.5740	0.0790	11638	415	0.1583	0.0120	0.0056
3.7660	0.0860	11038	388	0.1427	0.0107	0.0050
3.9730	0.0930	11971	406	0.1446	0.0108	0.0049
4.2000	0.1010	11669	392	0.1360	0.0102	0.0046
4.4450	0.1100	13082	400	0.1490	0.0108	0.0046
4.7130	0.1190	12276	388	0.1324	0.0097	0.0042
5.0010	0.1320	12941	408	0.1350	0.0100	0.0043
5.3250	0.1440	12277	424	0.1268	0.0095	0.0044
5.6780	0.1590	12425	439	0.1259	0.0095	0.0044
6.0640	0.1760	10453	418	0.1046	0.0081	0.0042
6.5000	0.1950	8458	378	0.0816	0.0064	0.0036
6.9690	0.2150	6465	363	0.0607	0.0052	0.0034
7.4980	0.2430	4891	343	0.0490	0.0047	0.0034
8.1050	0.2720	4337	338	0.0444	0.0045	0.0035
8.7730	0.3060	3643	309	0.0373	0.0040	0.0032
9.5200	0.3460	3118	322	0.0334	0.0041	0.0034
10.3920	0.3950	2636	305	0.0295	0.0039	0.0034
11.3730	0.4530	2305	311	0.0277	0.0042	0.0037
12.4990	0.5250	2111	370	0.0266	0.0050	0.0047
13.8240	0.6060	2220	312	0.0289	0.0045	0.0041
15.3590	0.7190	1741	268	0.0227	0.0038	0.0035
17.1830	0.8460	1863	295	0.0239	0.0041	0.0038
19.3360	1.0180	1730	304	0.0214	0.0040	0.0038

Figure 1: Schematic of the GEANIE (Germanium Array for Neutron Induced Excitations) spectrometer at LANSCE/WNR (Los Alamos Neutron Science Center/Weapons Neutron Research) facility.

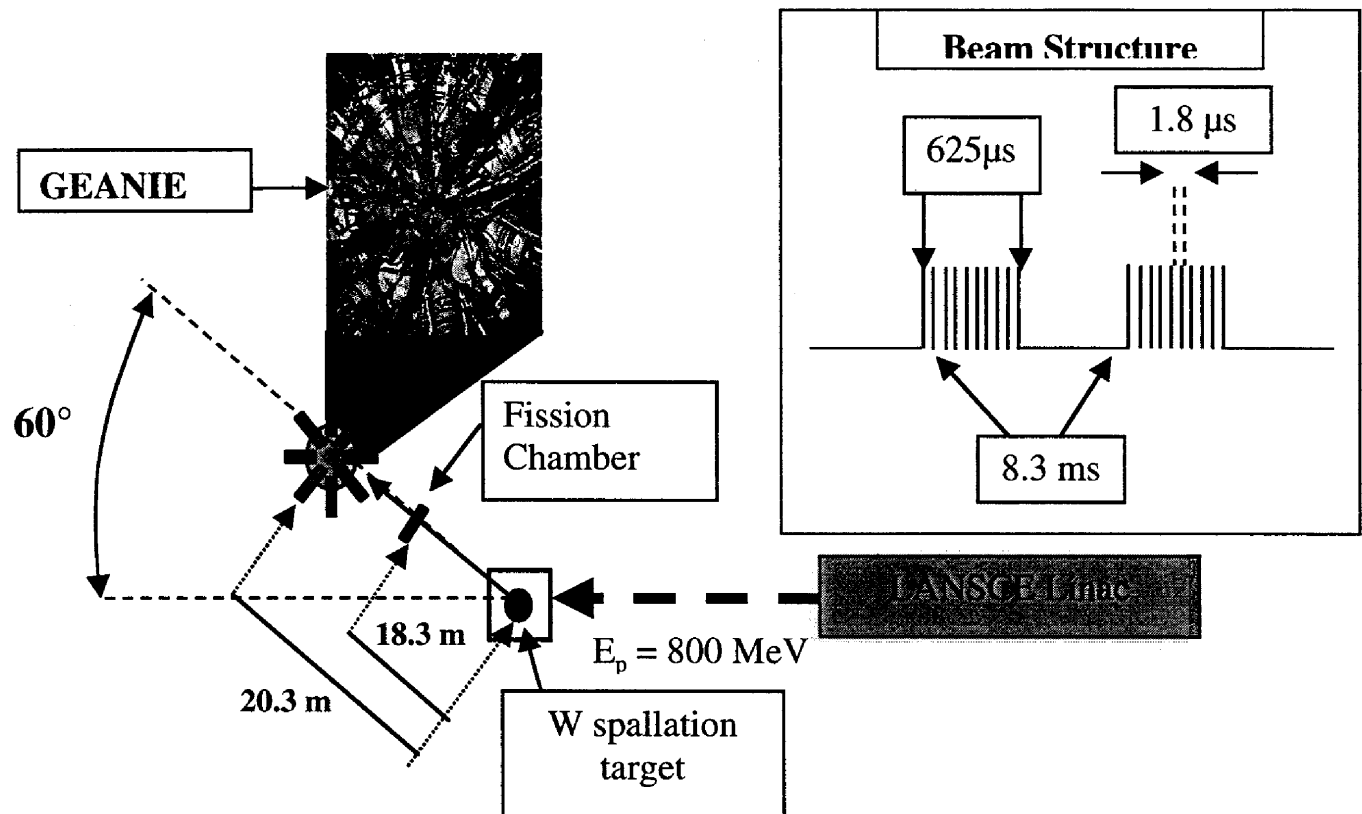


Figure 2: Time-of-Flight (TOF) Spectrum for the planar detectors. The TOF-random background subtraction level is shown by the red dashed line.

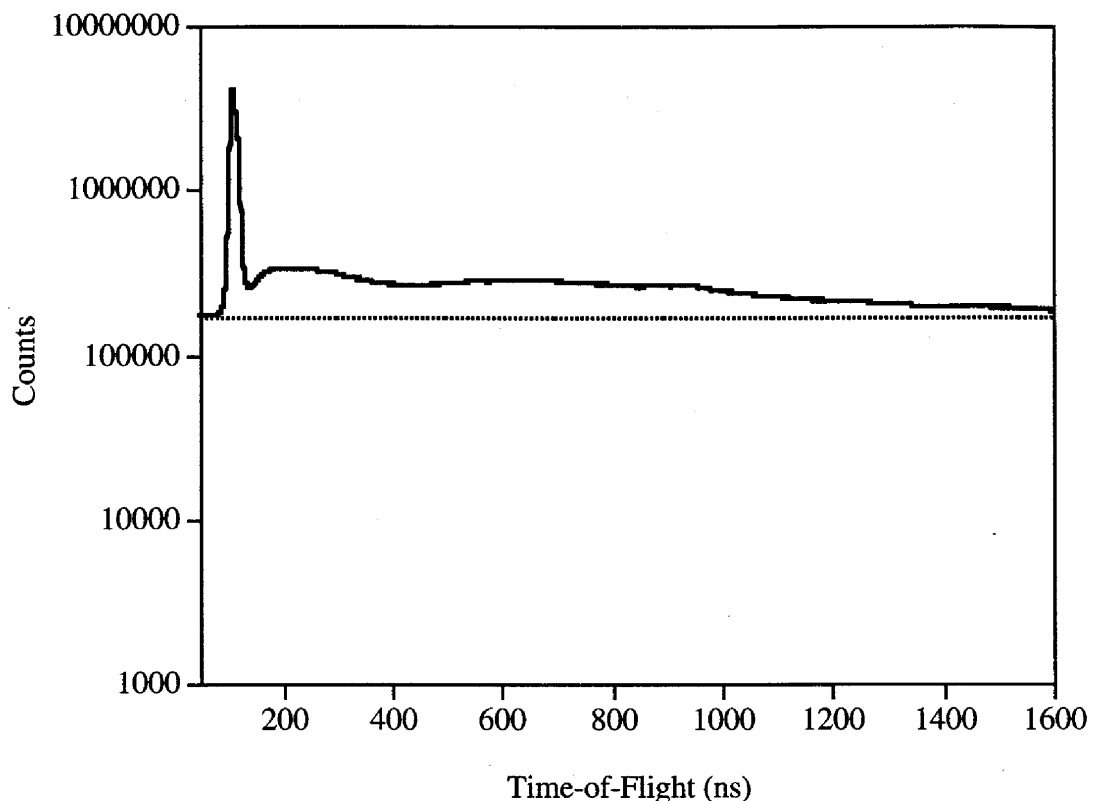


Figure 3a: Neutron energy gated spectra and fits in the energy region near the ^{238}Pu $6^+ \rightarrow 4^+$ with $E_\gamma = 157.4$ keV. The energy calibration is given by $E_\gamma = A + B(\text{channel})$ where $A = -0.171$ and $B = 0.1278$. Green arrows indicate the location of $6^+ \rightarrow 4^+$.

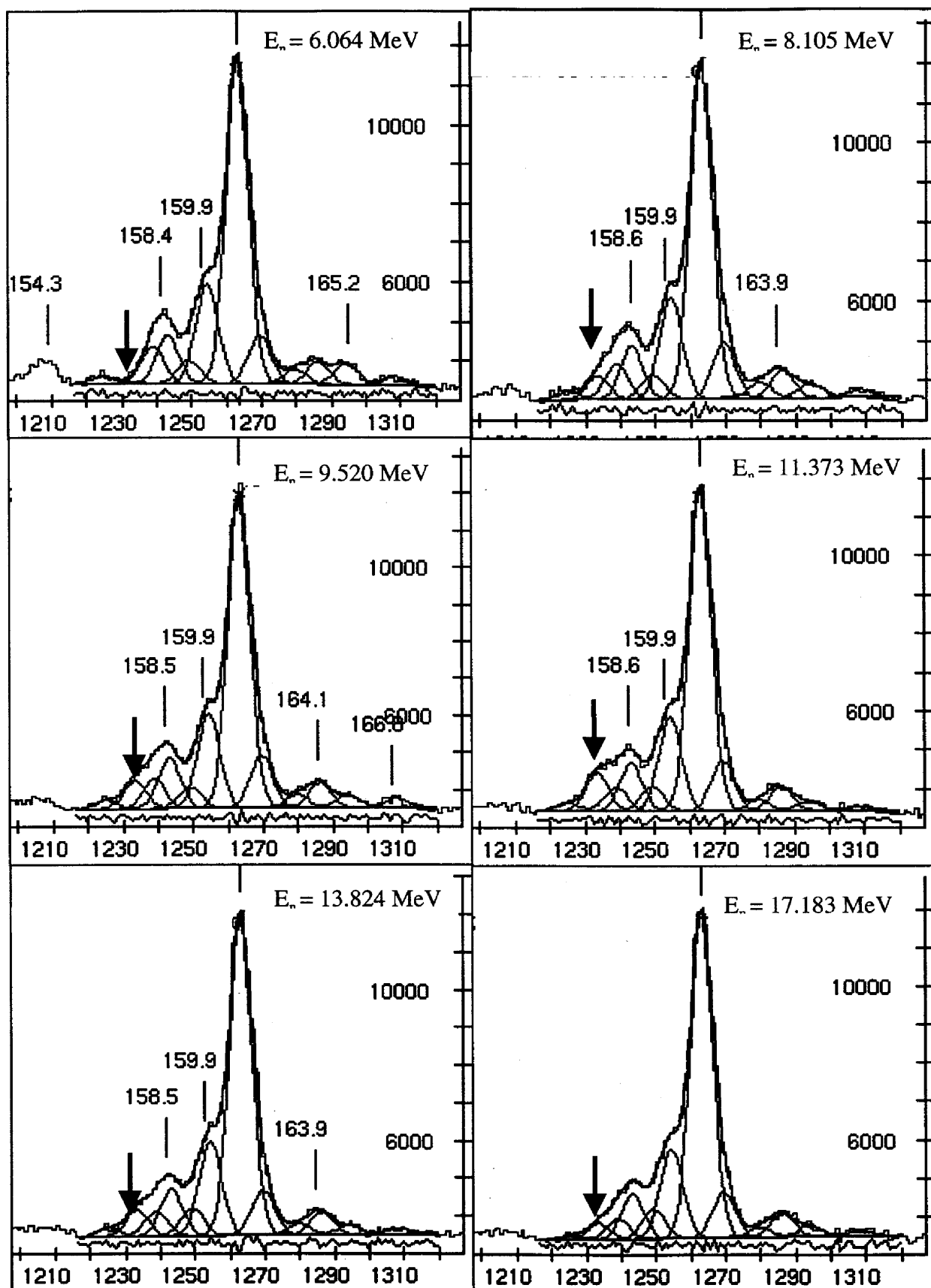


Figure 3b: Neutron energy gated spectra and fits in the energy region near the ^{238}Pu $8 \rightarrow 6$ with $E_n = 210.0$ keV. The energy calibration is given by $E_\gamma = A + B(\text{channel})$ where $A = -0.56$ and $B = 0.1278$. Green arrows indicate the location of $8^+ \rightarrow 6^+$.

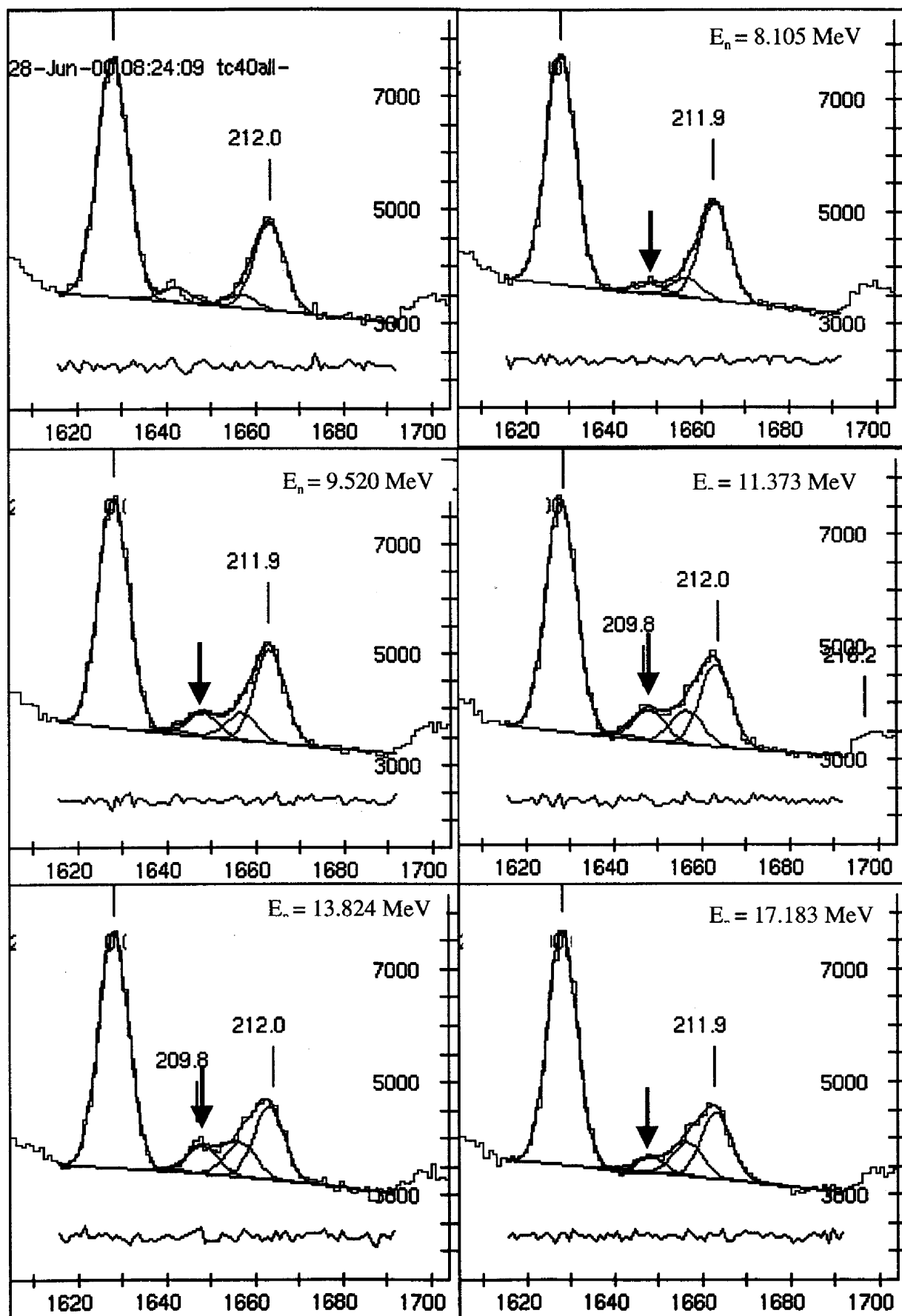


Figure 3c: Neutron energy gated spectra and fits near the ^{238}Pu $4^- \rightarrow 4^+$ and $2^- \rightarrow 2^+$ with $E_\gamma = 936.6$ and 924.0 keV respectively. The energy calibration is given by $E_\gamma = A + B(\text{channel})$ where $A = -1.80$ and $B = 0.1278$. Green arrows indicate the location of transitions.

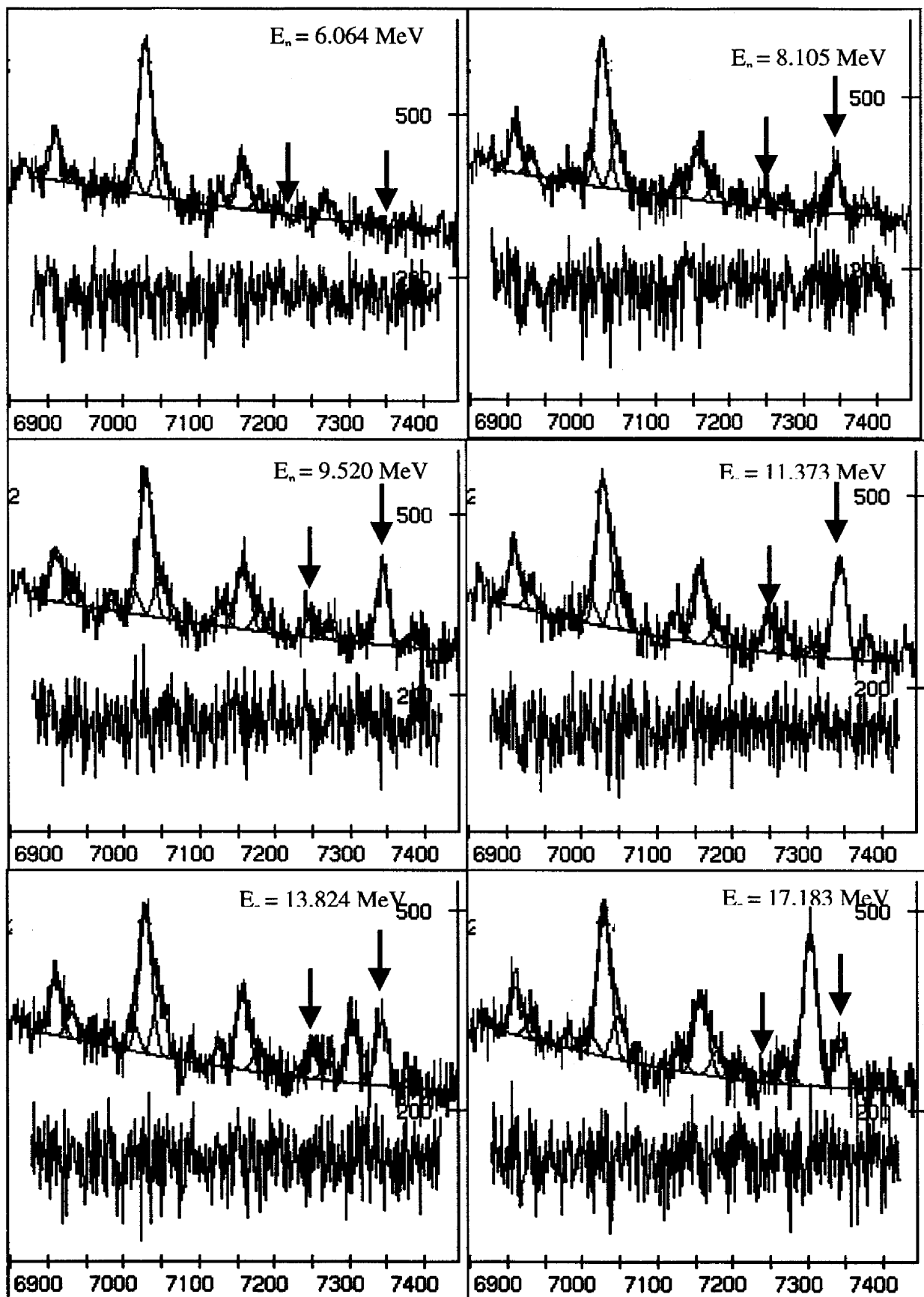


Figure 4a-b: Overlay plot (a) of the γ -ray spectra in the vicinity of the $6^+ \rightarrow 4^+$ transition in the ground state band of ^{238}Pu with $E_n = 11.373 \pm 0.453$ MeV. The green-dashed line indicates the location of the $6^+ \rightarrow 4^+$ transition. The red spectrum has had no background subtracted and the blue spectrum has had a “TOF-random” background spectrum subtracted from it. The second panel shows the peak area of the the $6 \rightarrow 4$ transition in ^{238}Pu as a function of incident neutron energy derived from the two different approaches.

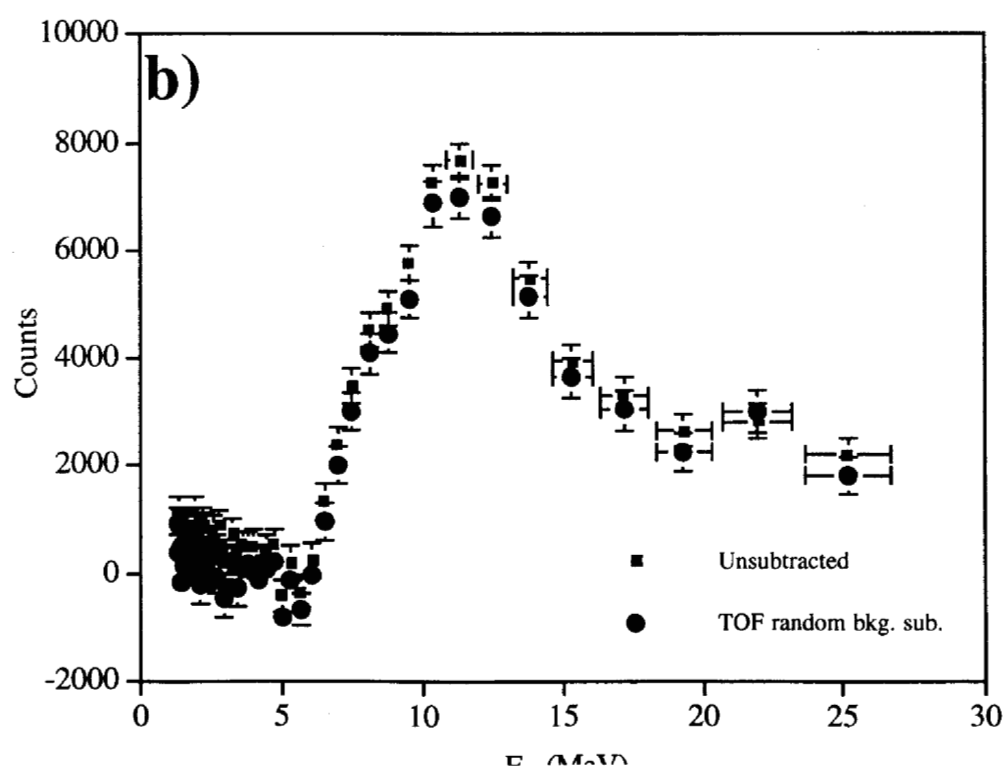
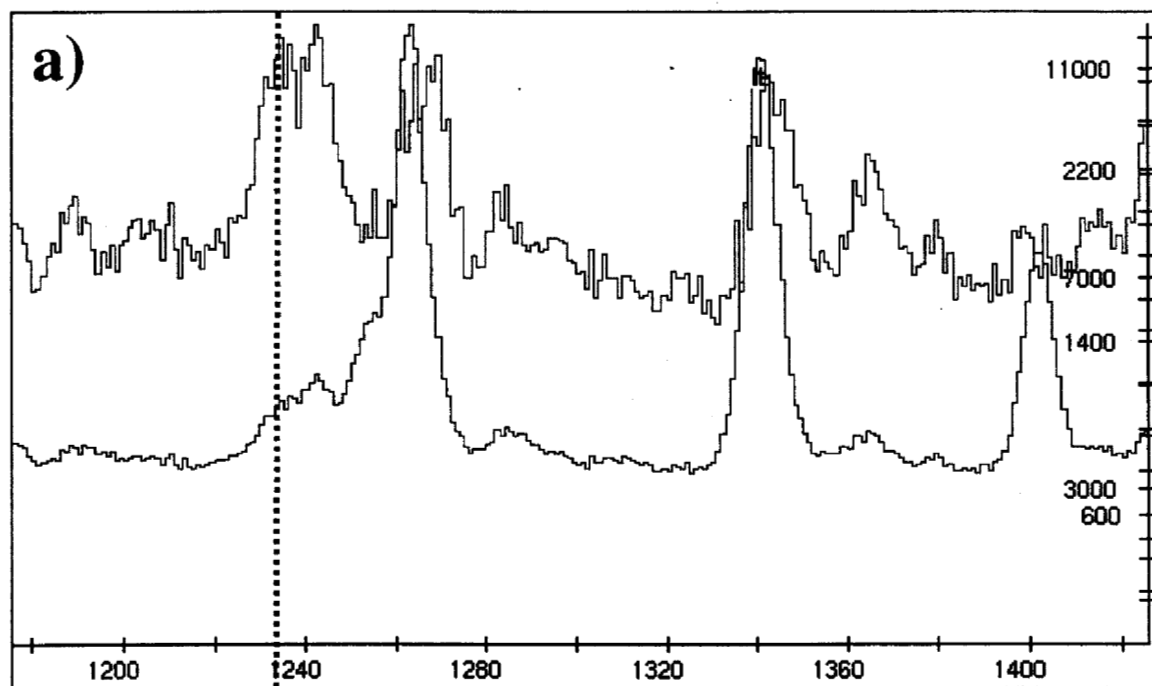


Figure 5: Pulse Height (a) and fission-gated TOF (b) projections from the E vs. TOF matrix for the ^{235}U fission chamber from the 1999 thin target run. The γ -flash location is shown in (b) figure by the solid green arrow. The dashed green lines in (a) figure indicate the fission gate used to obtain the spectrum in (b).

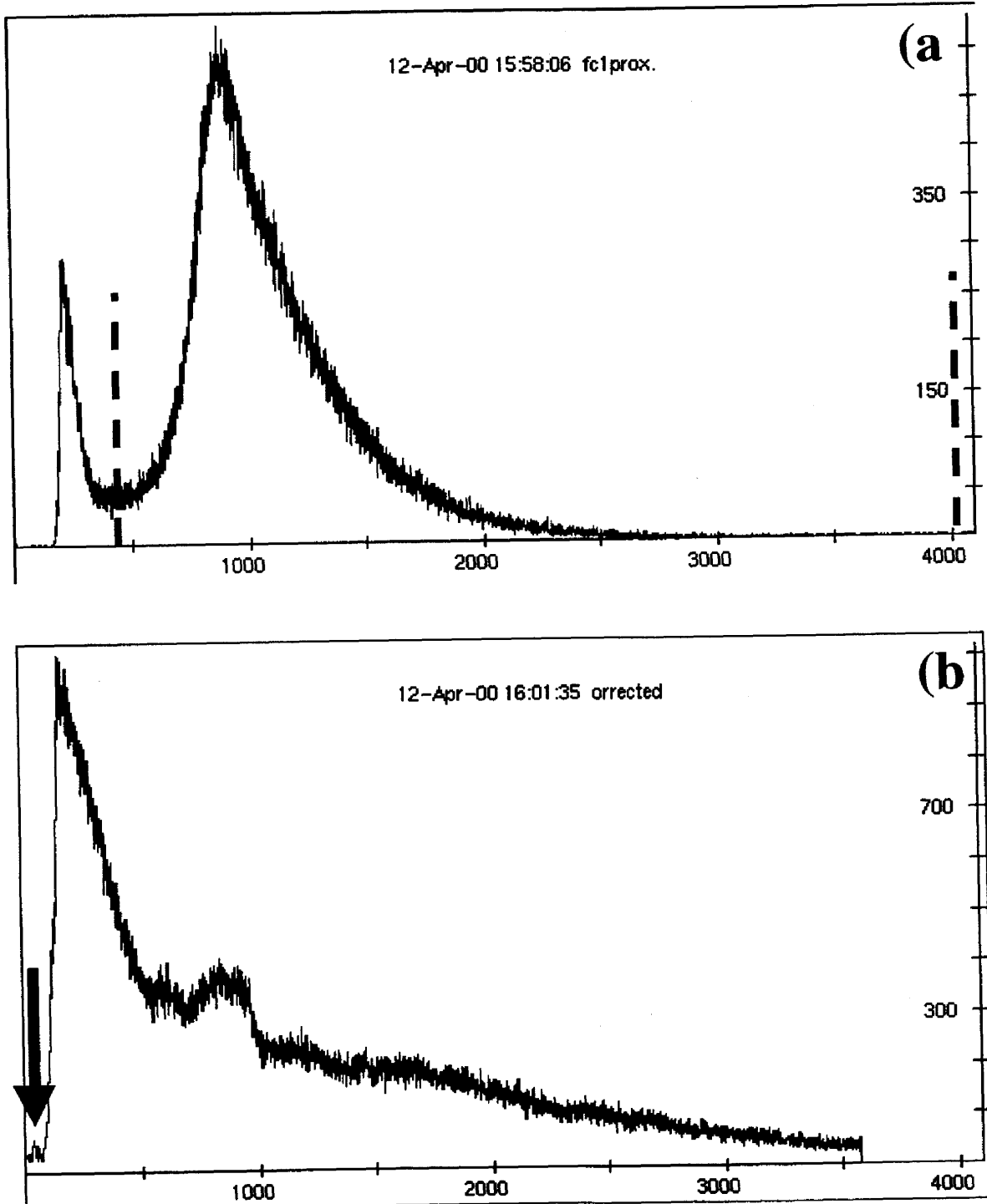


Figure 6: The neutron fluences determined from the 1999 thin target fission chambers using the procedure described in [You00]. The ^{235}U fission chamber is shown in the red and the ^{238}U fission chamber is shown in the black.

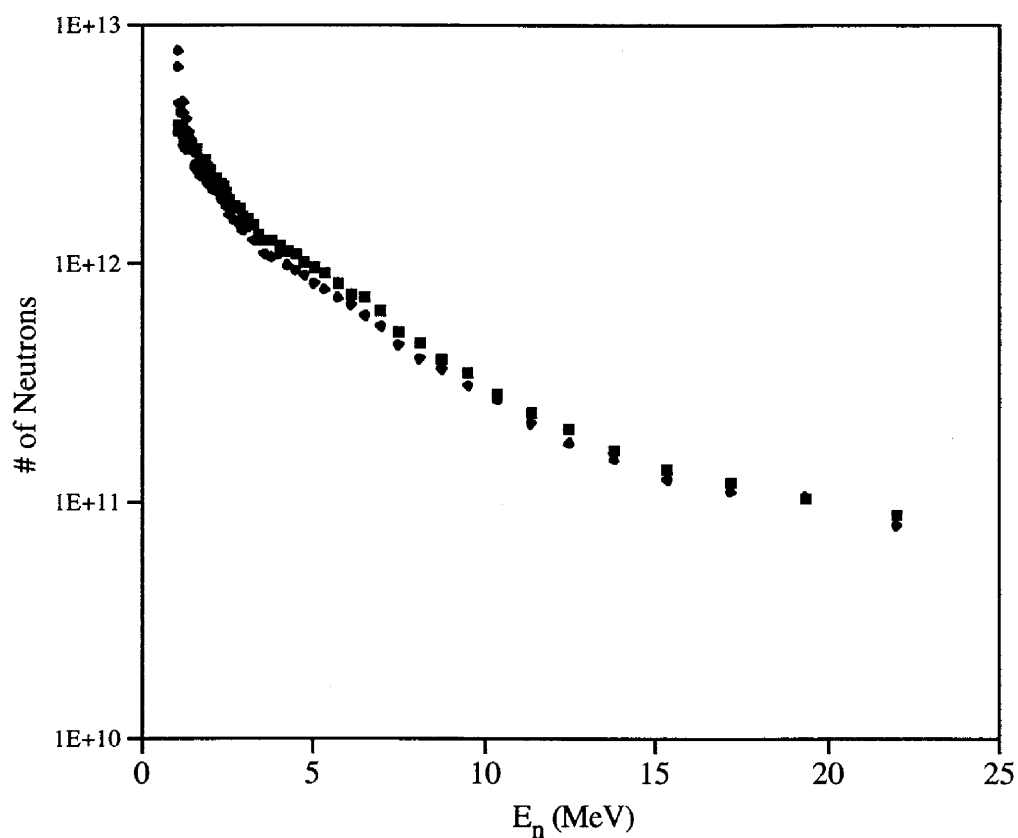


Figure 7: The partial γ -ray cross sections obtained for the ^{54}Fe 847 keV transition from the 1999 data set using the (a) ^{235}U and the (b) ^{238}U fission chamber foils. The point in green is the evaluated result from the reference [Sim98].

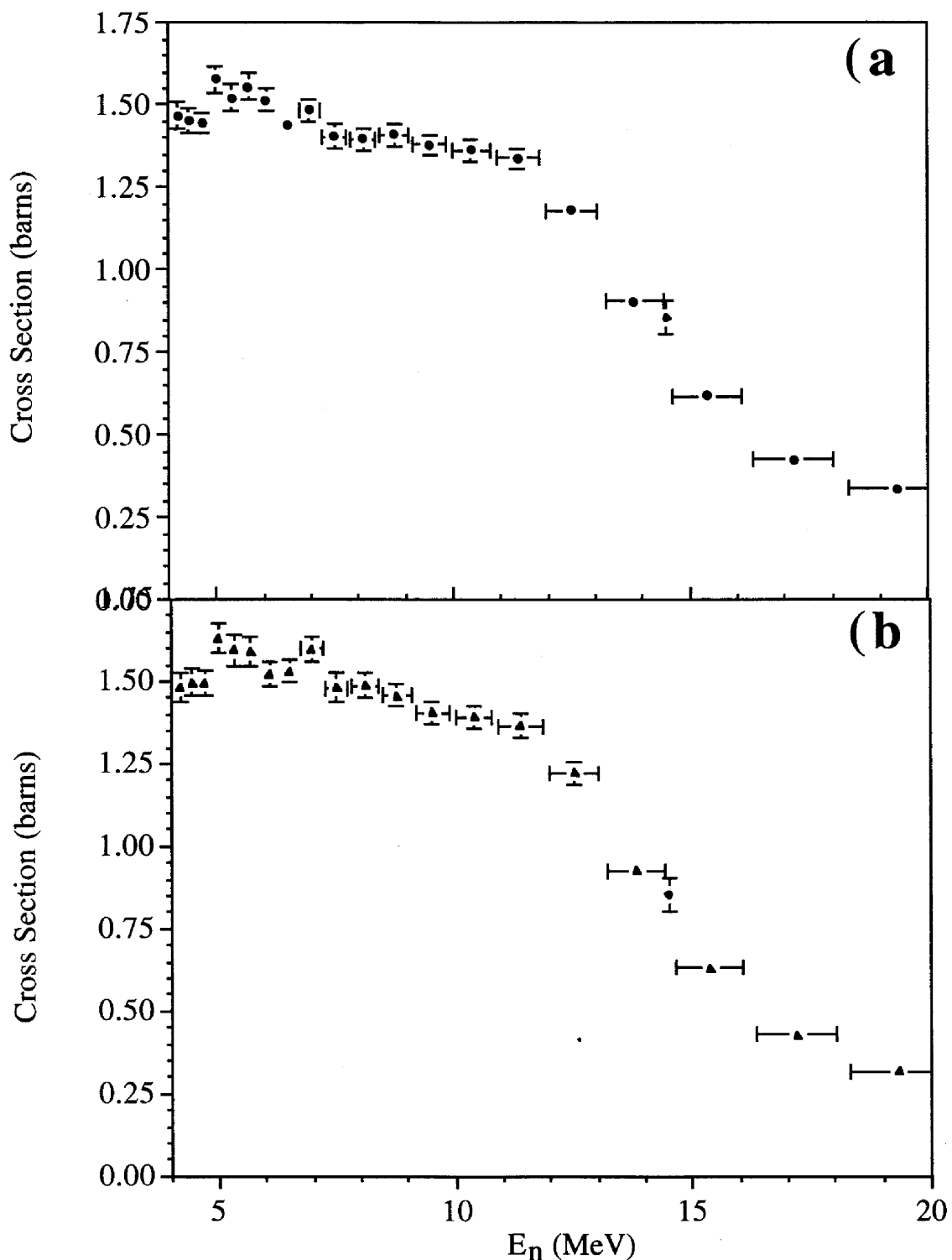


Figure 8: Intensity of the ^{238}Pu ground state band $6 \rightarrow 4$ transition in the 11 planar detectors as a function of detector angle normalized by the 161.3 keV target activity line [MIR00] (a) and the different detector efficiencies [McN00] and live-times (b). The bottom two plots show the average for each angle-grouping and the best fit for the angular distribution.

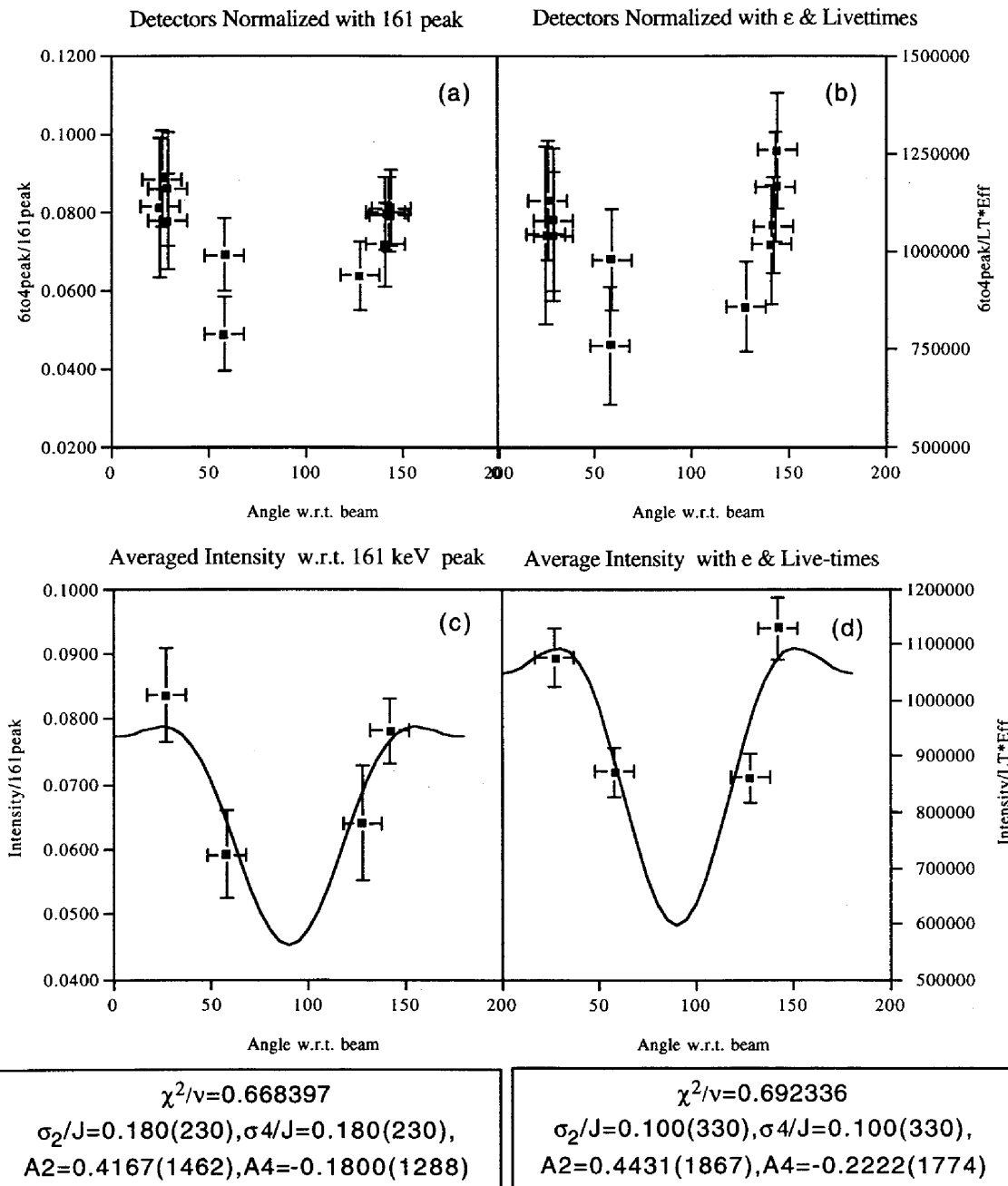


Figure 9: The extracted γ -ray partial cross sections obtained using the ^{235}U fission chamber for the 1998 thin (red), thick (green) and 1999 thin (blue) data sets (a) and the summed 1998 and 1999 data (b).

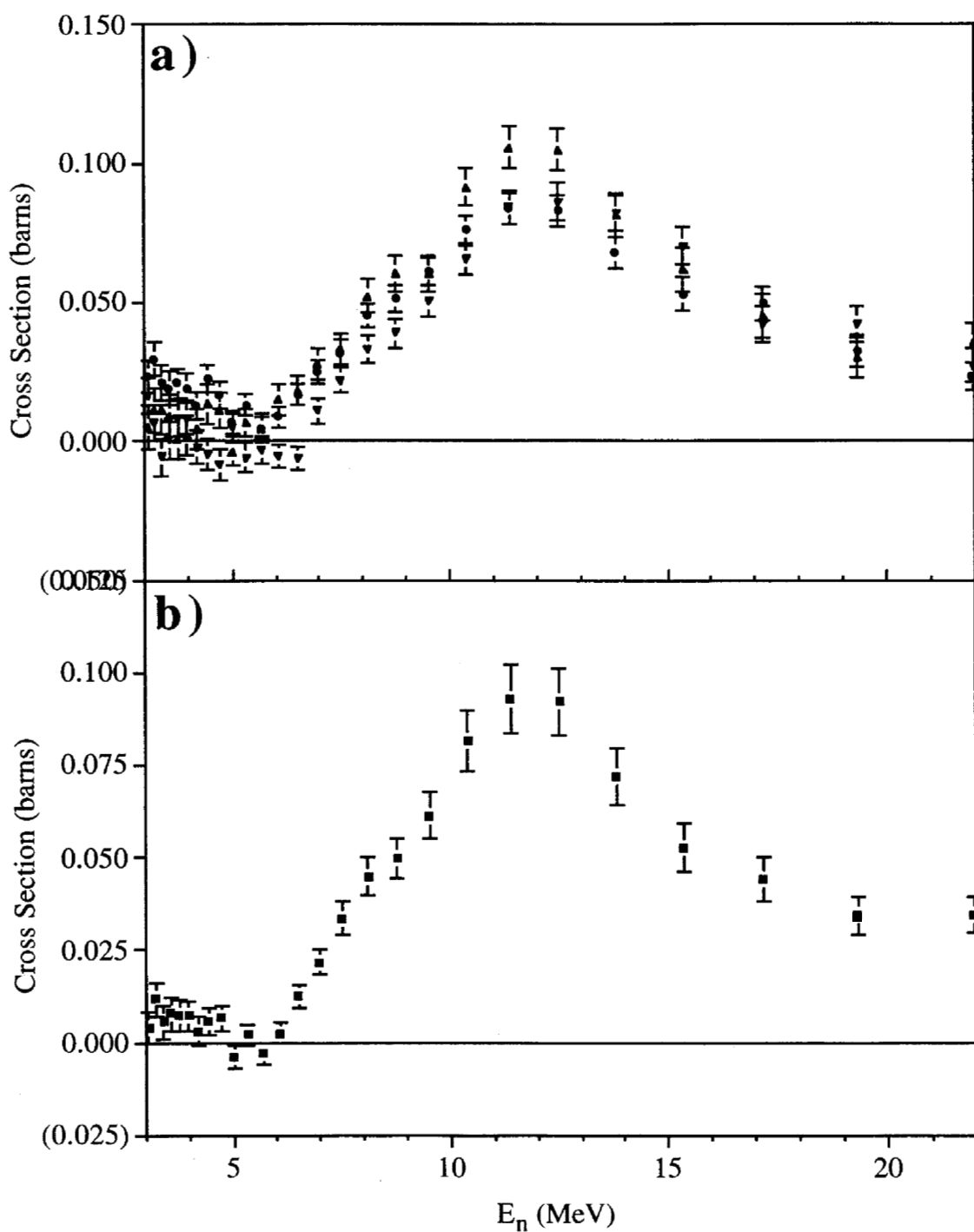


Figure 10: Energy calibration for the summed 1998+ 1999 data (a) and the residual. The equations for the curve fit are in the inset in the upper left hand corner.

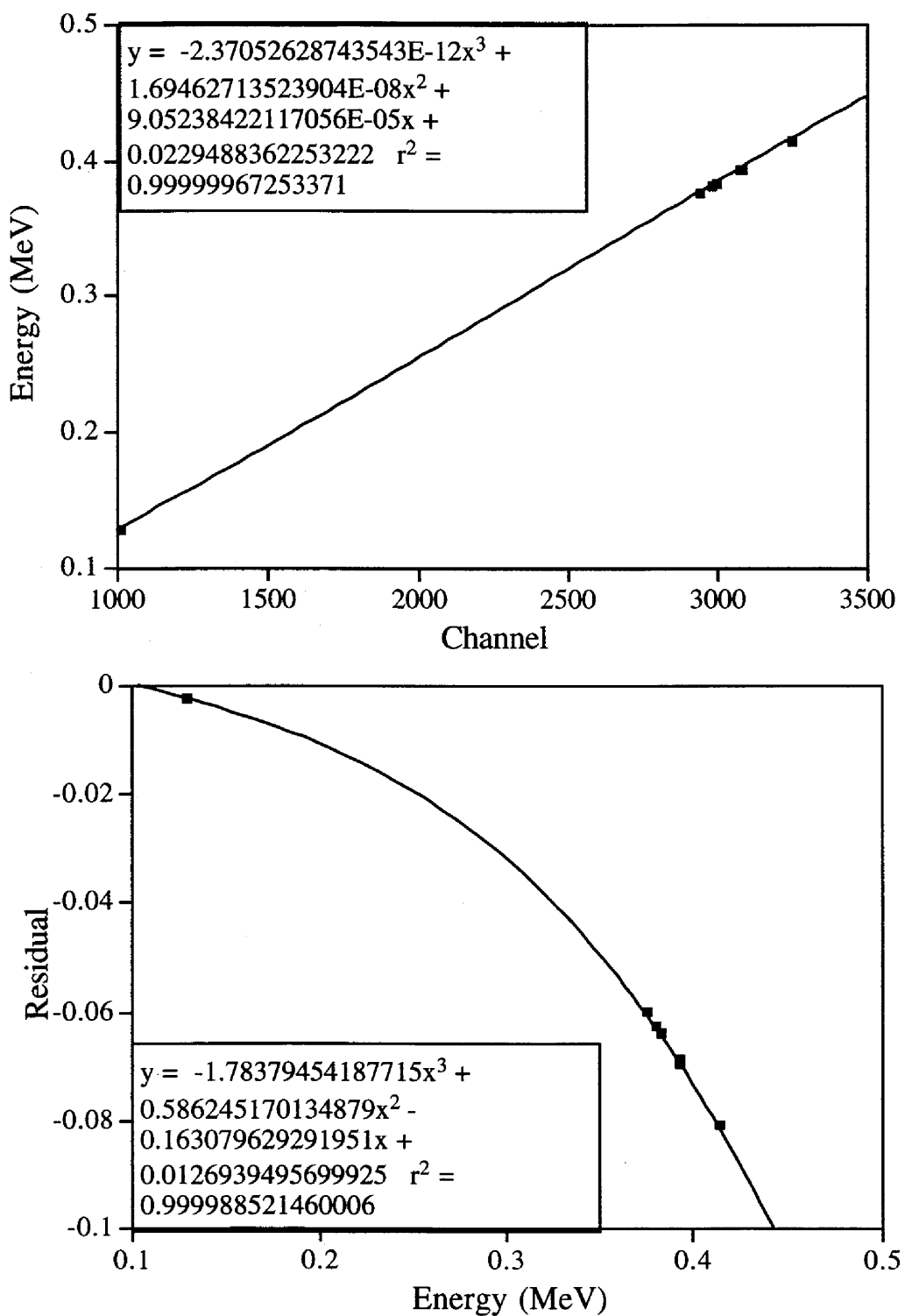


Figure 11: Absolute partial cross sections for the ground state band $6 \rightarrow 4$ (top) and $8 \rightarrow 6$ (bottom) in ^{238}Pu . GNASH calculations from [Cha99] (solid green lines) and [Cha00] (solid red lines) are also displayed.

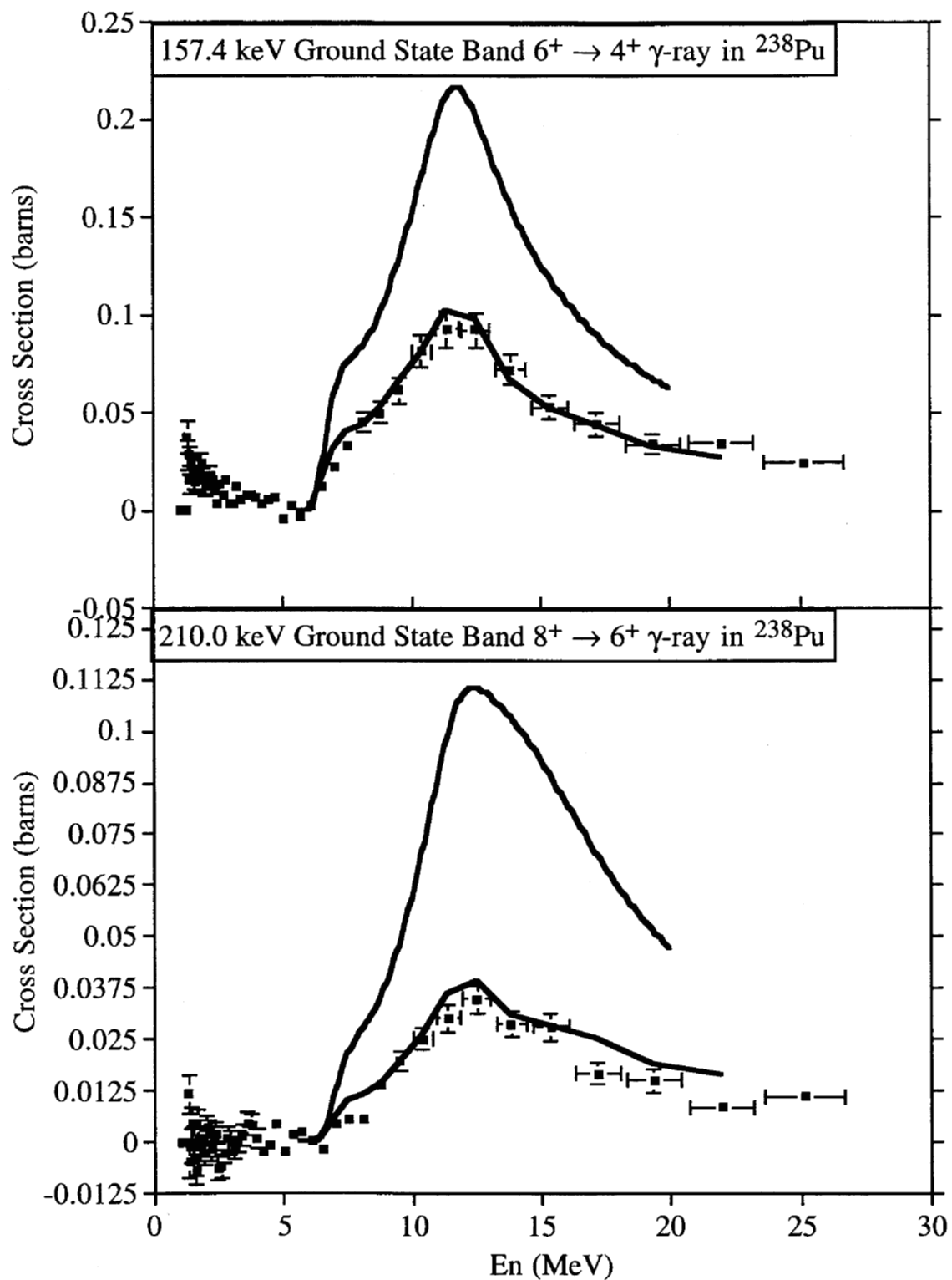


Figure 12: Absolute partial cross sections for the 4^- ($E_x=1028$ keV) $\rightarrow 4^+$ (top) and the 2^- ($E_x=968$ keV) $\rightarrow 2^+$ transitions in ^{238}Pu . GNASH calculations from [Cha99] (solid green lines) and [Cha00] (solid red lines) are also displayed.

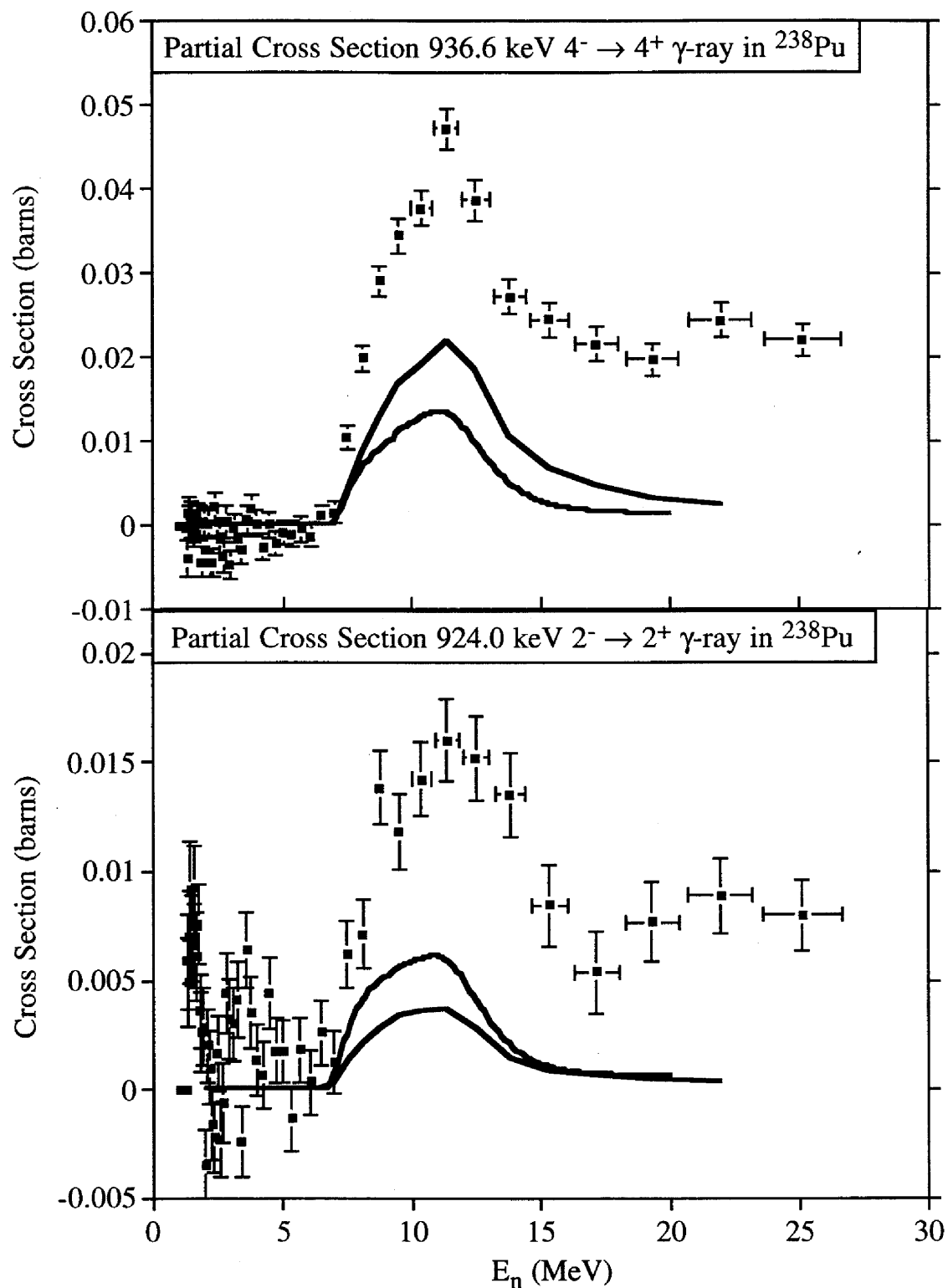


Figure 13: Absolute partial cross sections for the 1^- ($E_x=963$ keV) $\rightarrow 0$ (top) and the $^+ 1^-$ ($E_x=963$ keV) $\rightarrow 2^+$ (bottom) transitions in ^{238}Pu . Note that there appears to be a baseline offset for the $1^- \rightarrow 2^+$ transition of approximately ≈ 5 mb. GNASH calculations [Cha99] (green solid lines) are also displayed.

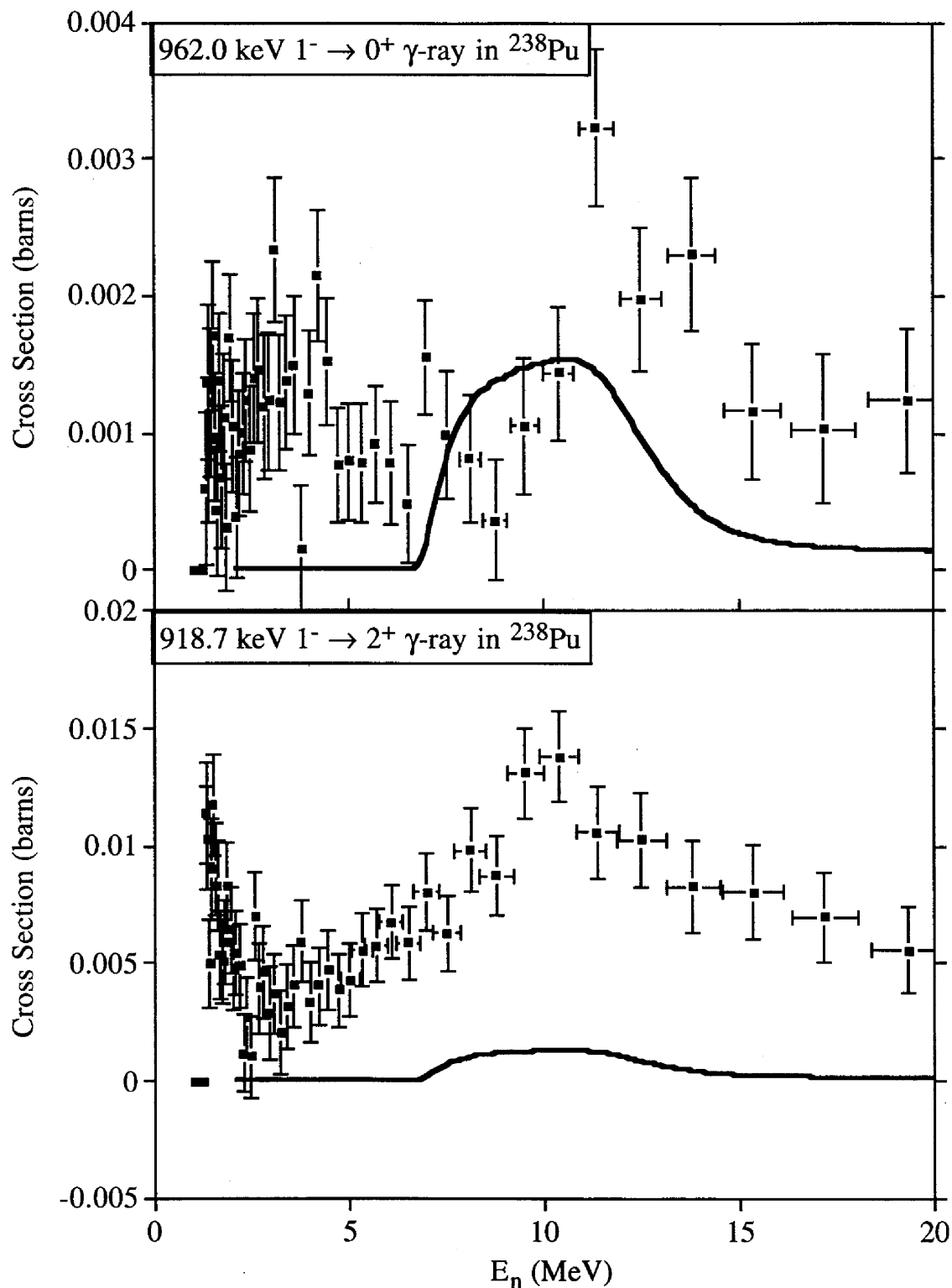


Figure 14: Absolute partial cross sections for the 5^- ($E_x=763.8$ keV) $\rightarrow 6^+$ (top) transitions and the 617.3 keV $5/3^- \rightarrow 4^+/2^+$ (bottom) transitions in ^{238}Pu . GNASH calculations [Cha99] (solid green lines) are also displayed. Note that both transitions appear to have slight offsets due to uncertainties in the background level.

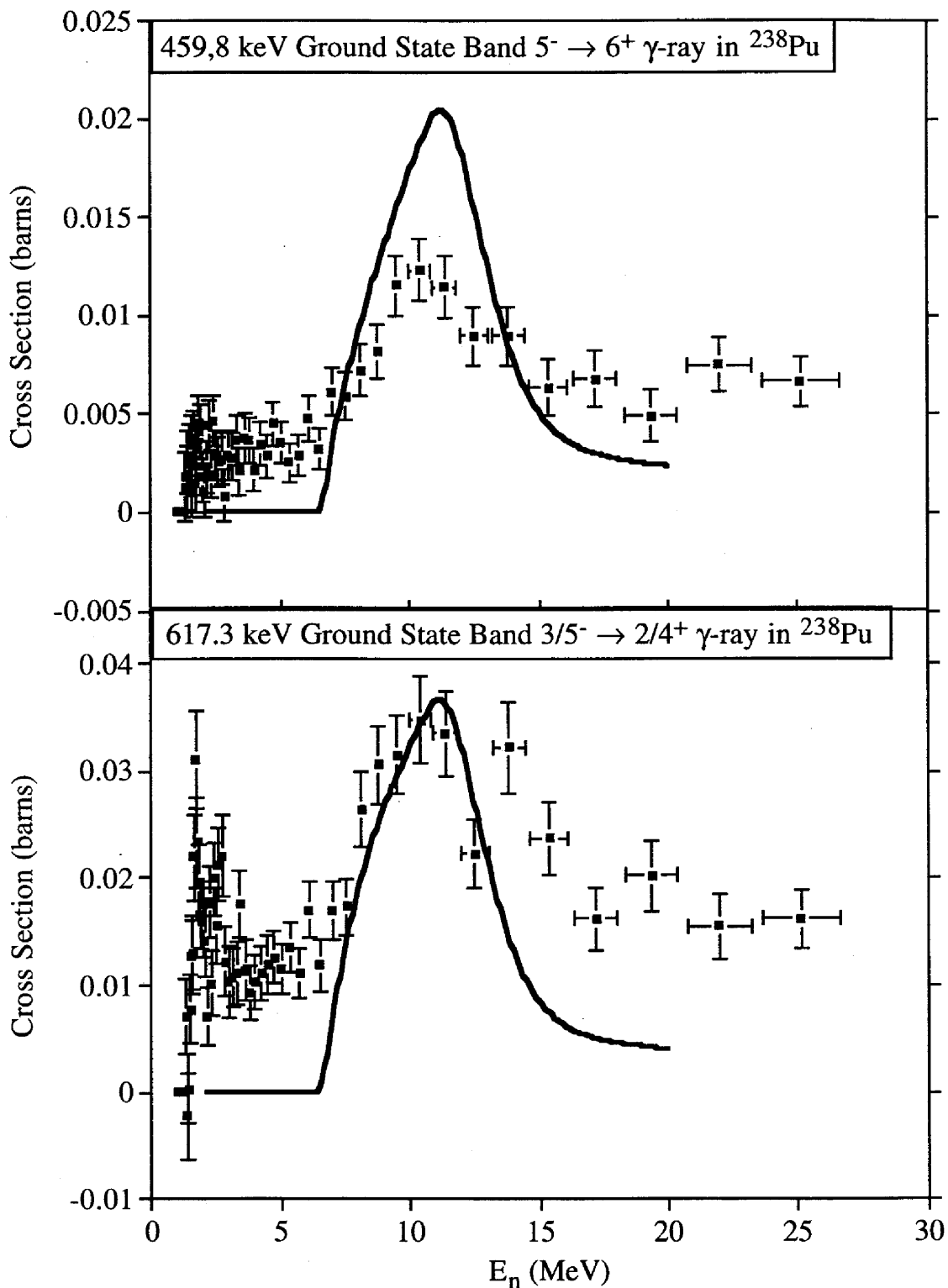


Figure 15: Absolute partial cross sections for the $13/2^+$ ($E_x=318.1$ keV) $\rightarrow 9/2^+$ (top) and the 226.4 keV $5/2^- \rightarrow 5/2^+$ (bottom) transitions in ^{239}Pu . GNASH calculations [Cha99] (solid green lines) are also displayed where available.

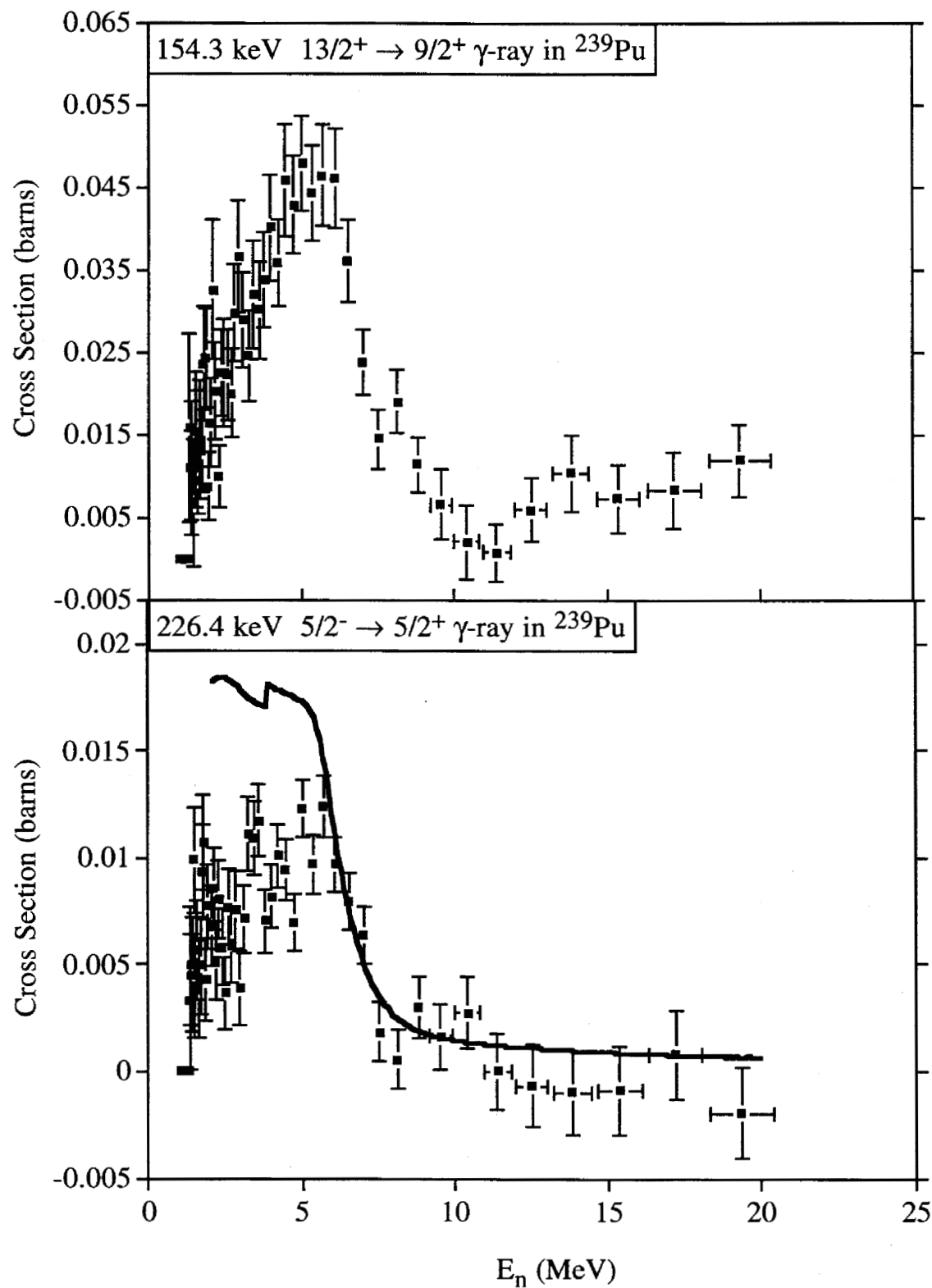


Figure 16: Absolute partial cross sections for the 228.2 keV $5/2^+$ ($E_{\gamma}=285.5$ keV) $\rightarrow 5/2^+$ (top) and the 277.6 keV $5/2^+ \rightarrow 3/2^+$ (bottom) transitions in ^{239}Pu . GNASH calculations [Cha99] are also displayed.

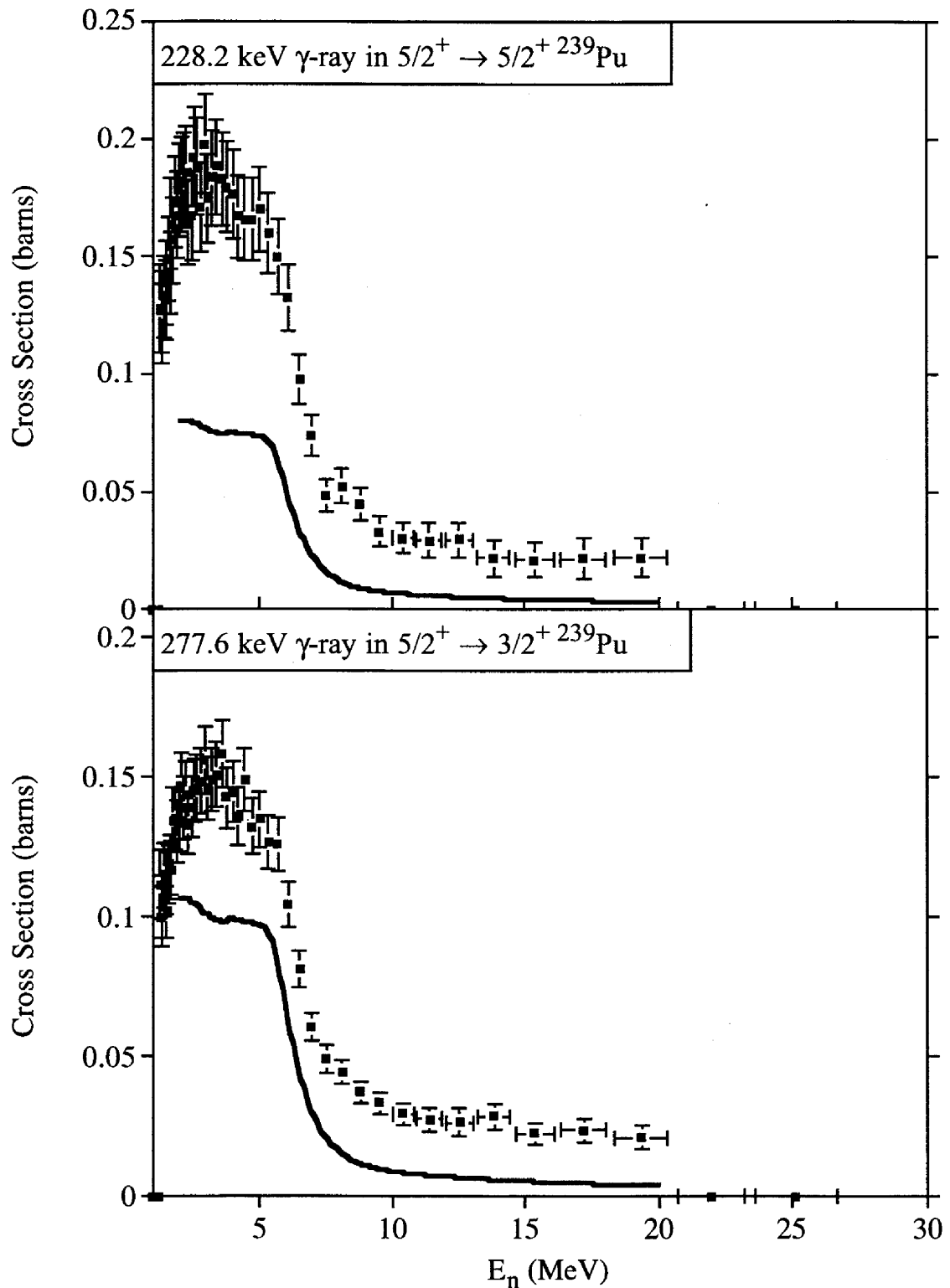


Figure 17: Absolute partial cross sections for the 273.3 keV $7/2^+$ ($E_x=321.0$ keV) $\rightarrow 9/2^-$ transition in ^{237}Pu , the $(n,3n)$ exit channel. GNASH calculations [Cha99] for the incident neutron energies available are also displayed.

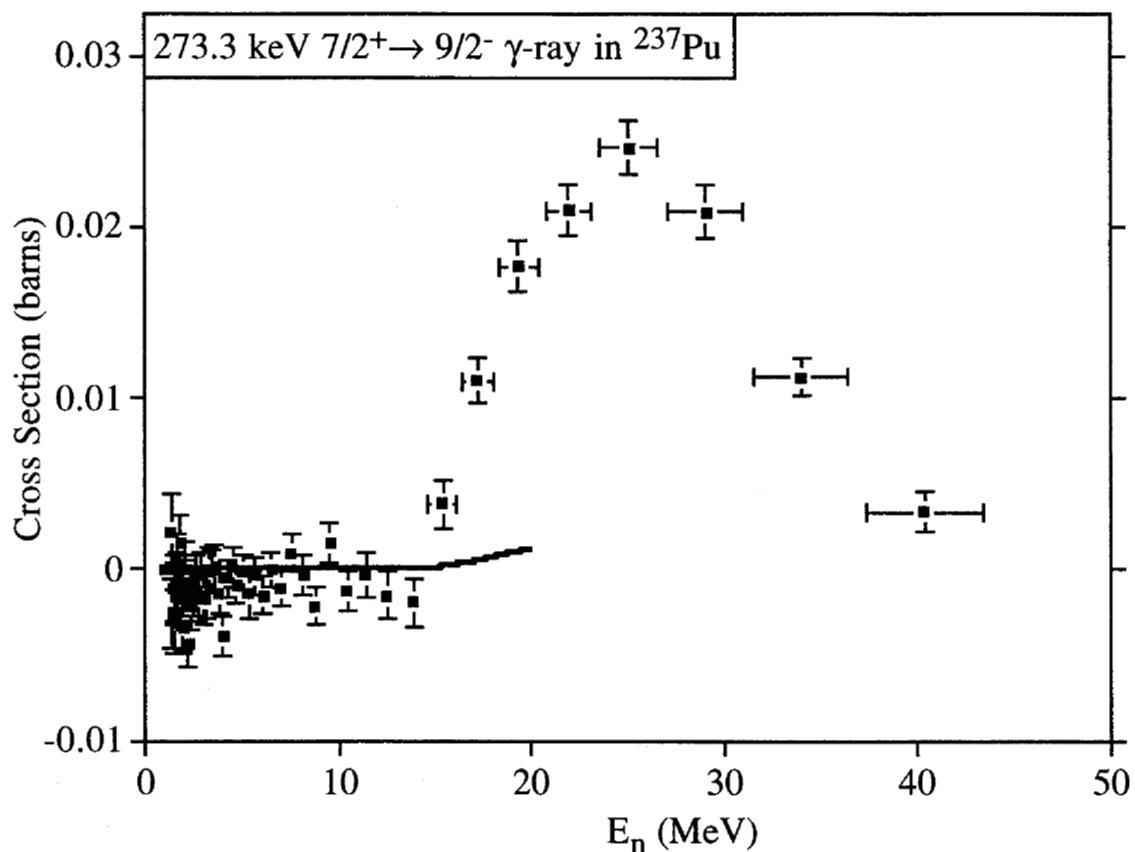


Figure 18: The low-lying levels in ^{238}Pu observed in this experiment. Dashed transitions were not observed. The thickness of the arrows is proportional to the peak intensity of the transition.

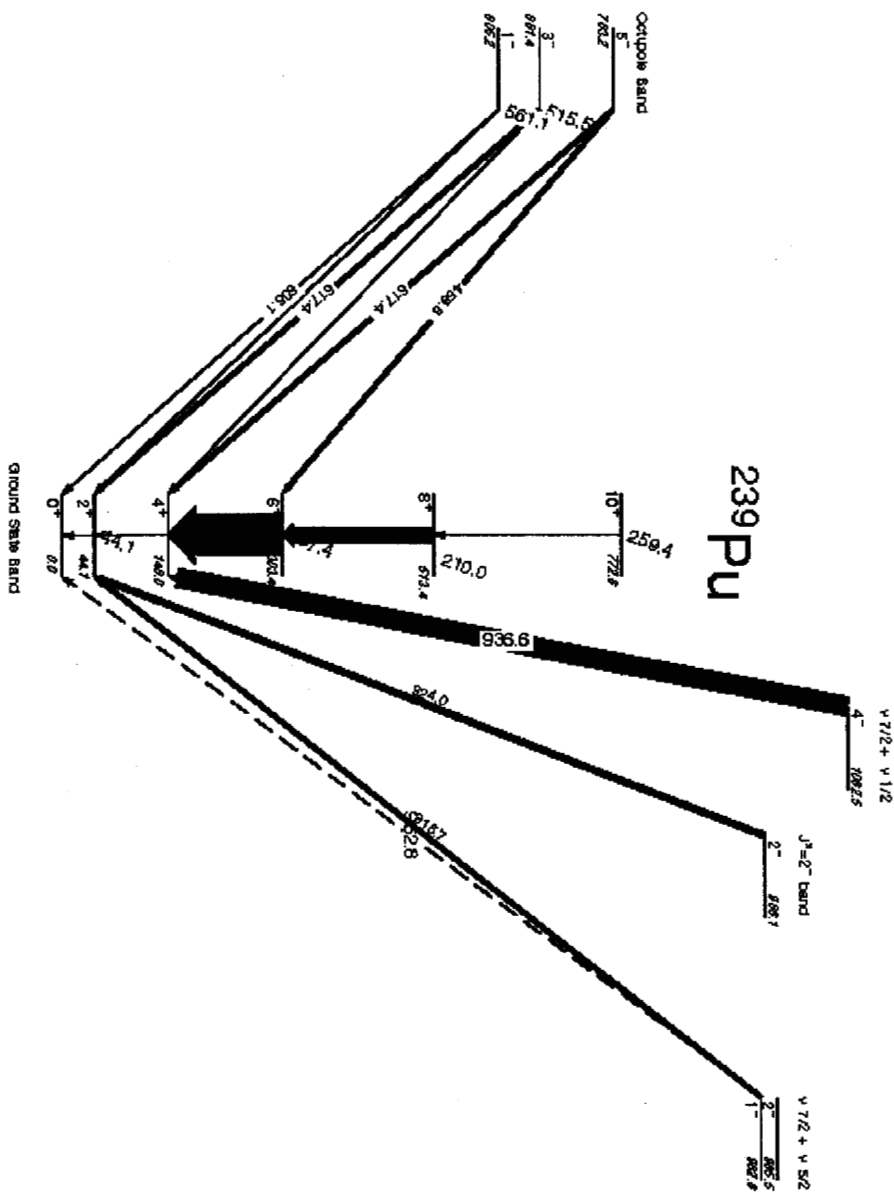


Figure 19a-b: The γ -ray spectrum from the planar detectors corresponding to neutron energies of 11.373 ± 0.453 MeV with $50 < E_n$ (keV) < 900 (a) and the region near the expected location of the $4 \rightarrow 2$ transition in the ground state band in ^{238}Pu .

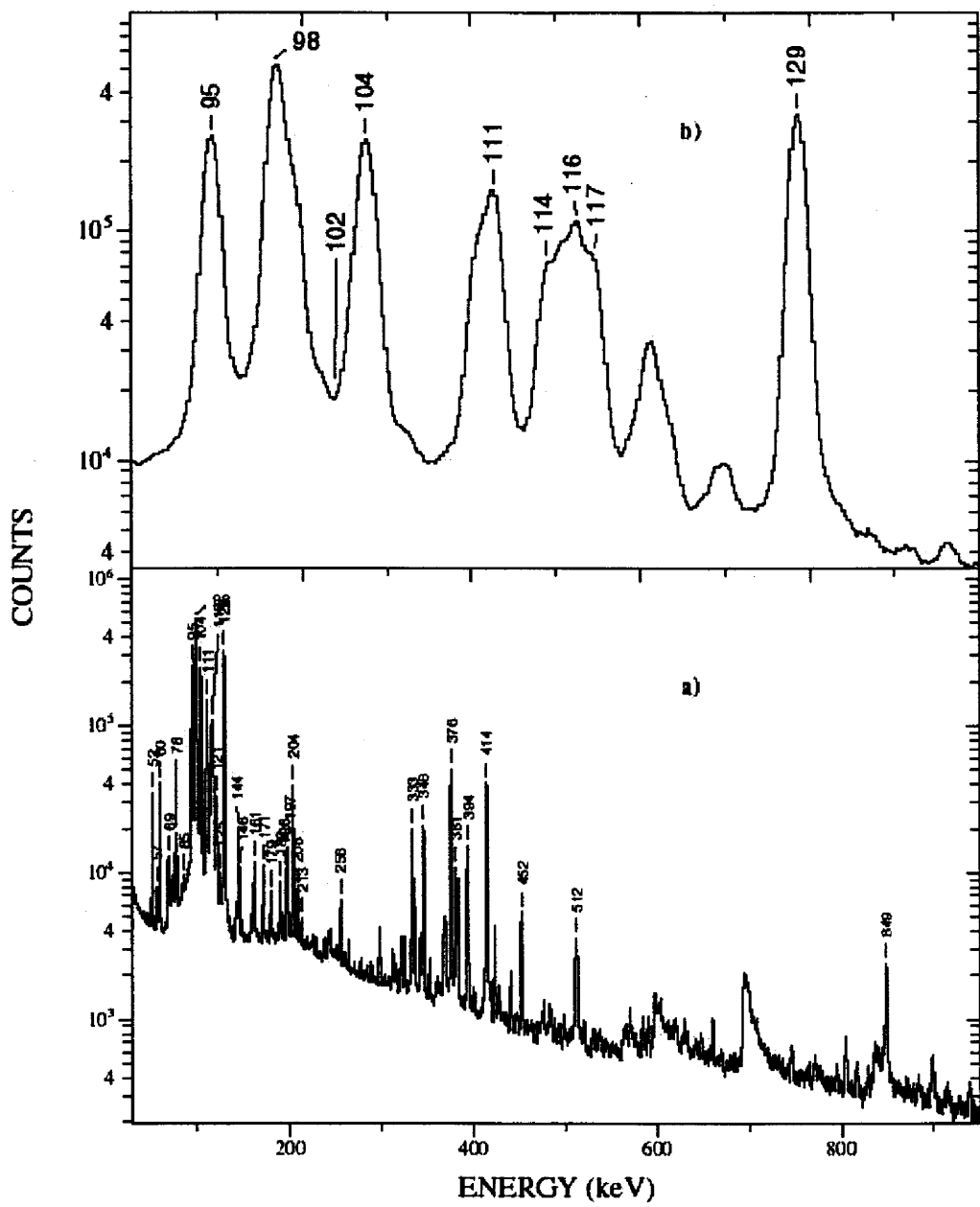


Figure 20: The ratio $6 \rightarrow 4 / 8 \rightarrow 6$ of the ground state band transitions (top) and the strongest side band transition over the $6 \rightarrow 4$ ground state band transition (bottom) from experiment (black points) and [Cha99] (green) and [Cha00] (red).

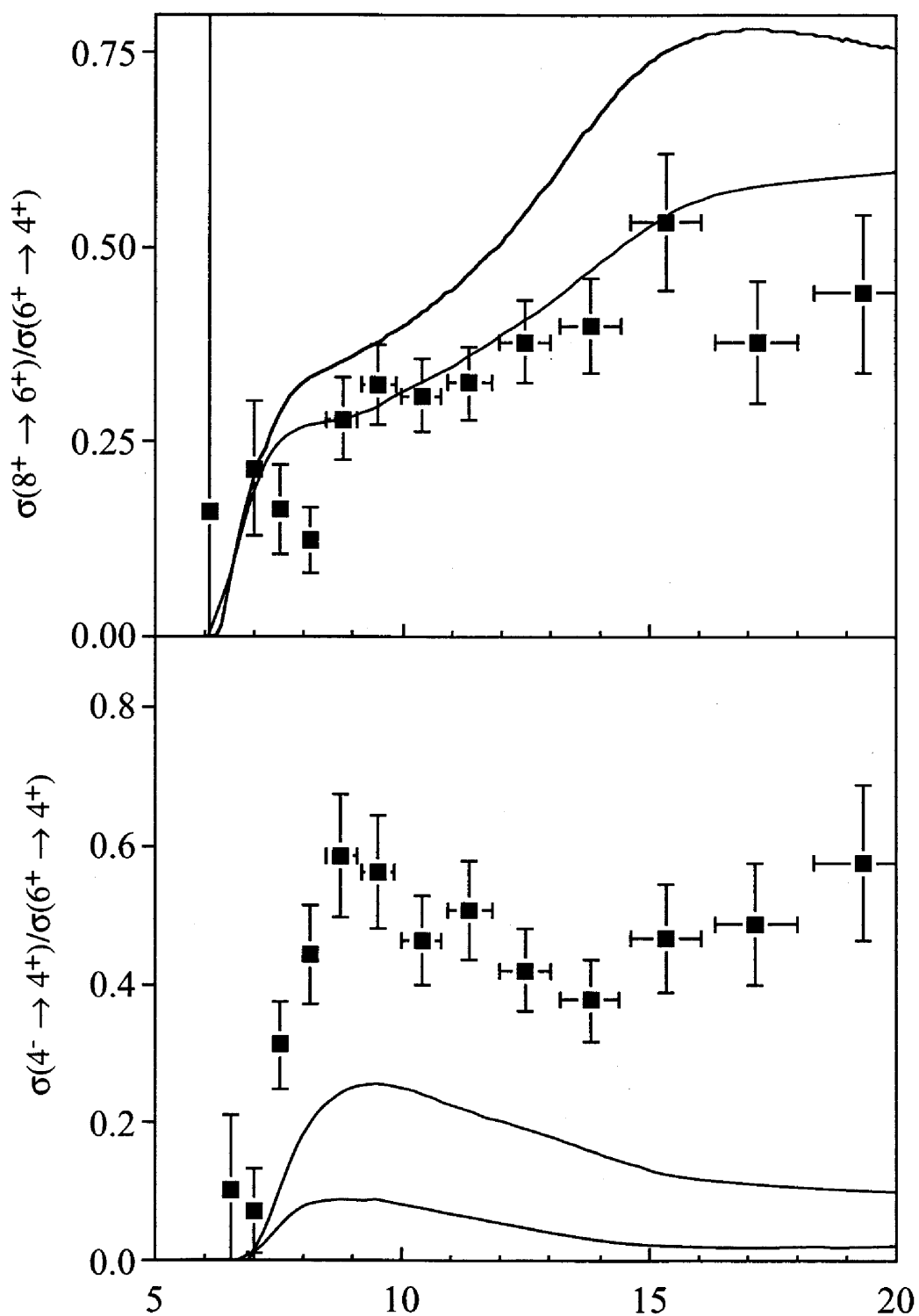


Figure A1: Partial cross sections for the $(n, 2n\gamma)$ lines from the separate 1998 10 mil, 20 mil and 1999 10 mil data sets. The following color scheme is used: 1999 thin target (black squares), 1998 thin target (blue circles), 1998 thick target (red diamonds).

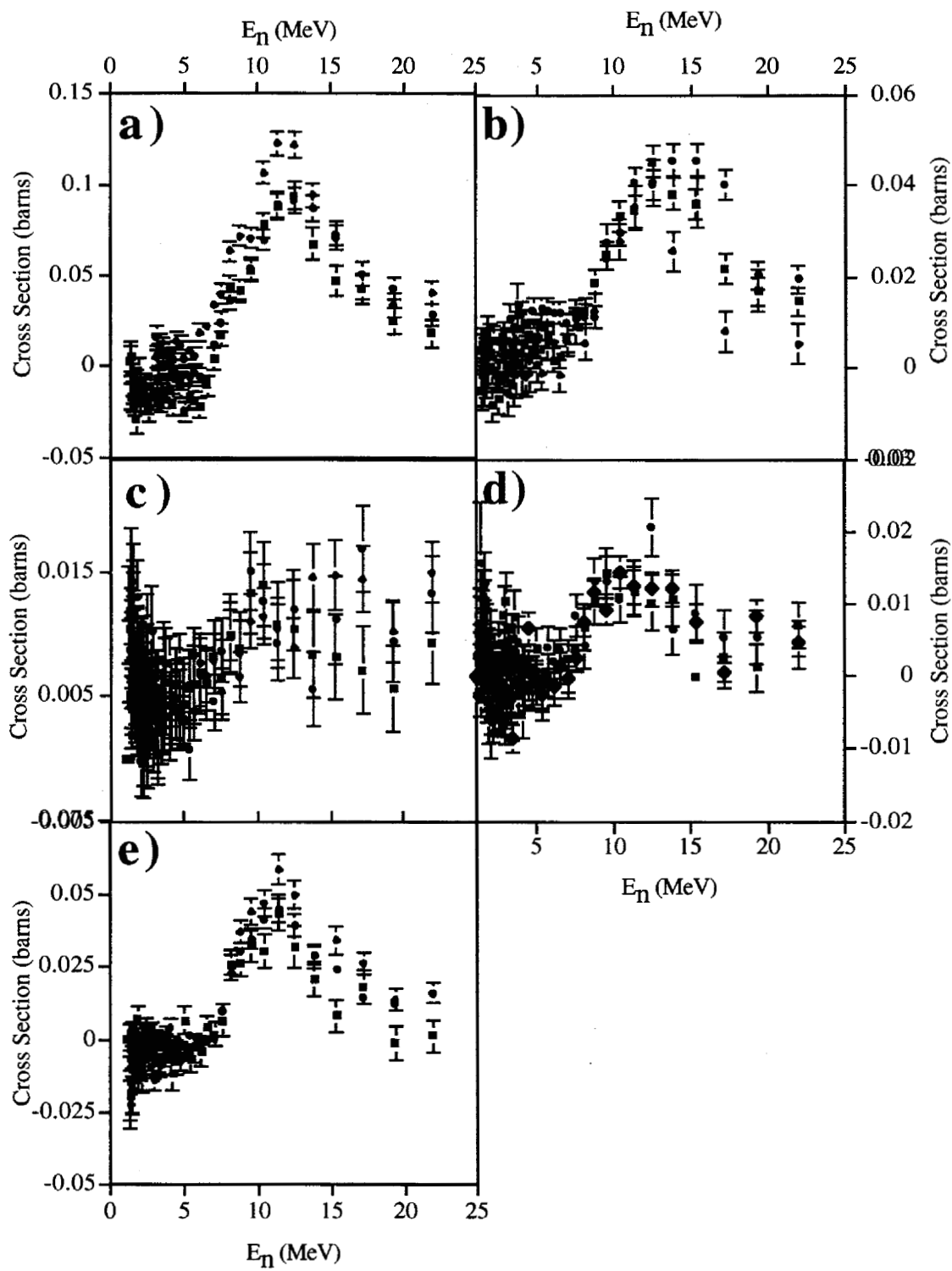
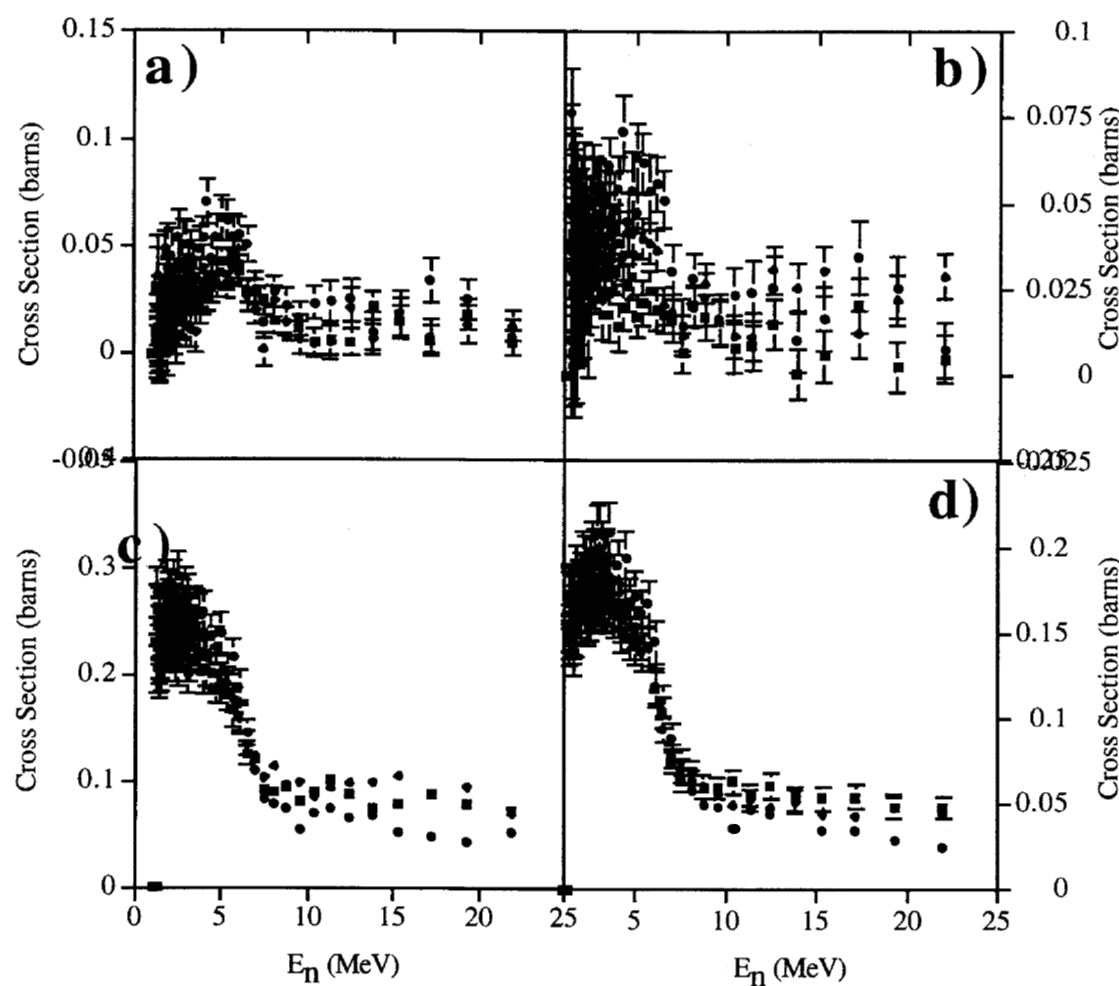


Figure A2: Partial cross sections for the $(n, 2n\gamma)$ lines from the separate 1998 10 mil, 20 mil and 1999 10 mil data sets. The following color scheme is used: 1999 thin target (black squares), 1998 thin target (blue circles), 1998 thick target (red diamonds).



Appendix A: The 1998 thin target, thick target and 1999 data sets.

This appendix contains the separate data for the $(n,xn\gamma)$ cross sections measured in the 1998 thin, 1998 thick and the 1999 thin target runs. The partial cross sections for the transitions marked with an asterisk were assigned using fits optimized using the summed 1998+1999 data sets. Not all of the transitions seen in the summed 1998+1999 data were visible in the separate data sets due to limited statistics. Those transitions that were seen in the individual data sets are listed in Table A1 below. The ^{235}U fission chamber was used to determine the neutron fluence for all data. Angular distribution corrections were not applied to any of the data.

Nucleus	Parent Level		Final Level (J^π, E_x)		E_γ (keV)	Conversion Coefficient
	J^π	E_x (keV)	J^π	E_x (keV)		
^{238}Pu	6^+	303.4	4^+	145.96	157.4	2.242
^{238}Pu	8^+	513.4	6^+	303.4	210.0	0.6891
^{238}Pu	1^-	962.77	2^+	44.1	918.7*	≈ 0
^{238}Pu	3^+	1069.95	4^+	145.96	924.0*	≈ 0
^{238}Pu	4^-	1082.57	4^+	145.96	936.5	≈ 0
^{239}Pu	$13/2^+$	318.1	$9/2^+$	163.76	154.3	2.352
^{239}Pu	$5/2^-$	505.5	$5/2^+$	285.46	226.37*	0.0779
^{239}Pu	$5/2^+$	285.46	$5/2^+$	75.71	228.18	2.734
^{239}Pu	$5/2^+$	285.46	$3/2^+$	7.86	277.60	1.548
^{237}Pu	$7/2^+$	321.0	$9/2^-$	47.7	273.3	0.2925

The following color scheme is used in both of the figures: black squares are the 1999 thin target, blue circles are the 1998 thin target, and red diamonds are the 1998 thick target data. Immediately following the cross sections are the neutron fluences used to determine the cross sections for all three data sets.

Table A2: Data from the ^{235}U fission chamber for the 1998 10 mil experiment.

E_n (MeV)	σE_n (MeV)	Counts	Δ_{Counts}	Neutrons	Δ_{Neutrons}	1/barns	$\Delta_{1/\text{barns}}$
1.321	0.021	2.927E+03	5.410E+01	2.106E+12	4.010E+10	2.513E+06	3.767E+04
1.363	0.021	3.410E+03	5.840E+01	2.331E+12	4.135E+10	2.852E+06	4.108E+04
1.407	0.022	3.479E+03	5.898E+01	2.256E+12	3.963E+10	2.966E+06	4.168E+04
1.454	0.024	3.672E+03	6.060E+01	2.257E+12	3.864E+10	3.075E+06	4.239E+04
1.503	0.025	3.784E+03	6.151E+01	2.202E+12	3.722E+10	3.187E+06	4.322E+04
1.555	0.026	4.138E+03	6.433E+01	2.277E+12	3.693E+10	3.430E+06	4.527E+04
1.608	0.027	4.289E+03	6.549E+01	2.231E+12	3.555E+10	3.515E+06	4.546E+04
1.665	0.029	4.235E+03	6.508E+01	2.081E+12	3.339E+10	3.505E+06	4.536E+04
1.726	0.031	4.347E+03	6.593E+01	2.015E+12	3.195E+10	3.612E+06	4.601E+04
1.79	0.032	4.958E+03	7.041E+01	2.167E+12	3.231E+10	3.968E+06	4.897E+04
1.856	0.034	5.024E+03	7.088E+01	2.069E+12	3.071E+10	4.096E+06	4.958E+04
1.927	0.036	4.990E+03	7.064E+01	1.939E+12	2.886E+10	4.160E+06	4.992E+04
2.002	0.037	5.543E+03	7.445E+01	2.029E+12	2.877E+10	4.322E+06	5.148E+04
2.082	0.041	5.186E+03	7.201E+01	1.788E+12	2.616E+10	4.318E+06	5.067E+04
2.167	0.042	5.742E+03	7.578E+01	1.868E+12	2.610E+10	4.651E+06	5.366E+04
2.255	0.045	6.036E+03	7.769E+01	1.854E+12	2.530E+10	4.769E+06	5.458E+04
2.351	0.048	5.742E+03	7.578E+01	1.665E+12	2.327E+10	4.727E+06	5.428E+04
2.453	0.052	5.749E+03	7.582E+01	1.574E+12	2.198E+10	4.792E+06	5.463E+04
2.561	0.054	6.270E+03	7.918E+01	1.616E+12	2.168E+10	5.019E+06	5.664E+04
2.676	0.059	5.836E+03	7.639E+01	1.419E+12	1.968E+10	4.978E+06	5.610E+04
2.8	0.062	5.962E+03	7.721E+01	1.372E+12	1.885E+10	5.029E+06	5.723E+04
2.935	0.069	6.069E+03	7.790E+01	1.317E+12	1.808E+10	5.100E+06	5.763E+04
3.075	0.071	6.391E+03	7.994E+01	1.307E+12	1.775E+10	5.520E+06	6.233E+04
3.226	0.078	6.370E+03	7.981E+01	1.226E+12	1.666E+10	5.415E+06	6.145E+04
3.392	0.084	6.030E+03	7.765E+01	1.089E+12	1.514E+10	5.390E+06	6.137E+04
3.57	0.092	5.946E+03	7.711E+01	1.009E+12	1.408E+10	5.421E+06	6.140E+04
3.763	0.097	6.571E+03	8.106E+01	1.040E+12	1.388E+10	5.749E+06	6.455E+04
3.971	0.107	6.558E+03	8.098E+01	9.645E+11	1.291E+10	6.047E+06	6.644E+04
4.194	0.114	6.997E+03	8.365E+01	9.585E+11	1.247E+10	6.401E+06	6.964E+04
4.441	0.126	7.189E+03	8.479E+01	9.153E+11	1.175E+10	6.598E+06	7.105E+04
4.706	0.137	7.210E+03	8.491E+01	8.515E+11	1.095E+10	6.854E+06	7.320E+04
4.998	0.15	7.225E+03	8.500E+01	7.996E+11	1.027E+10	7.023E+06	7.503E+04
5.318	0.165	7.436E+03	8.623E+01	7.606E+11	9.629E+09	7.106E+06	7.584E+04
5.672	0.182	7.229E+03	8.502E+01	6.759E+11	8.677E+09	7.265E+06	7.700E+04
6.058	0.201	8.066E+03	8.981E+01	6.377E+11	7.811E+09	7.443E+06	7.629E+04
6.496	0.222	1.020E+04	1.010E+02	6.098E+11	6.767E+09	7.755E+06	7.407E+04
6.962	0.244	1.196E+04	1.093E+02	5.613E+11	5.866E+09	8.050E+06	7.325E+04
7.489	0.277	1.239E+04	1.113E+02	4.725E+11	4.869E+09	7.609E+06	6.790E+04
8.096	0.312	1.285E+04	1.134E+02	4.166E+11	4.218E+09	7.360E+06	6.529E+04
8.763	0.348	1.272E+04	1.128E+02	3.627E+11	3.697E+09	7.394E+06	6.566E+04
9.515	0.396	1.210E+04	1.100E+02	3.085E+11	3.204E+09	7.150E+06	6.415E+04
10.373	0.447	1.183E+04	1.088E+02	2.679E+11	2.747E+09	6.820E+06	6.170E+04
11.354	0.521	1.031E+04	1.015E+02	2.054E+11	2.233E+09	6.279E+06	5.788E+04
12.496	0.601	1.034E+04	1.017E+02	1.704E+11	1.817E+09	5.911E+06	5.409E+04
13.824	0.694	1.167E+04	1.080E+02	1.485E+11	1.495E+09	5.811E+06	5.174E+04
15.36	0.82	1.152E+04	1.073E+02	1.205E+11	1.260E+09	5.755E+06	5.182E+04
17.193	0.976	1.144E+04	1.070E+02	1.039E+11	1.143E+09	5.829E+06	5.471E+04
19.339	1.146	1.186E+04	1.089E+02	9.366E+10	1.451E+09	6.097E+06	7.694E+04
21.99	1.425	1.260E+04	1.123E+02	7.681E+10	7.853E+08	6.258E+06	5.831E+04
25.211	1.733	1.476E+04	1.215E+02	7.225E+10	6.465E+08	7.010E+06	5.677E+04

Table A3: Data from the ^{235}U fission chamber for the 1998 20 mil experiment.

$E_{\gamma} (\text{MeV})$	$\phi_E (\text{MeV})$	Counts	ΔCounts	Neutrons	$\Delta \text{Neutrons}$	$1/\text{barms}$	$\Delta 1/\text{barms}$
1.321	0.021	3.360E+03	5.797E+01	2.419E+12	4.316E+10	5.181E+06	7.164E+04
1.363	0.022	3.656E+03	6.046E+01	2.498E+12	4.289E+10	5.615E+06	7.528E+04
1.407	0.023	3.612E+03	6.010E+01	2.344E+12	4.047E+10	5.722E+06	7.529E+04
1.454	0.024	4.060E+03	6.372E+01	2.494E+12	4.075E+10	6.052E+06	7.814E+04
1.503	0.025	4.008E+03	6.331E+01	2.331E+12	3.836E+10	6.250E+06	7.894E+04
1.555	0.026	4.187E+03	6.744E+01	2.304E+12	3.717E+10	6.429E+06	7.972E+04
1.608	0.027	4.548E+03	6.744E+01	2.366E+12	3.670E+10	6.751E+06	8.247E+04
1.665	0.029	4.426E+03	6.653E+01	2.174E+12	3.417E+10	6.716E+06	8.163E+04
1.726	0.031	4.473E+03	6.688E+01	2.074E+12	3.244E+10	6.788E+06	8.195E+04
1.79	0.032	4.817E+03	6.940E+01	2.104E+12	3.179E+10	7.049E+06	8.341E+04
1.856	0.034	4.932E+03	7.023E+01	2.031E+12	3.039E+10	7.365E+06	8.554E+04
1.927	0.036	5.050E+03	7.106E+01	1.961E+12	2.904E+10	7.553E+06	8.675E+04
2.002	0.037	5.221E+03	7.226E+01	1.912E+12	2.784E+10	7.633E+06	8.718E+04
2.082	0.041	5.128E+03	7.161E+01	1.768E+12	2.600E+10	7.534E+06	8.676E+04
2.167	0.042	5.418E+03	7.361E+01	1.768E+12	2.784E+10	7.633E+06	8.718E+04
2.255	0.045	5.955E+03	7.717E+01	1.827E+12	2.509E+10	8.586E+06	9.364E+04
2.351	0.048	5.618E+03	7.453E+01	1.629E+12	2.299E+10	8.483E+06	9.255E+04
2.453	0.052	5.569E+03	7.463E+01	1.525E+12	2.160E+10	8.497E+06	9.315E+04
2.561	0.054	5.891E+03	7.675E+01	1.518E+12	2.095E+10	8.719E+06	9.467E+04
2.676	0.059	5.787E+03	7.607E+01	1.407E+12	1.958E+10	8.719E+06	9.467E+04
3.075	0.071	6.185E+03	7.864E+01	1.265E+12	1.768E+10	9.601E+06	9.765E+04
3.226	0.078	5.918E+03	7.693E+01	1.139E+12	1.741E+10	9.601E+06	1.044E+05
3.392	0.084	5.820E+03	7.629E+01	1.052E+12	1.485E+10	9.425E+06	1.034E+05
3.57	0.092	5.900E+03	7.681E+01	1.001E+12	1.402E+10	9.693E+06	1.054E+05
3.763	0.097	6.199E+03	7.873E+01	9.817E+11	1.343E+10	1.009E+07	1.082E+05
3.971	0.107	6.489E+03	8.055E+01	9.543E+11	1.282E+10	1.083E+07	1.133E+05
4.194	0.114	6.606E+03	8.128E+01	9.051E+11	1.207E+10	1.113E+07	1.133E+05
4.441	0.126	6.664E+03	8.163E+01	8.486E+11	1.207E+10	1.113E+07	1.1538E+05
4.706	0.137	6.824E+03	8.261E+01	8.052E+11	1.059E+10	1.118E+07	1.162E+05
4.998	0.15	6.993E+03	8.362E+01	7.739E+11	1.008E+10	1.244E+07	1.262B+05
5.318	0.165	7.120E+03	8.438E+01	7.238E+11	9.390E+09	1.252E+07	1.273E+05
5.672	0.182	6.969E+03	8.348E+01	6.519E+11	8.499E+09	1.265E+07	1.284E+05
6.058	0.201	7.331E+03	8.678E+01	5.938E+11	7.484E+09	1.266E+07	1.247E+05
6.496	0.222	8.989E+03	9.481E+01	5.381E+11	7.484E+09	1.266E+07	1.161E+05
6.962	0.244	1.044E+04	1.022E+02	4.903E+11	5.402E+09	1.283E+07	1.120E+05
7.489	0.277	1.078E+04	1.038E+02	4.111E+11	4.472E+09	1.212E+07	1.035E+05
8.096	0.312	1.123E+04	1.060E+02	3.639E+11	3.879E+09	1.183E+07	1.003E+05
8.763	0.348	1.126E+04	1.061E+02	3.210E+11	3.429E+09	1.192E+07	1.007E+05
9.515	0.396	1.126E+04	1.061E+02	3.210E+11	3.429E+09	1.192E+07	1.007E+05
10.373	0.447	1.038E+04	1.028E+02	2.693E+11	2.948E+09	1.144E+07	9.781E+04
11.354	0.521	9.249E+03	9.617E+01	2.353E+11	2.545E+09	1.097E+07	9.502E+04
12.496	0.601	9.340E+03	9.664E+01	1.537E+11	1.712E+09	9.718E+06	8.520E+04
13.824	0.694	9.979E+03	9.989E+01	1.271E+11	1.369E+09	9.273E+06	7.882E+04
15.36	0.82	1.036E+04	1.018E+02	1.084E+11	1.183E+09	9.380E+06	8.071E+04
17.193	0.976	1.019E+04	1.009E+02	9.258E+10	1.063E+09	9.527E+06	8.573E+04
19.339	1.146	1.045E+04	1.022E+02	8.238E+10	1.309E+09	9.764E+06	1.207E+05
21.99	1.425	1.107E+04	1.052E+02	6.749E+10	7.282E+08	1.009E+07	9.024E+04
25.211	1.733	1.273E+04	1.128E+02	6.241E+10	5.952E+08	1.106E+07	8.457E+04

Table A4: Data from the ^{235}U fission chamber for the 1999 10 mil experiment.

E_n (MeV)	σE_n (MeV)	Counts	Δ_{Counts}	Neutrons	Δ_{Neutrons}	1/barns	$\Delta_{1/\text{barns}}$
1.321	0.021	3.749E+03	6.123E+01	2.700E+12	4.577E+10	4.693E+06	6.331E+04
1.363	0.021	3.807E+03	6.170E+01	2.601E+12	4.383E+10	4.945E+06	6.482E+04
1.407	0.022	4.037E+03	6.354E+01	2.619E+12	4.295E+10	5.198E+06	6.641E+04
1.454	0.024	4.427E+03	6.654E+01	2.719E+12	4.271E+10	5.469E+06	6.868E+04
1.503	0.025	4.456E+03	6.675E+01	2.590E+12	4.059E+10	5.659E+06	6.949E+04
1.555	0.026	4.608E+03	6.788E+01	2.536E+12	3.914E+10	5.916E+06	7.111E+04
1.608	0.027	4.894E+03	6.996E+01	2.547E+12	3.821E+10	5.996E+06	7.157E+04
1.665	0.029	4.825E+03	6.946E+01	2.369E+12	3.581E+10	6.090E+06	7.204E+04
1.726	0.031	5.140E+03	7.169E+01	2.383E+12	3.500E+10	6.444E+06	7.422E+04
1.79	0.032	5.610E+03	7.490E+01	2.452E+12	3.457E+10	6.771E+06	7.632E+04
1.856	0.034	5.596E+03	7.481E+01	2.305E+12	3.258E+10	6.925E+06	7.704E+04
1.927	0.036	5.752E+03	7.584E+01	2.234E+12	3.120E+10	7.095E+06	7.833E+04
2.002	0.037	5.808E+03	7.621E+01	2.127E+12	2.953E+10	7.048E+06	7.749E+04
2.082	0.041	5.884E+03	7.671E+01	2.030E+12	2.805E+10	7.265E+06	7.902E+04
2.167	0.042	6.428E+03	8.017E+01	2.090E+12	2.773E+10	7.668E+06	8.188E+04
2.255	0.045	6.348E+03	7.967E+01	1.947E+12	2.603E+10	7.883E+06	8.325E+04
2.351	0.048	6.330E+03	7.956E+01	1.836E+12	2.457E+10	7.905E+06	8.332E+04
2.453	0.052	6.569E+03	8.105E+01	1.798E+12	2.363E+10	7.958E+06	8.401E+04
2.561	0.054	6.332E+03	7.957E+01	1.631E+12	2.182E+10	8.007E+06	8.422E+04
2.676	0.059	6.497E+03	8.060E+01	1.580E+12	2.089E+10	8.129E+06	8.588E+04
2.8	0.062	6.284E+03	7.927E+01	1.444E+12	1.936E+10	8.020E+06	8.449E+04
2.935	0.069	6.809E+03	8.252E+01	1.477E+12	1.933E+10	8.701E+06	9.134E+04
3.075	0.071	6.528E+03	8.080E+01	1.335E+12	1.797E+10	8.609E+06	9.129E+04
3.226	0.078	6.553E+03	8.095E+01	1.260E+12	1.693E+10	8.514E+06	9.108E+04
3.392	0.084	6.528E+03	8.080E+01	1.179E+12	1.584E+10	8.799E+06	9.317E+04
3.57	0.092	6.762E+03	8.223E+01	1.147E+12	1.515E+10	9.219E+06	9.605E+04
3.763	0.097	7.374E+03	8.587E+01	1.167E+12	1.483E+10	9.845E+06	1.008E+05
3.971	0.107	7.401E+03	8.603E+01	1.089E+12	1.384E+10	1.021E+07	1.032E+05
4.194	0.114	7.426E+03	8.617E+01	1.017E+12	1.291E+10	1.050E+07	1.051E+05
4.441	0.126	8.025E+03	8.958E+01	1.022E+12	1.254E+10	1.103E+07	1.091E+05
4.706	0.137	7.889E+03	8.882E+01	9.320E+11	1.154E+10	1.133E+07	1.116E+05
4.998	0.15	7.804E+03	8.834E+01	8.638E+11	1.074E+10	1.150E+07	1.134E+05
5.318	0.165	8.185E+03	9.047E+01	8.370E+11	1.018E+10	1.187E+07	1.164E+05
5.672	0.182	8.233E+03	9.074E+01	7.700E+11	9.365E+09	1.253E+07	1.202E+05
6.058	0.201	9.989E+03	9.994E+01	7.864E+11	8.825E+09	1.387E+07	1.251E+05
6.496	0.222	1.256E+04	1.120E+02	7.539E+11	7.715E+09	1.429E+07	1.203E+05
6.962	0.244	1.276E+04	1.130E+02	6.007E+11	6.125E+09	1.311E+07	1.082E+05
7.489	0.277	1.278E+04	1.131E+02	4.871E+11	4.958E+09	1.202E+07	9.827E+04
8.096	0.312	1.360E+04	1.166E+02	4.417E+11	4.376E+09	1.174E+07	9.585E+04
8.763	0.348	1.263E+04	1.124E+02	3.603E+11	3.683E+09	1.113E+07	9.203E+04
9.515	0.396	1.232E+04	1.110E+02	3.134E+11	3.222E+09	1.066E+07	8.992E+04
10.373	0.447	1.119E+04	1.058E+02	2.530E+11	2.659E+09	1.014E+07	8.586E+04
11.354	0.521	1.091E+04	1.044E+02	2.170E+11	2.304E+09	1.000E+07	8.483E+04
12.496	0.601	1.204E+04	1.097E+02	1.978E+11	1.974E+09	1.009E+07	8.309E+04
13.824	0.694	1.222E+04	1.105E+02	1.554E+11	1.538E+09	9.548E+06	7.670E+04
15.36	0.82	1.223E+04	1.106E+02	1.280E+11	1.307E+09	9.207E+06	7.605E+04
17.193	0.976	1.243E+04	1.115E+02	1.127E+11	1.199E+09	9.391E+06	8.107E+04
19.339	1.146	1.305E+04	1.142E+02	1.026E+11	1.611E+09	1.039E+07	1.256E+05
21.99	1.425	1.459E+04	1.208E+02	8.910E+10	8.721E+08	1.102E+07	9.275E+04
25.211	1.733	1.695E+04	1.302E+02	8.311E+10	7.019E+08	1.218E+07	8.615E+04

Table A5: $\sigma(157.4 \text{ keV } 6^+ \rightarrow 4^+) {}^{238}\text{Pu}$ ground state band transition in all three data sets.

E_n (MeV)	δE_n (MeV)	$\sigma(98\text{-thin})$	$\Delta\sigma(98\text{-thin})$	$\sigma(98\text{-thick})$	$\Delta\sigma(98\text{-thick})$	$\sigma(99\text{-thin})$	$\Delta\sigma(99\text{-thin})$
3.0780	0.0630	0.0060	0.0090	0.0160	0.0060	(0.0157)	(0.0065)
3.2310	0.0680	0.0120	0.0090	0.0060	0.0060	(0.0079)	(0.0065)
3.3960	0.0740	0.0120	0.0090	(0.0060)	(0.0060)	(0.0185)	(0.0067)
3.5740	0.0790	0.0090	0.0090	0.0000	0.0060	(0.0158)	(0.0066)
3.7660	0.0860	0.0010	0.0080	0.0080	0.0060	(0.0138)	(0.0061)
3.9730	0.0930	0.0020	0.0080	0.0080	0.0060	(0.0118)	(0.0060)
4.2000	0.1010	0.0050	0.0080	(0.0020)	(0.0060)	(0.0207)	(0.0059)
4.4450	0.1100	0.0150	0.0080	(0.0050)	(0.0050)	(0.0066)	(0.0059)
4.7130	0.1190	0.0120	0.0070	(0.0080)	(0.0050)	(0.0110)	(0.0057)
5.0010	0.1320	(0.0050)	(0.0070)	0.0050	0.0050	(0.0250)	(0.0057)
5.3250	0.1440	0.0090	0.0070	(0.0060)	(0.0050)	(0.0166)	(0.0056)
5.6780	0.1590	0.0060	0.0070	(0.0030)	(0.0050)	(0.0189)	(0.0053)
6.0640	0.1760	0.0190	0.0070	(0.0060)	(0.0050)	(0.0227)	(0.0054)
6.5000	0.1950	0.0230	0.0070	(0.0070)	(0.0050)	(0.0102)	(0.0055)
6.9690	0.2150	0.0360	0.0070	0.0120	0.0050	0.0043	0.0058
7.4980	0.2430	0.0420	0.0080	0.0240	0.0050	0.0177	0.0061
8.1050	0.2720	0.0670	0.0080	0.0360	0.0050	0.0439	0.0062
8.7730	0.3060	0.0760	0.0080	0.0420	0.0050	0.0415	0.0061
9.5200	0.3460	0.0750	0.0080	0.0540	0.0060	0.0525	0.0062
10.3920	0.3950	0.1120	0.0080	0.0700	0.0060	0.0776	0.0070
11.3730	0.4530	0.1290	0.0090	0.0890	0.0070	0.0883	0.0070
12.4990	0.5250	0.1280	0.0090	0.0910	0.0070	0.0938	0.0075
13.8240	0.6060	0.0990	0.0100	0.0870	0.0070	0.0674	0.0086
15.3590	0.7190	0.0750	0.0100	0.0730	0.0070	0.0470	0.0085
17.1830	0.8460	0.0540	0.0090	0.0430	0.0070	0.0425	0.0083
19.3360	1.0180	0.0360	0.0090	0.0430	0.0060	0.0252	0.0070
21.9600	1.2250	0.0430	0.0090	0.0280	0.0060	0.0183	0.0076
25.1210	1.5160	0.0420	0.0080	0.0260	0.0060	0.0144	0.0073

Table A6: $\sigma(210.0 \text{ keV } 8^+ \rightarrow 6^+)$ ^{238}Pu ground state band transition in all three data sets.

E_n (MeV)	δE_n (MeV)	σ (98-thin)	$\Delta\sigma$ (98-thin)	σ (98-thick)	$\Delta\sigma$ (98-thick)	σ (99-thin)	$\Delta\sigma$ (99-thin)
3.0780	0.0630	0.006	0.009	0.006	0.003	0.0004	0.0031
3.2310	0.0680	0.012	0.009	0.011	0.003	-0.0008	-0.0032
3.3960	0.0740	0.012	0.009	0.005	0.003	0.0047	0.0033
3.5740	0.0790	0.009	0.009	0.009	0.003	0.0025	0.0033
3.7660	0.0860	0.001	0.008	0.008	0.003	0.0034	0.003
3.9730	0.0930	0.002	0.008	0.012	0.003	0.0032	0.003
4.2000	0.1010	0.005	0.008	0.01	0.003	0.005	0.0029
4.4450	0.1100	0.015	0.008	0.007	0.003	0.0021	0.0029
4.7130	0.1190	0.012	0.007	0.013	0.003	0.0029	0.0028
5.0010	0.1320	-0.005	-0.007	0.006	0.003	0.007	0.0027
5.3250	0.1440	0.009	0.007	0.013	0.003	0.009	0.0028
5.6780	0.1590	0.006	0.007	0.013	0.003	0.0073	0.0027
6.0640	0.1760	0.019	0.007	0.012	0.003	0.0018	0.0025
6.5000	0.1950	0.023	0.007	0.012	0.002	0.0026	0.0025
6.9690	0.2150	0.036	0.007	0.01	0.002	0.0066	0.0028
7.4980	0.2430	0.042	0.008	0.011	0.002	0.0121	0.0028
8.1050	0.2720	0.067	0.008	0.012	0.003	0.0127	0.0029
8.7730	0.3060	0.076	0.008	0.011	0.003	0.019	0.0028
9.5200	0.3460	0.075	0.008	0.024	0.003	0.0248	0.003
10.3920	0.3950	0.112	0.008	0.03	0.003	0.0333	0.0033
11.3730	0.4530	0.129	0.009	0.041	0.003	0.0345	0.0034
12.4990	0.5250	0.128	0.009	0.04	0.003	0.0454	0.0035
13.8240	0.6060	0.099	0.01	0.046	0.003	0.0383	0.0034
15.3590	0.7190	0.075	0.01	0.046	0.003	0.0361	0.0034
17.1830	0.8460	0.054	0.009	0.04	0.003	0.022	0.0033
19.3360	1.0180	0.036	0.009	0.02	0.003	0.0169	0.0031
21.9600	1.2250	0.043	0.009	0.019	0.003	0.0148	0.0031
25.1210	1.5160	0.042	0.008	0.018	0.003	0.016	0.0032

E_a (MeV)	δE_a (MeV)	$\Delta g_{(98\text{-thin})}$	$g_{(98\text{-thin})}$	$\Delta g_{(98\text{-thick})}$	$g_{(98\text{-thick})}$	$\Delta g_{(99\text{-thin})}$	$g_{(99\text{-thin})}$	$\Delta g_{(99\text{-thick})}$
1.3210	0.0180	0	0.0061	0.0026	0.0158	0.0039	0.0039	
1.3650	0.0190	0.0041	0.0032	0.004	0.0024	0.0169	0.008	
1.4090	0.0190	0.0220	0.0102	0.0078	0.0037	0.0119	0.0025	0.0116
1.4550	0.0210	0.0041	0.0032	0.007	0.0026	0.008	0.0025	0.0046
1.5040	0.0230	0.0116	0.0035	0.0035	0.0119	0.0025	0.0025	0.004
1.5560	0.0230	0.0058	0.0036	0.0066	0.0022	0.0124	0.0039	0.0039
1.6100	0.0240	0.0058	0.0033	0.0077	0.0025	0.0104	0.0038	0.0038
1.6670	0.0250	0.0062	0.0034	0.0033	0.0021	0.0074	0.0039	0.0039
1.7280	0.0270	0.0051	0.003	0.0055	0.0022	0.0055	0.0055	0.0039
1.7920	0.0280	0.0034	0.003	0.0083	0.0024	0.005	0.005	0.0034
1.8580	0.0290	0.004	0.003	0.003	0.0114	0.0025	0.0025	0.0038
1.9290	0.0320	0.0083	0.0031	0.0066	0.0024	0.0061	0.0061	0.0035
2.0040	0.0330	0.0034	0.0033	0.0052	0.0021	0.007	0.0036	-0.0035
2.0840	0.0350	-0.0003	0.0033	0.0052	0.0021	0.0106	0.004	
2.1690	0.0370	-0.0003	0.0028	0.0076	0.0023	0.0079	0.0023	-0.0015
2.2590	0.0400	-0.0004	0.0029	-0.0029	0.0034	0.0021	0.0001	0.0035
2.3340	0.0420	0.0036	0.0029	0.0048	0.0021	0.0006	0.0006	0.0035
2.4550	0.0450	0.0041	0.003	0.0013	0.0022	0.0022	0.0004	0.0036
2.5640	0.0480	0.0079	0.0033	0.0096	0.0023	0.0031	0.0031	0.0037
2.6800	0.0520	0.0049	0.0035	0.0045	0.0023	0.0041	0.0041	0.0041
2.8020	0.0550	0.0107	0.0037	0.0035	0.0024	0.0046	0.0046	0.004
2.9380	0.0600	0.0034	0.0034	0.0071	0.0023	0.0001	0.0001	0.0042
3.1760	0.1150	0.007	0.004	0.0073	0.0025	0.0018	0.0037	0.0034
3.250	0.1440	0.008	0.0008	0.0025	0.0056	0.002	0.0102	0.0033
3.7680	0.1590	0.004	0.0025	0.0078	0.002	0.0042	0.0042	0.0033
4.7130	0.1190	0.0035	0.0026	0.0073	0.002	0.0006	0.0006	-0.0034
4.4450	0.1100	0.0063	0.003	0.0036	0.0021	0.005	0.005	0.0033
4.2000	0.1010	0.0041	0.0028	0.0044	0.002	0.002	0.0036	0.0037
3.9730	0.0930	0.0045	0.0028	0.0071	0.0021	0.0072	0.0072	0.0037
3.7660	0.0860	0.008	0.003	0.004	0.0021	0.0043	0.0043	0.0036
3.5740	0.0790	0.0083	0.0032	0.0026	0.0022	0.0062	0.0062	0.0038
3.3960	0.0740	0.0039	0.0032	0.0024	0.0021	0.0021	0.0034	0.0038
3.2310	0.0680	0.0058	0.0032	0.0002	0.002	0.002	0.0034	0.0038
3.0780	0.0630	0.006	0.003	0.0043	0.0022	0.0011	0.0011	0.0035
2.9380	0.0600	0.0034	0.0034	0.0071	0.0023	0.0001	0.0001	0.0042
2.8020	0.0550	0.0107	0.0037	0.0035	0.0024	0.0046	0.0046	0.004
2.6800	0.0520	0.0049	0.0035	0.0045	0.0023	0.0041	0.0041	0.0041
2.4550	0.0450	0.0041	0.003	0.0013	0.0022	0.0004	0.0004	0.0036
2.5640	0.0480	0.0079	0.0033	0.0096	0.0023	0.0031	0.0031	0.0037
2.6800	0.0480	0.0079	0.0033	0.0096	0.0023	0.0031	0.0031	0.0037
2.8020	0.0550	0.0107	0.0037	0.0035	0.0024	0.0046	0.0046	0.004
3.1760	0.0740	0.0039	0.0032	0.0024	0.0021	0.0072	0.0072	0.0037
3.5740	0.0860	0.0083	0.0032	0.0026	0.0022	0.0043	0.0043	0.0036
3.3960	0.0740	0.0039	0.0032	0.0024	0.0021	0.0062	0.0062	0.0038
3.2310	0.0680	0.0058	0.0032	0.0002	0.002	0.002	0.0034	0.0038
3.0780	0.0630	0.006	0.003	0.0043	0.0022	0.0011	0.0011	0.0035
2.9380	0.0600	0.0034	0.0034	0.0071	0.0023	0.0001	0.0001	0.0042
2.8020	0.0550	0.0107	0.0037	0.0035	0.0024	0.0046	0.0046	0.004
3.1760	0.1590	0.004	0.0025	0.0078	0.0021	0.0072	0.0072	0.0037
4.4450	0.1100	0.0063	0.003	0.0044	0.002	0.002	0.0036	0.0037
4.2000	0.1010	0.0041	0.0028	0.0044	0.002	0.002	0.0036	0.0037
3.9730	0.0930	0.0045	0.0028	0.0071	0.0021	0.0072	0.0072	0.0037
3.7660	0.0860	0.008	0.003	0.004	0.0021	0.0062	0.0062	0.0038
3.5740	0.0790	0.0083	0.0032	0.0026	0.0022	0.0043	0.0043	0.0036
3.3960	0.0740	0.0039	0.0032	0.0024	0.0021	0.0062	0.0062	0.0038
3.2310	0.0680	0.0058	0.0032	0.0002	0.002	0.002	0.0034	0.0038
3.0780	0.0630	0.006	0.003	0.0043	0.0022	0.0011	0.0011	0.0035
2.9380	0.0600	0.0034	0.0034	0.0071	0.0023	0.0001	0.0001	0.0042
2.8020	0.0550	0.0107	0.0037	0.0035	0.0024	0.0046	0.0046	0.004
3.1760	0.1590	0.004	0.0025	0.0078	0.0021	0.0072	0.0072	0.0037
4.4450	0.1100	0.0063	0.003	0.0044	0.002	0.002	0.0036	0.0037
4.2000	0.1010	0.0041	0.0028	0.0044	0.002	0.002	0.0036	0.0037
3.9730	0.0930	0.0045	0.0028	0.0071	0.0021	0.0072	0.0072	0.0037
3.7660	0.0860	0.008	0.003	0.004	0.0021	0.0062	0.0062	0.0038
3.5740	0.0790	0.0083	0.0032	0.0026	0.0022	0.0043	0.0043	0.0036
3.3960	0.0740	0.0039	0.0032	0.0024	0.0021	0.0062	0.0062	0.0038
3.2310	0.0680	0.0058	0.0032	0.0002	0.002	0.002	0.0034	0.0038
3.0780	0.0630	0.006	0.003	0.0043	0.0022	0.0011	0.0011	0.0035
2.9380	0.0600	0.0034	0.0034	0.0071	0.0023	0.0001	0.0001	0.0042
2.8020	0.0550	0.0107	0.0037	0.0035	0.0024	0.0046	0.0046	0.004
3.1760	0.1590	0.004	0.0025	0.0078	0.0021	0.0072	0.0072	0.0037
4.4450	0.1100	0.0063	0.003	0.0044	0.002	0.002	0.0036	0.0037
4.2000	0.1010	0.0041	0.0028	0.0044	0.002	0.002	0.0036	0.0037
3.9730	0.0930	0.0045	0.0028	0.0071	0.0021	0.0072	0.0072	0.0037
3.7660	0.0860	0.008	0.003	0.004	0.0021	0.0062	0.0062	0.0038
3.5740	0.0790	0.0083	0.0032	0.0026	0.0022	0.0043	0.0043	0.0036
3.3960	0.0740	0.0039	0.0032	0.0024	0.0021	0.0062	0.0062	0.0038
3.2310	0.0680	0.0058	0.0032	0.0002	0.002	0.002	0.0034	0.0038
3.0780	0.0630	0.006	0.003	0.0043	0.0022	0.0011	0.0011	0.0035
2.9380	0.0600	0.0034	0.0034	0.0071	0.0023	0.0001	0.0001	0.0042
2.8020	0.0550	0.0107	0.0037	0.0035	0.0024	0.0046	0.0046	0.004
3.1760	0.1590	0.004	0.0025	0.0078	0.0021	0.0072	0.0072	0.0037
4.4450	0.1100	0.0063	0.003	0.0044	0.002	0.002	0.0036	0.0037
4.2000	0.1010	0.0041	0.0028	0.0044	0.002	0.002	0.0036	0.0037
3.9730	0.0930	0.0045	0.0028	0.0071	0.0021	0.0072	0.0072	0.0037
3.7660	0.0860	0.008	0.003	0.004	0.0021	0.0062	0.0062	0.0038
3.5740	0.0790	0.0083	0.0032	0.0026	0.0022	0.0043	0.0043	0.0036
3.3960	0.0740	0.0039	0.0032	0.0024	0.0021	0.0062	0.0062	0.0038
3.2310	0.0680	0.0058	0.0032	0.0002	0.002	0.002	0.0034	0.0038
3.0780	0.0630	0.006	0.003	0.0043	0.0022	0.0011	0.0011	0.0035
2.9380	0.0600	0.0034	0.0034	0.0071	0.0023	0.0001	0.0001	0.0042
2.8020	0.0550	0.0107	0.0037	0.0035	0.0024	0.0046	0.0046	0.004
3.1760	0.1590	0.004	0.0025	0.0078	0.0021	0.0072	0.0072	0.0037
4.4450	0.1100	0.0063	0.003	0.0044	0.002	0.002	0.0036	0.0037
4.2000	0.1010	0.0041	0.0028	0.0044	0.002	0.002	0.0036	0.0037
3.9730	0.0930	0.0045	0.0028	0.0071	0.0021	0.0072	0.0072	0.0037
3.7660	0.0860	0.008	0.003	0.004	0.0021	0.0062	0.0062	0.0038
3.5740	0.0790	0.0083	0.0032	0.0026	0.0022	0.0043	0.0043	0.0036
3.3960	0.0740	0.0039	0.0032	0.0024	0.0021	0.0062	0.0062	0.0038
3.2310	0.0680	0.0058	0.0032	0.0002	0.002	0.002	0.0034	0.0038
3.0780	0.0630	0.006	0.003	0.0043	0.0022	0.0011	0.0011	0.0035
2.9380	0.0600	0.0034	0.0034	0.0071	0.0023	0.0001	0.0001	0.0042
2.8020	0.0550	0.0107	0.0037	0.0035	0.0024	0.0046	0.0046	0.004
3.1760	0.1590	0.004	0.0025	0.0078	0.0021	0.0072	0.0072	0.0037
4.4450	0.1100	0.0063	0.003	0.0044	0.002	0.002	0.0036	0.0037
4.2000	0.1010	0.0041	0.0028	0.0044	0.002	0.002	0.0036	0.0037

Table A8: $\sigma(924.0 \text{ keV } 3^+ \rightarrow 4^+) {}^{238}\text{Pu}$ ground state band transition in all three data sets.

$E_n (\text{MeV})$	$\delta E_n (\text{MeV})$	$\sigma(98\text{-thin})$	$\Delta\sigma(98\text{-thin})$	$\sigma(98\text{-thick})$	$\Delta\sigma(98\text{-thick})$	$\sigma(99\text{-thin})$	$\Delta\sigma(99\text{-thin})$
1.3210	0.0180	0.017	0.0092	0.0025	0.0023	0.0011	0.0035
1.3650	0.0190	0.0074	0.0046	-0.0023	-0.0021	0.0058	0.0066
1.4090	0.0190	0.0003	0.0041	0.0041	0.0022	0.0071	0.0039
1.4550	0.0210	0.0083	0.0048	0.0008	0.0022	0.0102	0.0046
1.5040	0.0220	0.0058	0.0044	0.0014	0.002	0.0112	0.0039
1.5560	0.0230	0.0018	0.0041	0.0022	0.002	0.0071	0.0037
1.6100	0.0240	0.0141	0.0045	0.0013	0.0021	0.01	0.0037
1.6670	0.0250	-0.0024	-0.0043	0.0018	0.002	0.002	0.0036
1.7280	0.0270	-0.0014	-0.0038	0.0038	0.0021	0.0064	0.0038
1.7920	0.0280	0.0008	0.0038	0.0024	0.0021	-0.002	-0.0031
1.8580	0.0290	0.0033	0.0038	0.002	0.0021	-0.006	-0.0035
1.9290	0.0320	0.0063	0.0038	0.0008	0.0021	0.0034	0.0033
2.0040	0.0330	-0.0085	-0.0039	-0.0051	-0.0018	-0.0012	-0.0033
2.0840	0.0350	-0.0062	-0.0036	0.0002	0.002	-0.0003	-0.0035
2.1690	0.0370	-0.005	-0.0035	-0.0011	-0.0021	0.0026	0.0035
2.2590	0.0400	-0.0017	-0.0037	-0.0034	-0.0019	0.0002	0.0033
2.3540	0.0420	-0.0021	-0.0036	-0.0049	-0.0019	-0.0032	-0.0032
2.4550	0.0450	-0.0052	-0.0037	0.001	0.0021	0.0044	0.0036
2.5640	0.0480	-0.0038	-0.0039	-0.0027	-0.0021	-0.0025	-0.0036
2.6800	0.0520	-0.0034	-0.0043	-0.0053	-0.0021	0.0005	0.004
2.8020	0.0550	-0.0061	-0.0042	0.0023	0.0023	0.0089	0.004
2.9380	0.0600	-0.0037	-0.0041	-0.0017	-0.0021	0.0109	0.0042
3.0780	0.0630	0.0042	0.0037	-0.0031	-0.002	0.003	0.0035
3.2310	0.0680	-0.0031	-0.0038	0.0027	0.002	0.0018	0.0036
3.3960	0.0740	-0.0057	-0.0038	-0.0077	-0.0019	0.0054	0.0037
3.5740	0.0790	0.0037	0.004	0.0019	0.002	0.0087	0.0037
3.7660	0.0860	0.0053	0.0037	-0.0009	-0.0019	-0.0026	-0.0035
3.9730	0.0930	-0.0056	-0.0035	0.002	0.0019	-0.0006	-0.0036
4.2000	0.1010	0.0011	0.0035	0.0005	0.0018	-0.0014	-0.0034
4.4450	0.1100	0.0002	0.0037	0.0062	0.002	0.0006	0.0032
4.7130	0.1190	-0.0018	-0.0032	0.0007	0.0018	-0.0014	-0.0033
5.0010	0.1320	-0.0009	-0.0033	-0.0002	-0.0017	0.0038	0.0032
5.3250	0.1440	-0.0033	-0.0033	-0.0024	-0.0018	-0.002	-0.003
5.6780	0.1590	0.0044	0.0033	-0.0006	-0.0018	0.0002	0.0031
6.0640	0.1760	0.0023	0.0031	-0.0012	-0.0016	-0.001	-0.0032
6.5000	0.1950	0.0041	0.0032	0.0014	0.0018	0.0017	0.0029
6.9690	0.2150	-0.0002	-0.003	-0.0003	-0.0019	0.0025	0.0029
7.4980	0.2430	0.0091	0.0031	0.0026	0.0018	0.004	0.0033
8.1050	0.2720	0.0046	0.0034	0.0075	0.0019	0.0073	0.0034
8.7730	0.3060	0.0142	0.0035	0.0115	0.002	0.011	0.0033
9.5200	0.3460	0.0143	0.0036	0.0091	0.002	0.0152	0.0037
10.3920	0.3950	0.0116	0.0035	0.014	0.0021	0.0117	0.0037
11.3730	0.4530	0.0134	0.004	0.012	0.0023	0.0125	0.0038
12.4990	0.5250	0.0223	0.0043	0.0118	0.0023	0.0108	0.0041
13.8240	0.6060	0.0072	0.0039	0.0119	0.0024	0.0112	0.0039
15.3590	0.7190	0.0095	0.0043	0.0073	0.0024	0	
17.1830	0.8460	0.0059	0.0039	0.0006	0.0022	0.0028	0.0036
19.3360	1.0180	0.0058	0.004	0.0082	0.0022	0.0012	0.0036
21.9600	1.2250	0.005	0.0036	0.0048	0.0021	0.0076	0.0035
25.1210	1.5160	0.0082	0.0034	0.0054	0.002	0.003	0.0033

E_n (MeV)	βE_n (MeV)	$\Delta\phi_{98}$ (98-thin)	$\Delta\phi_{99}$ (98-thick)	$\Delta\phi_{98}$ (98-thick)	$\Delta\phi_{99}$ (99-thin)	$\Delta\phi_{99}$ (99-thin)
1.3210	0.0180	-0.0242	-0.0087	-0.003	-0.0022	-0.0003
1.3650	0.0190	-0.0077	-0.0041	-0.0016	-0.0022	-0.0145
1.4090	0.0190	0.0015	0.0041	0.0023	0.0022	-0.0194
1.4550	0.0210	0.002	0.0044	-0.0046	-0.0022	-0.0177
1.5040	0.0220	-0.006	-0.0041	-0.0006	-0.0021	-0.004
1.5560	0.0230	-0.0073	-0.004	-0.0004	-0.0006	-0.0058
1.6670	0.0250	0.0017	0.0042	-0.0016	-0.0002	-0.0056
1.7280	0.0270	-0.0035	-0.0038	-0.0007	-0.0021	-0.0081
1.7920	0.0280	-0.0068	-0.0036	-0.0001	-0.0021	-0.0068
1.8580	0.0290	-0.0036	-0.0036	-0.0032	-0.0021	-0.0123
1.9290	0.0320	-0.0018	-0.0038	-0.0011	-0.0021	-0.0008
2.0040	0.0330	-0.0103	-0.0038	-0.0011	-0.0019	-0.0053
2.0840	0.0350	0.0019	0.0036	-0.0029	-0.0002	-0.0125
2.1690	0.0370	-0.0065	-0.0034	-0.0006	-0.0021	-0.0125
2.2590	0.0400	-0.0067	-0.0035	-0.0021	-0.0019	-0.0053
2.3540	0.0420	-0.0018	-0.0036	-0.0003	-0.0019	-0.0054
2.4550	0.0450	-0.0067	-0.0035	-0.0021	-0.0002	-0.0015
2.5640	0.0480	0.0027	0.0039	-0.0015	-0.0021	-0.0019
2.6800	0.0520	-0.0102	-0.0042	-0.0036	-0.0021	-0.0005
2.8020	0.0550	0.0025	0.0042	-0.0021	-0.0022	-0.0054
3.0780	0.0630	-0.0152	-0.004	-0.0002	-0.0021	-0.0078
3.2310	0.0680	-0.009	-0.0036	-0.0018	-0.0002	-0.0063
3.3960	0.0740	-0.0097	-0.0037	-0.0019	-0.0006	-0.0056
3.5740	0.0790	-0.006	-0.0037	-0.0013	-0.0002	-0.0029
3.7660	0.0860	-0.0016	-0.0036	-0.0019	-0.0001	-0.0058
4.7130	0.1190	-0.0078	-0.0031	-0.0018	-0.0005	-0.0053
4.4450	0.1100	-0.0037	-0.0036	-0.0002	-0.0002	-0.0075
4.2000	0.1010	-0.0019	-0.0034	-0.00041	-0.0018	-0.0122
5.0010	0.1320	-0.0058	-0.0032	-0.00032	-0.0025	-0.0067
5.3250	0.1440	-0.0052	-0.0032	-0.0011	-0.0019	-0.0048
5.6780	0.1590	0.0009	0.0032	-0.0002	-0.0018	-0.0031
6.5000	0.1950	-0.0003	-0.0003	-0.0007	-0.0017	-0.0042
6.0640	0.1760	-0.0015	-0.0003	-0.0003	-0.0017	-0.0053
7.4980	0.2430	0.0003	0.0029	0.0013	0.0019	0.0018
6.9690	0.2150	-0.0003	-0.0003	0.0	0.0042	0.0044
8.7730	0.3060	0.0401	0.0043	0.0032	0.0226	0.027
8.1050	0.2720	0.0278	0.0039	0.0093	0.0019	0.0069
7.4980	0.2430	0.0003	0.0029	0.0013	0.0019	0.0018
6.9690	0.2150	-0.0003	-0.0003	-0.0007	-0.0017	-0.0042
9.5200	0.3460	0.0476	0.0047	0.034	0.0031	0.0045
10.3920	0.3950	0.0509	0.048	0.0405	0.0035	0.0032
11.3730	0.4530	0.0633	0.0048	0.043	0.0035	0.0062
12.4990	0.5250	0.0539	0.0058	0.0042	0.0124	0.0025
13.3360	0.8460	0.0284	0.0044	0.0144	0.0026	0.0191
17.1830	0.7190	0.0371	0.0051	0.0235	0.003	0.0086
15.3590	0.7190	0.0312	0.0046	0.028	0.0032	0.0219
13.8240	0.6060	0.0312	0.0046	0.028	0.0036	0.0077
21.9600	1.2250	0.0174	0.0039	0.0155	0.0025	0.0013
21.9600	1.0180	0.0149	0.0042	0.0124	0.0013	-0.0061
17.1830	0.8460	0.0284	0.0044	0.0144	0.0026	0.0191
15.3590	0.7190	0.0371	0.0051	0.0235	0.003	0.0057
25.1210	1.5160	0.015	0.0035	0.0083	0.0021	0.002

Table A9: $\text{g}(938.0 \text{ keV} 4^+ \rightarrow 4^+_1 \text{Pu})$ ground state band transition in all three data sets.

E_{γ} (MeV)	βE_{γ} (MeV)	$\sigma(98\text{-thin})$	$\Delta\sigma(98\text{-thin})$	$\sigma(98\text{-thick})$	$\Delta\sigma(98\text{-thick})$	$\sigma(99\text{-thin})$	$\Delta\sigma(99\text{-thin})$
1.3210	0.0180	0.0337	0.0197	0.0038	0.0111	0.01	0.0096
1.3650	0.0190	0.0111	0.0111	0.0038	0.0111	0.01	0.0096
1.4090	0.0190	0.0055	0.0187	0.029	0.0152	0.0063	0.0099
1.4450	0.0210	0.0072	0.0072	0.0166	0.0006	0.0123	0.0043
1.5040	0.0220	0.0028	0.0144	-0.0099	-0.0104	0.0194	0.0101
1.5560	0.0230	0.0028	0.0144	-0.0099	-0.0104	0.0194	0.0101
1.6670	0.0250	0.0184	0.0162	0.009	0.0088	0.0197	0.0087
1.7280	0.0270	0.0195	0.0161	0.0161	0.0262	0.0095	0.0174
1.7920	0.0280	0.0167	0.0126	0.009	0.0104	0.0104	0.0094
1.8580	0.0290	0.0521	0.0133	0.0133	0.0196	0.0099	0.0222
1.9290	0.0320	0.0183	0.014	0.014	0.0099	0.0099	0.0072
2.0040	0.0330	0.0323	0.0143	0.0143	0.016	0.0098	0.0217
2.0840	0.0350	0.017	0.0114	0.0114	0.0194	0.0097	0.0071
2.1690	0.0370	0.0486	0.014	0.014	0.0161	0.0085	0.0082
2.2590	0.0400	0.0136	0.0142	0.0203	0.0266	0.0084	0.0116
2.3540	0.0420	0.0358	0.0116	0.0116	0.0266	0.0084	0.0116
2.5640	0.0450	0.0450	0.0271	0.0121	0.0121	0.0274	0.0287
2.6800	0.0480	0.0584	0.0139	0.0139	0.0123	0.0077	0.0065
2.8020	0.0500	0.0547	0.0132	0.0132	0.0143	0.0083	0.0038
3.2310	0.0630	0.0545	0.012	0.012	0.0115	0.0092	0.0352
3.3960	0.0680	0.0479	0.0129	0.0129	0.0279	0.0081	0.0072
3.5740	0.0740	0.0439	0.0128	0.0128	0.0103	0.0091	0.0305
3.5740	0.0790	0.0365	0.0104	0.0104	0.0092	0.0092	0.0277
3.7660	0.0860	0.052	0.0115	0.0115	0.0196	0.007	0.0078
3.7930	0.0930	0.0588	0.0104	0.0104	0.0369	0.0091	0.0263
4.4450	0.1010	0.0764	0.0117	0.0117	0.0246	0.0072	0.0268
4.2000	0.1010	0.1100	0.0482	0.0482	0.0094	0.0324	0.0071
4.7130	0.1190	0.0583	0.0118	0.0118	0.0311	0.0072	0.0338
5.0010	0.1320	0.0682	0.0108	0.0108	0.0349	0.0065	0.0062
5.3250	0.1440	0.0667	0.0098	0.0098	0.0343	0.007	0.0335
5.6780	0.1590	0.0579	0.0118	0.0118	0.0371	0.007	0.0475
6.0640	0.1760	0.0601	0.0086	0.0086	0.0392	0.0069	0.0401
6.5000	0.1950	0.0553	0.0098	0.0098	0.039	0.0066	0.0065
6.9690	0.2150	0.0325	0.0084	0.0084	0.0195	0.0064	0.0309
7.4980	0.2430	0.0158	0.008	0.008	0.018	0.0077	0.0263
8.1050	0.2720	0.0306	0.0079	0.0079	0.0242	0.0072	0.0263
8.7730	0.3060	0.0242	0.008	0.008	0.0143	0.0066	0.0062
10.3920	0.3460	0.0174	0.0082	0.0082	0.0067	0.0078	0.0127
11.3730	0.4350	0.0255	0.0084	0.0084	0.0043	0.0065	0.0054
12.4990	0.5250	0.0271	0.0106	0.0106	0.002	0.0076	0.0066
13.8240	0.620	0.0107	0.0095	0.0095	0.0064	0.007	0.0069
15.3590	0.7190	0.0177	0.0097	0.0097	0.0102	0.0162	0.0081
17.1830	0.8460	0.037	0.0115	0.0115	0.0185	0.007	0.0149
19.3360	1.0180	0.0277	0.01	0.0133	0.009	0.0199	0.0078
21.9600	1.2250	0.008	0.0086	0.0086	0.0129	0.0071	0.0062
25.1210	1.5160	0.0191	0.0086	0.0086	0.0118	0.0078	0.0088

Table A11: $\sigma(154.3 \text{ keV } 13/2^+ \rightarrow 9/2^+)$ ^{239}Pu ground state band transition in all three data sets.

Table A12: $\sigma(226.4 \text{ keV } 5/2^- \rightarrow 5/2^+)$ ^{239}Pu ground state band transition in all three data sets.

E_n (MeV)	δE_n (MeV)	$\sigma(98\text{-thin})$	$\Delta\sigma(98\text{-thin})$	$\sigma(98\text{-thick})$	$\Delta\sigma(98\text{-thick})$	$\sigma(99\text{-thin})$	$\Delta\sigma(99\text{-thin})$
1.3210	0.0180	0.1493	0.0246	0.0446	0.0102	0.0477	0.0116
1.3650	0.0190	0.1407	0.0216	0.0616	0.01	0.0374	0.0111
1.4090	0.0190	0.1006	0.0213	0.0541	0.0096	0.0236	0.0101
1.4550	0.0210	0.1286	0.0205	0.0501	0.0092	0.0413	0.0101
1.5040	0.0220	0.1357	0.0202	0.0494	0.009	0.0365	0.0096
1.5560	0.0230	0.1227	0.0185	0.0463	0.0088	0.0298	0.0097
1.6100	0.0240	0.1108	0.0184	0.0473	0.0085	0.0327	0.0094
1.6670	0.0250	0.1215	0.0184	0.0428	0.0085	0.0388	0.0092
1.7280	0.0270	0.1061	0.0178	0.0412	0.0087	0.0182	0.0092
1.7920	0.0280	0.1005	0.0166	0.0369	0.0085	0.0368	0.0088
1.8580	0.0290	0.1074	0.0166	0.0376	0.0083	0.0334	0.0085
1.9290	0.0320	0.1022	0.0158	0.0484	0.0078	0.0326	0.0083
2.0040	0.0330	0.1073	0.0159	0.0523	0.0077	0.0262	0.0083
2.0840	0.0350	0.1155	0.0162	0.0478	0.0077	0.0353	0.0087
2.1690	0.0370	0.112	0.0155	0.0436	0.0074	0.0195	0.0079
2.2590	0.0400	0.1106	0.015	0.0391	0.0075	0.0348	0.0083
2.3540	0.0420	0.0898	0.014	0.0417	0.0072	0.0492	0.0082
2.4550	0.0450	0.0795	0.0143	0.0329	0.0074	0.0382	0.0081
2.5640	0.0480	0.1079	0.0148	0.0451	0.0073	0.0273	0.008
2.6800	0.0520	0.1118	0.0147	0.0498	0.0074	0.0261	0.0084
2.8020	0.0550	0.1074	0.0145	0.0296	0.0074	0.0296	0.008
2.9380	0.0600	0.1008	0.0148	0.0488	0.0074	0.0303	0.0082
3.0780	0.0630	0.084	0.0134	0.0414	0.0068	0.0177	0.0071
3.2310	0.0680	0.0732	0.0131	0.0469	0.0071	0.0311	0.008
3.3960	0.0740	0.0903	0.0137	0.0553	0.007	0.0174	0.0079
3.5740	0.0790	0.0827	0.0134	0.0337	0.0072	0.0414	0.0078
3.7660	0.0860	0.09	0.0132	0.0388	0.0066	0.0301	0.0069
3.9730	0.0930	0.0848	0.0127	0.0353	0.0063	0.0141	0.0068
4.2000	0.1010	0.0731	0.0113	0.0317	0.006	0.0197	0.0067
4.4450	0.1100	0.0588	0.0113	0.0381	0.006	0.0257	0.0067
4.7130	0.1190	0.0882	0.0114	0.0384	0.0059	0.0289	0.0065
5.0010	0.1320	0.0978	0.0118	0.0439	0.0056	0.0172	0.0062
5.3250	0.1440	0.0696	0.0107	0.037	0.0056	0.0211	0.0063
5.6780	0.1590	0.0584	0.0106	0.0357	0.0054	0.0243	0.0061
6.0640	0.1760	0.0715	0.0107	0.0342	0.0056	0.0193	0.0059
6.5000	0.1950	0.0483	0.0096	0.0194	0.0054	0.0178	0.0056
6.9690	0.2150	0.0474	0.0093	0.018	0.0055	0.0161	0.006
7.4980	0.2430	0.0459	0.0095	0.0113	0.0055	0.0067	0.0059
8.1050	0.2720	0.0425	0.0099	0.0194	0.0057	0.0204	0.0061
8.7730	0.3060	0.0302	0.0096	0.0262	0.0058	0.0172	0.0064
9.5200	0.3460	0.062	0.0104	0.0151	0.006	0.0158	0.0065
10.3920	0.3950	0.0392	0.0106	0.0109	0.006	0.0079	0.0071
11.3730	0.4530	0.0427	0.0116	0.0108	0.0065	0.0086	0.007
12.4990	0.5250	0.0518	0.0122	0.0296	0.0068	0.0149	0.0073
13.8240	0.6060	0.0395	0.012	0.0246	0.0072	0.0005	0.0074
15.3590	0.7190	0.0233	0.0126	0.0295	0.007	0.0058	0.0075
17.1830	0.8460	0.0413	0.0119	0.0117	0.0067	0.0204	0.0076
19.3360	1.0180	0.0448	0.0115	0.0212	0.007	0.0024	0.0071
21.9600	1.2250	0.0347	0.0117	0.028	0.0064	0.0048	0.0069
25.1210	1.5160	0.0348	0.0105	0.0056	0.0061	-0.0032	-0.0066

Table A13: $\sigma(228.2 \text{ keV } 5/2^+ \rightarrow 7/2^+) {}^{239}\text{Pu}$ ground state band transition in all three data sets.

E_n (MeV)	δE_n (MeV)	$\sigma(98\text{-thin})$	$\Delta\sigma(98\text{-thin})$	$\sigma(98\text{-thick})$	$\Delta\sigma(98\text{-thick})$	$\sigma(99\text{-thin})$	$\Delta\sigma(99\text{-thin})$
1.3210	0.0180	0.2999	0.0233	0.1852	0.0161	0.2603	0.0217
1.3650	0.0190	0.2318	0.0187	0.2098	0.0175	0.2644	0.0221
1.4090	0.0190	0.2151	0.0175	0.191	0.0162	0.248	0.0206
1.4550	0.0210	0.2708	0.0211	0.1771	0.0151	0.2541	0.0207
1.5040	0.0220	0.2508	0.0196	0.1943	0.016	0.2313	0.019
1.5560	0.0230	0.2628	0.0204	0.1835	0.0154	0.2417	0.02
1.6100	0.0240	0.2841	0.0218	0.1918	0.0156	0.2314	0.019
1.6670	0.0250	0.2787	0.0213	0.1924	0.0157	0.2271	0.0186
1.7280	0.0270	0.2827	0.0216	0.217	0.0172	0.2467	0.0199
1.7920	0.0280	0.2673	0.0207	0.2001	0.0163	0.2436	0.0196
1.8580	0.0290	0.3083	0.0233	0.2172	0.0172	0.2441	0.0194
1.9290	0.0320	0.2959	0.0223	0.207	0.0162	0.2469	0.0194
2.0040	0.0330	0.2892	0.0221	0.2092	0.0164	0.2676	0.0209
2.0840	0.0350	0.2984	0.0227	0.2199	0.0171	0.2515	0.02
2.1690	0.0370	0.3077	0.0235	0.2039	0.0161	0.2333	0.0188
2.2590	0.0400	0.285	0.0216	0.2137	0.0165	0.2497	0.0196
2.3540	0.0420	0.2803	0.021	0.1898	0.0149	0.2408	0.0187
2.4550	0.0450	0.2818	0.0213	0.1866	0.0149	0.236	0.0187
2.5640	0.0480	0.3156	0.0239	0.2091	0.0164	0.2466	0.0196
2.6800	0.0520	0.2768	0.021	0.2049	0.016	0.241	0.0193
2.8020	0.0550	0.289	0.0219	0.1993	0.0158	0.2323	0.0186
2.9380	0.0600	0.3007	0.0228	0.2189	0.0169	0.2605	0.0204
3.0780	0.0630	0.2951	0.0223	0.1804	0.0143	0.2437	0.0191
3.2310	0.0680	0.2733	0.0209	0.1905	0.0151	0.2535	0.02
3.3960	0.0740	0.282	0.0214	0.2133	0.0164	0.2417	0.0192
3.5740	0.0790	0.2816	0.0211	0.2125	0.0163	0.238	0.0184
3.7660	0.0860	0.2768	0.0208	0.2011	0.0154	0.2309	0.0178
3.9730	0.0930	0.2798	0.0208	0.1957	0.0148	0.2116	0.0166
4.2000	0.1010	0.236	0.0179	0.1851	0.0142	0.2262	0.0176
4.4450	0.1100	0.2556	0.0193	0.1831	0.0141	0.21	0.0165
4.7130	0.1190	0.2442	0.0183	0.17	0.0131	0.211	0.0163
5.0010	0.1320	0.2585	0.0192	0.1702	0.013	0.2007	0.0156
5.3250	0.1440	0.2181	0.0165	0.1738	0.0132	0.1917	0.015
5.6780	0.1590	0.2335	0.0175	0.1604	0.0123	0.1762	0.014
6.0640	0.1760	0.2039	0.0156	0.144	0.0114	0.1679	0.0135
6.5000	0.1950	0.1566	0.0123	0.1222	0.0101	0.1337	0.0112
6.9690	0.2150	0.1192	0.0098	0.1112	0.0096	0.1276	0.0112
7.4980	0.2430	0.0893	0.0077	0.0934	0.0086	0.0971	0.0096
8.1050	0.2720	0.0852	0.0075	0.1028	0.0093	0.095	0.0094
8.7730	0.3060	0.0807	0.0072	0.0879	0.0084	0.1007	0.01
9.5200	0.3460	0.059	0.0055	0.0903	0.0088	0.0859	0.0093
10.3920	0.3950	0.0743	0.0068	0.0779	0.0082	0.0953	0.0104
11.3730	0.4530	0.079	0.0073	0.0845	0.0088	0.106	0.0108
12.4990	0.5250	0.0716	0.0066	0.0889	0.0092	0.0936	0.0103
13.8240	0.6060	0.0722	0.0067	0.0898	0.0095	0.0782	0.0099
15.3590	0.7190	0.0568	0.0056	0.0947	0.0096	0.0835	0.0101
17.1830	0.8460	0.0522	0.0051	0.0797	0.0087	0.0927	0.0105
19.3360	1.0180	0.0472	0.0047	0.0855	0.0093	0.0827	0.0099
21.9600	1.2250	0.0571	0.0056	0.0639	0.0078	0.0757	0.0093
25.1210	1.5160	0.0447	0.0045	0.0544	0.0072	0.0798	0.0093

Table A14: $\sigma(277.6 \text{ keV } 5/2^+ \rightarrow 3/2^+)$ ^{239}Pu ground state band transition in all three data sets.

E_n (MeV)	δE_n (MeV)	$\sigma(98\text{-thin})$	$\Delta\sigma(98\text{-thin})$	$\sigma(98\text{-thick})$	$\Delta\sigma(98\text{-thick})$	$\sigma(99\text{-thin})$	$\Delta\sigma(99\text{-thin})$
1.3210	0.0180	0.1657	0.0146	0.1351	0.0125	0.1697	0.0158
1.3650	0.0190	0.1602	0.0137	0.1167	0.0111	0.1727	0.0164
1.4090	0.0190	0.1639	0.0147	0.1244	0.0117	0.1737	0.0153
1.4550	0.0210	0.1673	0.0142	0.1385	0.0123	0.1519	0.0139
1.5040	0.0220	0.1835	0.0152	0.1237	0.0114	0.1534	0.0138
1.5560	0.0230	0.1481	0.0124	0.1228	0.0109	0.1487	0.0134
1.6100	0.0240	0.178	0.0145	0.1352	0.0119	0.1614	0.0142
1.6670	0.0250	0.176	0.015	0.1382	0.0119	0.1678	0.0147
1.7280	0.0270	0.2014	0.0165	0.1275	0.0108	0.1623	0.0142
1.7920	0.0280	0.1854	0.0151	0.1506	0.0131	0.1763	0.0149
1.8580	0.0290	0.178	0.0146	0.1509	0.0125	0.1832	0.0156
1.9290	0.0320	0.1914	0.0155	0.1399	0.0117	0.1714	0.0145
2.0040	0.0330	0.1976	0.0158	0.1421	0.0118	0.1658	0.0137
2.0840	0.0350	0.2097	0.0168	0.1602	0.0135	0.1764	0.0148
2.1690	0.0370	0.1953	0.0158	0.1516	0.0125	0.1718	0.0144
2.2590	0.0400	0.2072	0.0166	0.1473	0.0121	0.1828	0.015
2.3540	0.0420	0.1969	0.0155	0.1421	0.0116	0.1631	0.0133
2.4550	0.0450	0.2053	0.0164	0.1477	0.0121	0.1661	0.0136
2.5640	0.0480	0.2145	0.0172	0.1526	0.0126	0.1757	0.0147
2.6800	0.0520	0.2104	0.017	0.1535	0.0125	0.1729	0.0142
2.8020	0.0550	0.2243	0.0179	0.1536	0.0124	0.1733	0.0143
2.9380	0.0600	0.2267	0.0181	0.1579	0.0127	0.1792	0.0146
3.0780	0.0630	0.2154	0.0172	0.1531	0.0126	0.173	0.0142
3.2310	0.0680	0.2097	0.0167	0.1542	0.0125	0.172	0.014
3.3960	0.0740	0.2112	0.0168	0.1485	0.0123	0.1821	0.0147
3.5740	0.0790	0.2263	0.0176	0.1526	0.0123	0.1832	0.0149
3.7660	0.0860	0.1956	0.0154	0.1459	0.0116	0.1728	0.0139
3.9730	0.0930	0.2048	0.0159	0.1531	0.012	0.1672	0.0133
4.2000	0.1010	0.1819	0.0142	0.1445	0.0114	0.159	0.0128
4.4450	0.1100	0.2102	0.0163	0.1492	0.0117	0.1723	0.0137
4.7130	0.1190	0.1828	0.0141	0.1418	0.0111	0.1545	0.0124
5.0010	0.1320	0.1865	0.0144	0.1426	0.0111	0.15	0.0119
5.3250	0.1440	0.1751	0.0136	0.1291	0.0103	0.1543	0.0124
5.6780	0.1590	0.1815	0.0142	0.1316	0.0104	0.149	0.0122
6.0640	0.1760	0.1568	0.0127	0.1124	0.0092	0.1232	0.0104
6.5000	0.1950	0.1194	0.0099	0.0901	0.0076	0.1092	0.0094
6.9690	0.2150	0.0965	0.0083	0.0763	0.0068	0.08	0.0075
7.4980	0.2430	0.0757	0.0068	0.0733	0.007	0.0681	0.007
8.1050	0.2720	0.0634	0.0059	0.0633	0.0062	0.073	0.0073
8.7730	0.3060	0.0539	0.0051	0.0595	0.0058	0.0638	0.0068
9.5200	0.3460	0.0524	0.0051	0.0552	0.0058	0.063	0.0071
10.3920	0.3950	0.0394	0.0041	0.0481	0.0054	0.0667	0.007
11.3730	0.4530	0.0502	0.0051	0.0511	0.0061	0.0582	0.0069
12.4990	0.5250	0.0475	0.0049	0.0461	0.0058	0.0638	0.0079
13.8240	0.6060	0.0629	0.0062	0.0502	0.0063	0.0568	0.0071
15.3590	0.7190	0.0377	0.004	0.0431	0.0054	0.0568	0.007
17.1830	0.8460	0.0378	0.0039	0.042	0.0058	0.0577	0.0069
19.3360	1.0180	0.0315	0.0032	0.0472	0.0061	0.0519	0.0068
21.9600	1.2250	0.0271	0.0028	0.0434	0.0053	0.0513	0.0066
25.1210	1.5160	0.019	0.0021	0.0459	0.0058	0.0457	0.006

